LICENTIATE THESIS

L

Assessment of Hydrogeological and Water Quality Parameters, Using MRS and VES in the Vientiane Basin, Laos

Nils Perttu

"My books are like water; those of the great geniuses are wine.
(Fortunately) everybody drinks water"

Mark Twain

Abstract

Water is essential for all life on the planet, sustaining and ensuring the earth's ecosystem. Groundwater from a global perspective provides about 50% of the potable water supplies, 40% of the industrial water and 20% of the irrigated agriculture. For drinking water, deep groundwater has many advantages compared to surface water and shallow groundwater, since it demands little or no treatment and the access is secured against temporary droughts. However, salinity in deep groundwater is common in coastal areas and in areas where rock salt is occurring naturally in the soil and bedrock. Drilling wells is expensive and unprofitable if it is made without knowing the groundwater potential and the location of salt affected groundwater. Vertical Electrical Soundings (VES) has been widely used to characterize aquifers and to identify salt affected water since there may be a relation between the conductivity of the aquifer and the salinity of the water. However, it is not possible to distinguish high conductive groundwater from e.g. increased clay content. Magnetic Resonance Sounding (MRS) gives a direct image of the water content of the ground and hence the vertical distribution of an aquifer. By combining MRS with VES, salt affected groundwater could be distinguished from high conductive sediments and freshwater aquifers. The aim of this study is to define and characterize water bearing geological formation and to test the possibility of using geophysical techniques to determine hydrogeological parameters and water quality parameters relating to salinity in the Vientiane basin, Laos. The investigation area is part of the Khorat Plateau where halite is naturally occurring as shallow as 50 m in depth in the Thangon Formation.

In total, 32 sites and 28 sampled wells, located in three different areas were investigated. MRS and VES recognized the stratigraphic unit N_2Q_{1-3}, consisting of alluvial unconsolidated sediments, as the main water bearing unit. The aquifer thickness varies between 10 to 40 m and the depth to the main aquifer range from 5 to 15 m. The water content is here relatively high, up to 16 % and decay times varying between 100 and 400 ms, suggest a mean pore size equivalent to medium sand to gravel. The resistivity is highly variable, but usually around 10-100 ohm-m, which suggests fresh water. Hydraulic and storage related parameters such as transmissivity, hydraulic column, specific yield and specific storage have been estimated from MRS and transverse resistance has been estimated from VES. MRS together with VES has also shown to be a useful and important tool in identifying the salt related clay layer of the Thangon Formation. This layer is characterized by low water content and a resistivity lower than 5 ohm-m. This formation can be found in all 3 areas on depth of 20 to 50 m.

Several approaches have been used to look for a relation between the water conductivity collected from wells and the aquifer conductivity determined from VES, including Archie's law. The best correlation is achieved using a linear fit between VES conductivity and water conductivity for deep wells (EC[μS/cm]= 0.3821VES[μS/cm], R^2=0.81). The conductivity of water from shallow wells does not show any relation to VES conductivity (R^2=0.09). This is probably because deep wells usually have higher conductivity than shallow wells and hence contributing more to the aquifer conductivity. Interpolated maps of TDS in area 3 from deep wells together with maps of the conductivity of the bottom layer and aquifer layer, MRS transmissivity and hydrostatic column indicates that the salt originate from the underlying layer situated beneath the main aquifer. The most important water quality parameters influencing the water conductivity are TDS, hardness and chloride, which all have a high correlation to the EC of water and thus VES conductivity. This makes MRS and VES a very promising tool for guidance of future drillings and water quality estimation.

Keywords: magnetic resonance sounding; vertical electrical sounding; resistivity; conductivity; transmissivity; transverse resistance; hydrostatic column; storativity; salinity; groundwater quality; Vientiane Basin, Laos; Khorat Plateau.

Acknowledgement

Table of Contents

Paper I:
    Perttu N., Wattanasen K., Elming S-Å., Phommasone K. 2008.
    Characterization of Aquifers in the Vientiane Basin, Laos,
    Using Magnetic Resonance Sounding and Vertical Electrical Sounding.
    (Manuscript).

Paper II:
    Perttu N., Wattanasen K., Elming S-Å., Phommasone K. 2008.
    Determining Water Quality Parameters of Aquifers in the Vientiane Basin, Laos,
    Using Geophysical and Water Chemistry Data.
    (Manuscript).

Nomenclature of Selected Parameters

|			
f_L	Larmor frequency	T_{MRS}	Transmissivity from MRS
ω_L	Angular larmor frequency	T	Absolute temperature
B_0	Amplitude of the static geomagnetic field	z	Depth
B_1	Amplitude of the excitation magnetic field	Δz	Depth interval/thickness
$B_{1\perp}$	Amplitude of the perpendicular part of the excitation magnetic field	ρ	Apparent resistivity
q	Amplitude of the excitation pulse	ρ	Resistivity of aquifer
I_0	Current amplitude	ρ_0	Resistivity of water
τ	Duration of excitation pulse	σ	Conductivity of aquifer
h	Planck's constant	EC	Conductivity of water
γ	Gyromagnetic ratio of protons	m	cementation factor
$e(t)$	Amplitude of water signal	n	Saturation exponent
E_0	Initial amplitude of the water signal	a	Structural parameter
T_1 & T_2	Longitudinal and transversal time decay constants	F	Formation resistivity factor
T_2^*	Measured transversal time decay constant		
$w(r)$	Water content distribution in the model		
M_0	Macroscopic magnetic moments of protons		
θ	Tilt angle of M in respect to B_0		
r	Coordinate vector		
φ	Phase shift of the signal		
η	Total porosity		
η_e	Effective porosity		
η_t	Trapped porosity		
V_{pore}	Volume of the pore		
S_{pore}	Surface area of the pore		
ρ	Surface relaxivity factor		
S	Storativity		
S_y	Specific Yield		
S_r	Specific Retention		
S_y	Specific yield		
S_r	Specific retention		
S_e	Elastic storage		
S_s	Specific storage		
θ_{MRS}	MRS modelled water content		
θ_f	Free water content		
θ_b	Bound water		
θ_c	Capillary water		
θ_g	Gravitational water		
θ_m	Mobile water		
θ_t	Trapped water		
K	Hydraulic conductivity		
T_p	Transmissivity from pumping test		

1. Introduction

1.1 Background

Water is essential for all life on the planet, sustaining and ensuring the earth's ecosystem. Less than 3% of the entire world's water is fresh, the remaining part is seawater and hence undrinkable. Of the 3% of freshwater, 68.7% is frozen and bound to the poles and glaciers, and therefore inaccessible. Thus, the lasting 32.3% is accessible to man and the whole ecosystem's freshwater need. Most of that water, 30.1%, is stored as groundwater, whereas the rest is found in lakes, rivers, reservoirs and rainfall (UNESCO, 2003). The water is not evenly distributed around the globe and seasonal variation, drought and floods can create extreme situations. North Africa and the Middle East have a great shortage of freshwater (Fig. 1.1a), whereas countries like Canada and northern Europe have fresh water in excess (WRI, 2000). The Intergovernmental Panel on Climate Change (IPCC) collects and summarizes objectively, the worldwide scientific literature relevant to understand human induced climate change. Their conclusion is that "freshwater resources are vulnerable and have the potential to be strongly impacted by climate change". Among other things, they emphasize that higher water temperature and changes in extremes, including floods and droughts, are destined to affect water quality with increased content of nutrients, salts and pathogens (Bates et al., 2008). Already today, 3900 children die each day due to dirty water or poor hygiene and 1.8 million people die every year in diarrhoeal diseases (WHO, 2004). Climate change together with a growing world population, increasing water stress (Shiklomanov, 1999; Fig. 1.1b) and pollution can in the future exhaust an already weakened natural resource.

Groundwater from a global perspective provides about 50% of the potable water supplies, 40% of the industrial water and 20% of the irrigated agriculture, although the relative use vary significantly between different countries. Deep groundwater has many advantages compared to surface water and shallow groundwater, since it demands little or no treatment and the access is

secured against temporary droughts. However, salinity in deep groundwater is common in coastal areas and sea-level rise from global warming is anticipated to increase salinisation even more (Bates et al., 2008). In some places, salt, precipitated from water and followed by a concentration of dissolved solids by evaporation are naturally occurring in sediments and bedrock (Wannakomol, 2005). Since some deep wells penetrate down to salt affected groundwater the wells becomes useless.

Deep wells are expensive and unprofitable if drilling is made without knowing the groundwater potential and the location of salt affected groundwater. Therefore, basic information that can guide drilling is essential. In 1993 the "Project for Groundwater Development in Vientiane Province, Laos" was implemented by Japan International Cooperation Agency (JICA), aiming to raise the water supply ratio in the rural areas by drilling deep wells (Takayanagi, 1993). Due to bad water quality and maintenance problems, only 30% of the total 118 deep wells were in use in year 2000 (JICA, 2000). The bad water quality was partially due to salinity caused by halite (rock salt) (JICA, 2000). Salinity problems are common in central Laos and north-east Thailand and have been studied by among others Wannakomol, (2005); Srisuk et al. (1999) and Williamson et al. (1989).

Geophysical methods have been successfully used in groundwater exploration, since they are usually non-invasive and relatively cheap. Many of the measured physical properties of the earth, is to a large extent influenced by the water content, e.g. electrical conductivity, velocity of seismic waves (seismic methods) and dielectric permittivity (Ground Penetrating Radar). The most common methods for groundwater studies are based on electrical resistivity. The resistivity of a geological structure can vary significantly, depending on the water content and salinity. This enables both a quantification of the water content and an estimation of the groundwater quality (i.e. salt content). However, the resistivity for different materials, are not unique. For instance, salt affected groundwater can easily be mistaken for high conductive sediments like clay. Magnetic Resonance Sounding (MRS) is a relatively
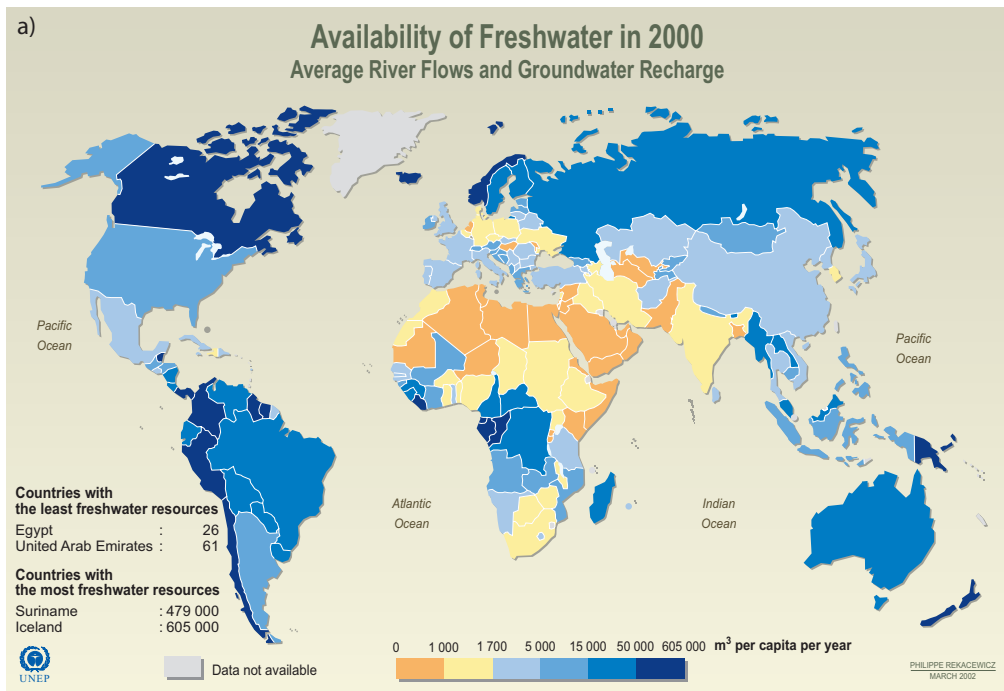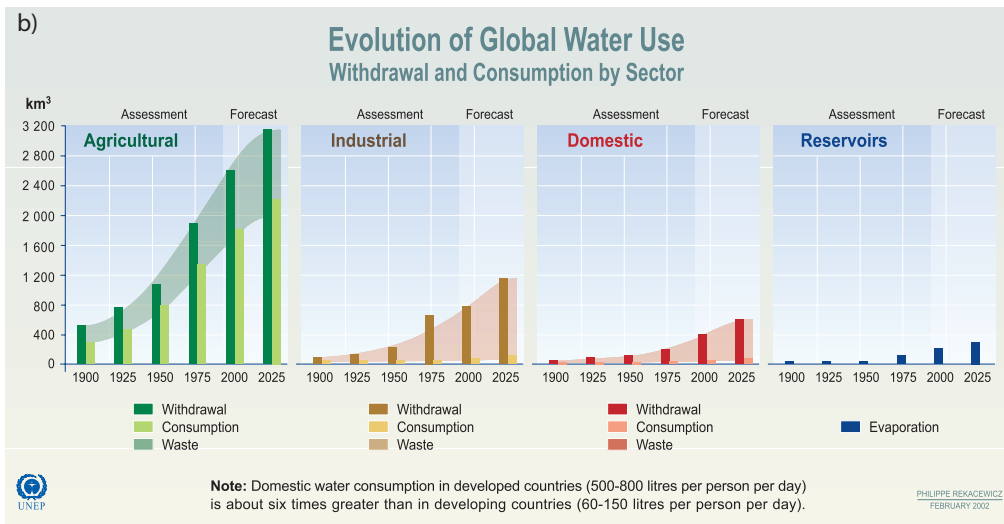
Fig. 1.1 a) Availability of freshwater from rivers and groundwater in the year 2000 expressed in m³/capita (UNEP/GRID-Arendal, 2002a) and b) The evolution and forecast of water use for different sectors (UNEP/GRID-Arendal, 2002b).

new technique, which in contrary to other geophysical techniques gives a direct measure of the water content, and also of the pore size distribution with depth (Legchenko and Valla, 2002). MRS is hence able to determine both storage and hydraulic related parameters far less ambiguous than classical geophysical techniques (Lubczynski and Roy, 2003). If combining MRS measurements with electrical resistivity methods, freshwater aquifer may be identified and distinguished from salt affected water.

1.2 Aims

The objectives of this thesis can be divided into three parts:

- Define and characterize water bearing geological formation according to their relative hydraulic and storage related properties (Paper I).
- Exploring the possibility to distinguish freshwater aquifers from salt affected groundwater (Paper I, Paper II).
- Investigate the possibility to determine the quality of the groundwater directly from geophysical parameters and water chemistry data (Paper II).

2. Study Area

The Vientiane Province is located in central Laos (Fig. 2.1), between latitude 18° and 18.67° and longitude 102° and 103°. The central part of the province is situated in the Vientiane Basin with an average elevation of 170 to 190 m. This fertile flat low-land is mainly used for agriculture with big irrigation systems. The surrounding mountain area is covered by forests with elevations ranging up to 1600 m. The whole region is within the drainage basin of Nam Gnum and Mekong Rivers. Laos has a tropical monsoon climate with a rainy season from May to October, followed by a cool dry season from November to February and a hot dry period from March to April. The average rainfall is about 1 780 mm, but it varies regionally. Temperature ranges from as high as

Fig. 2.1 The Vientiane Province, with the Vientiane Basin in the drainage basin of Nam Gnum and Mekong rivers. The three study areas defined with rectangles.

40°C in the Mekong lowlands during the hot months to as low as 5°C in the mountain area in the winter (Stuart-Fox; Rooney, 2006).

2.1 Geology and Hydrogeology

The Vientiane Basin is located on the very northern part of the Sakhon Nakhon Basin in the Khorat Plateau (Fig. 2.2). The Khorat Plateau covers an area of 170 000 km^2 between latitudes 101° and 106° and longitudes 14° and 19° in the region of north-eastern Thailand and central Laos. During the Cretaceous, due to relative sea-level rise, the plateau underwent periods of marine influx but was sporadically isolated from the oceans. This created the Maha Sarakham Formation, a three layer salt unit separated by red-coloured siliciclastics of fluvial origin. Tectonics during the early Tertiary lead to severe folding and deformation of the salt beds, creating a variety of different salt structures such as domes, anticlines, synclines and ridges as shallow as 50 m below the surface. The upper and middle parts of the salt beds are often missing due to dissolution from groundwater percolation. The evaporites include thick successions of halite, anhydrite and potassic minerals like sylivite and carnalite (Tabakh, et al, 1999).

Fig. 2.2 Geology of Vientiane province (Long et al. 1986). Keymap showing the extent of the Khorat Plateau after Tabakh et al. (1999). The rectangle defines the area where halite depths have been determined from borehole data. A and B, E and F, G and H defines profiles along which geophysical and geological data are presented.

4

Period			Symbol		Thickness [m]	Vientiane Stratigraphy	Thai Equivalent
Neogene – Quaternary			Q_4	Phon Hong Group	0.5		
			Q_{2-3}		20-25		
			N_2Q_{1-2}		70	Vientiane Fm.	
Cretaceous	Late		K_2sb		150	Saysomboun Fm.	Phu Thok Fm.
			K_2tn		>550	Thangon Fm.	Maha Sarakham Fm.
	Early		K_2cp	Khorat Group	400	Champa Fm.	Phu Phan Fm.
Jurassic Cretaceous			J-Kpn		350	Phu Phanang Fm.	Phra Wihan Fm.

Fig. 2.3 Stratigraphy of the Vientiane Basin after Long (1986) and Lovatt Smith et al. (1996).

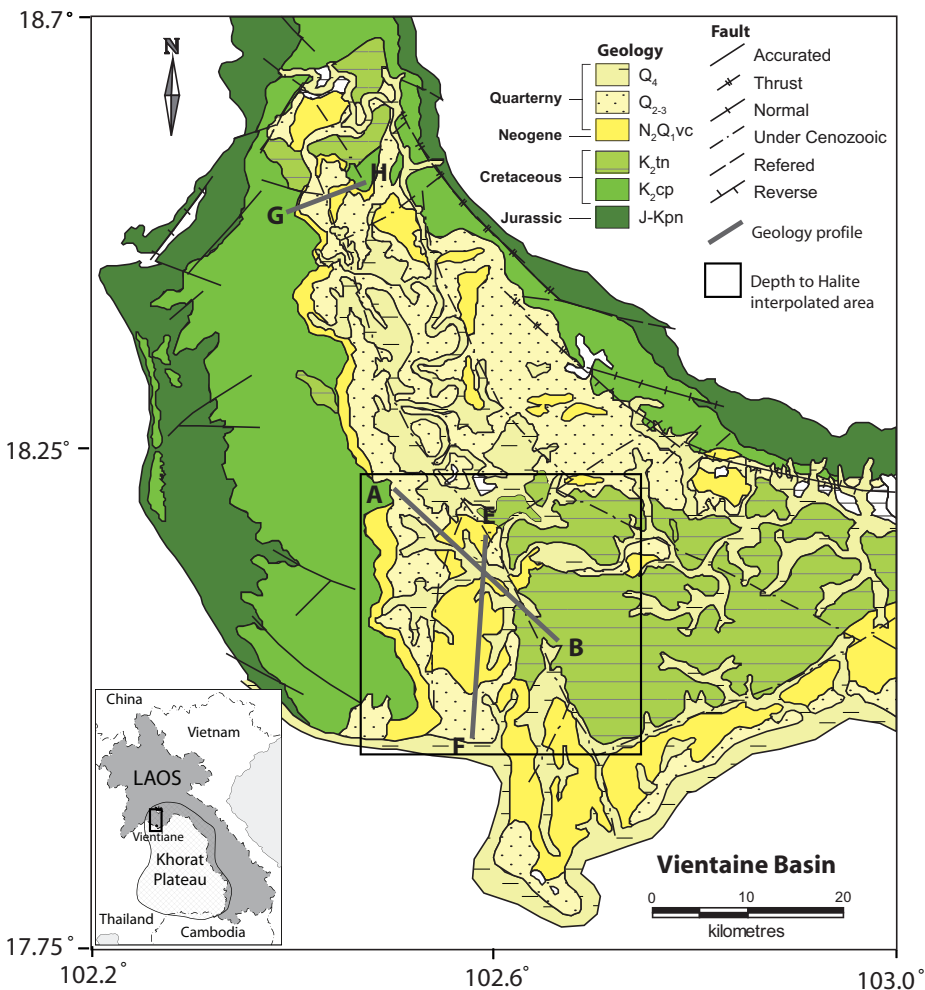The geology (Fig. 2.2) and stratigraphy (Fig. 2.3) are summarized in the section below using Lao nomenclature proposed by Long et al (1986) with modifications based on Thai stratigraphy (Lovatt Smith et al., 1996) and hydrogeological data (Srisuk et al., 1999, Takayanagi, 1993). The equivalent to the Maha Sarakham Formation in the Vientiane Basin is the middle Cretaceous Thangon formation (K_2tn). It is most easily found in the south-eastern part of the Vientiane basin, where the salt beds have been mobilized into pillows and small diapirs. It is mainly composed of salt-layer bearing anhydrite interbedded with claystone with a thickness less than 550 m and a maximum halite thickness of of 340 m (Lovatt Smith et al., 1996). The depth to the salt layer generally ranges between 50 to 200 m in the southern part of the province (Long et al., 1986). The hydraulic conductivity (K) ranges between 10^{-14} to 10^{-8} m/s, the specific yield is in the range of (S_y) 10^{-7} and the average specific storage (S_s) is $2*10^{-9}$, which makes K_2tn an aquiclude or non water bearing formation (Srisuk et al., 1999).

The Thangon formation is overlain by the Saysomboun Formation (K_2sb) (not in map). This formation originates from upper Cretaceous and constitutes red-brown claystone that gradually change to siltstone. The maximum thickness of K_2sb is 150 m. K_2sb is found in the middle and northern part of the basin with a relative low K ranging from 10^{-8} to 10^{-5} m/s, a S_y of around 0.01 and a S_s 10^{-6}. The Neogene to Quaternary Vientiane Formation (N_2Q_1vc) has a thickness no more than 70 m. This formation is overlain by the stratigraphic units: Q_{2-3} (<25 m) and Q_4 (<0.5

m) of Quaternary origin. The N_2Q_1vc and Q_{2-3} are alluvial deposits found in abandoned river channels, and contain mostly gravel, sand and clay. Since they share the same characteristics they will be referred to as the N_2Q_{1-3} unit in this paper. The equivalent Thai units have K ranging from 10^{-6} to 10^{-4} m/s, with S_y around 0.15 and S_s around 2 to $3*10^{-3}$. The possibility for developing groundwater in these units is regarded as high. The above mentioned units are all part of the Phon Hong Group. Underlying the Thangon Formation is the Khorat Group, which among others consists of the Champa- (K_2cp) and Phu Pha Nang formations (J-Kpn). These up to 400 m and 350 m thick units, respectively, are found primarily in the western and eastern part of the basin on the border to the mountain area. They are largely composed of sandstone of Cretaceous and Jurassic ages, with K ranging from 10^{-8} to 10^{-5} m/s, S_y of around 0.05 and S_s of about $5*10^{-6}$.

2.1.1 Sources of Salinity

Salinity can arise from natural causes or from human activities. The major source of salinity within the Vientiane Basin, originates primarily from the salt structures of the Thangon formation.

Salinity in shallow groundwater, originates from weathered salt accumulated in the upper clastic sediments transported from higher altitudes to nearby lowlands and valleys. Here, the water evaporates, leaving the salt in the upper surface (Löffler and Kubiniok, 1988). Salinity can also arise from deep groundwater flows, when water in a recharge area penetrates down to the rock salt and then is transported to lowland discharge areas. Salt groundwater can also be transported upward through faults and fractures caused by artesian, convective and capillarity flow (Srisuk et al., 1994). Human activity affects the transport of salt in many different ways. Within the Khorat Plateau, soil salinity has been reported due to deforestation, construction of water reservoirs, salt manufacturing and irrigation (Arunin, 1987).

3. Magnetic Resonance Sounding (MRS)

The Magnetic Resonance Sounding (MRS) technique, also known as Proton Magnetic Resonance (PMR) and Surface Nuclear Magnetic Resonance (SNMR), was developed in Russia during the 1980's, but became commercially available first in the late 1990's by the French company Iris instrument and their instrument Numis. The principal behind the method is governed from Nuclear Magnetic Resonance (NMR) and has been utilized in medical tomography (MRI), well logging, oil exploration- and chemistry applications.

3.1 Theory of Method

MRS is based on the principal of Nuclear Magnetic Resonance (NMR), where the spin of protons is crucial to understand the basic phenomena. Spin comes in multiples of ½, where, individual unpaired protons possess a spin of $\pm 1/2$. The spin of the proton can be seen as a magnetic moment vector (μ), causing the proton to behave like a tiny magnet with a north and south pole. When placed in a magnetic field of strength B_0, the proton aligns itself with the magnetic field in a low energy state (Fig. 3.1a). A proton can absorb an electro magnetic wave, of frequency ω_L (the larmor frequency). The frequency depends on the gyromagnetic ratio (γ)

a)

Fig. 3.1 a) Energy diagram, showing the two spin states of the proton. The energy of the EM wave must match the energy difference between the two states for absorption to occur, given by the static magnetic field (B_0). b) The proton transmits a secondary EM wave when returning to its low energy state.

$$\omega_L = 2\pi \cdot f_L = \gamma \cdot B_0 \qquad (3.1)$$

for hydrogen:

$$f_L (Hz) = 0.04258 \cdot B_0 (nT) \qquad (3.2)$$

This will cause the proton to switch to a higher energy state. The energy of the electro magnetic wave needed to cause a transition between the two spin states (Fig. 3.1a) is given by

$$E = 2\pi \cdot h \cdot f_L \qquad (3.3)$$

where h is the Planck constant. As the proton returns to its low-energy state it will emit a secondary electro magnetic wave (Fig. 3.1b). The phenomena can also be explained from Fig. 3.2a, where the magnetic moment (μ) of the proton is aligned with the static magnetic field (B_0) in a precessional motion, with the angular frequency ω_L. When a resonance magnetic field, B_1 is applied (Fig. 3.2b), μ is deflected from its equilibrium state with an angle of θ, where only the perpendicular component of B_1 contribute to the deflecting force. As B_1 is turned off, μ returns back to its equilibrium state (Fig. 3.2c) generating a secondary relaxation magnetic field while realigning with B_0 in a precessional motion in the larmor frequency. The amplitude of the secondary magnetic wave is proportional to the sum of flux from all precessing magnetic moments $M_\perp = M_0 * \sin \theta$ with

$$M_0 = N \cdot B_0 \frac{\gamma^2 h^2}{4kT} \qquad (3.4)$$

where N is the number of hydrogen protons per unit volume, *T* is the absolute temperature and *k* is the Boltzmann constant.

3.1.1 The Principle of MRS

MRS measurements are usually conducted with a square or circular loop, where the energizing field, B_1 is created by a pulse, $q=I_0*\tau$, of alternating current (I_0) and duration (τ) in the larmor frequency

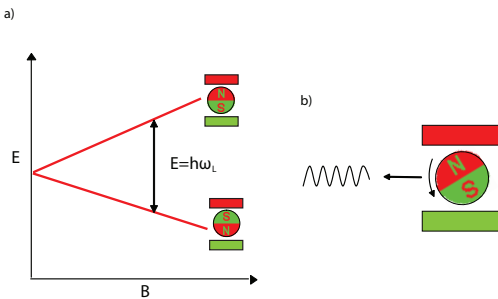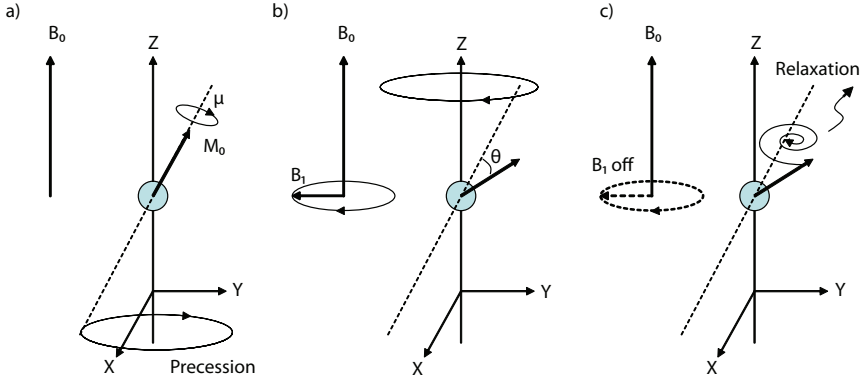$$i(t) = I_0 \cdot \cos(\omega_L t), 0 < t \leq \tau \qquad (3.5)$$

Fig. 3.2 a) Proton in a precessional orbit around the geomagnetic field (B_0), where μ is the magnetic moment vector aligned with B_0. b) μ is deflected by an angle of θ, due to the excitation field (B_1), where only the perpendicular component of B_1 acts on μ. c) When B_1 is removed, the proton generates a relaxation magnetic field, as it returns to B_0 in a precessional motion.

The pulse moment is followed by a 30 ms "dead time", where the system switches from transmitting mode to receiving mode. The decaying signal $e(t,q)$ induced in the antenna (Fig. 3.3a) by the relaxation of the protons can be approximated by

$$e(t,q) = E_0(q)e^{-t/T_d}\cos(\omega_L t + \varphi) \qquad (3.6)$$

where T_d is the decay time or relaxation of the signal, φ is the phase shift. E_0 is the initial amplitude of the signal:

$$E_0(q) = \omega_0 M_0 \int_V B_{1\perp} \sin\left(\frac{1}{2}\gamma B_{1\perp}q\right)w(r)dV(r) \quad (3.7)$$

M_0 is the nuclear magnetization of protons, $B_{1\perp}$ is the transmitting magnetic field component perpendicular to the B_0, w(r) is the water content in a unit volume dV at the location r(x,y,z).

From Equation (3.5) and (3.6) it can be deduced that E_0 is directly related to the water content, (w(r)). T_d is the characteristic time for which the signal has diminished to 1/3 of its initial value and is related to the mean pore size of the material, and hence the grain size and hydraulic conductivity. The recorded larmor frequency ($f_L = \omega_L/2\pi$) is associated to the magnetic inhomogeneities within the investigated volume and the phase shift (φ) is related to conductivity variation of the subsurface. By systematically

increasing the pulse moment (q), the energizing field penetrates deeper into the investigated volume and information of E_0, T_d together with f_L and φ and can be retrieved from deeper parts of the subsurface (Fig. 3.3b). The maximum investigated volume could be approximated by an area 1.5 times the loop size for a depth corresponding to the loop diameter (Yaramanci et al., 2004). The magnetic field produced by the protons varies between 10^{-12} and $4*10^{-9}$ T, which corresponds to 10 to 4000 nV in a wire loop of 100 m in diameter as receiving antenna (Legchenko and Valla, 2003).

3.1.2 Relaxation of the Signal

The realignment of the magnetization vector to its equilibrium state (Fig. 3.2c and Fig. 3.5b), can be described by two characteristic times: T_1 (the longitudinal relaxation) and T_2 (the transverse relaxation) and describes how efficiently the magnetic energy of the protons is transferred its surrounding. T_1 is the relaxation in the direction of the geomagnetic field (B_0), whereas T_2 is the relaxation perpendicular to B_0, and is directly attainable with the MRS system. The measured transverse relaxation time T_2^*, is somewhat shorter due to two simultaneous phenomena (Fig. 3.4); (1) As the magnetic susceptibility of the surrounding rock is nonzero, magnetic field gradients will be generated at the pore-grain

7
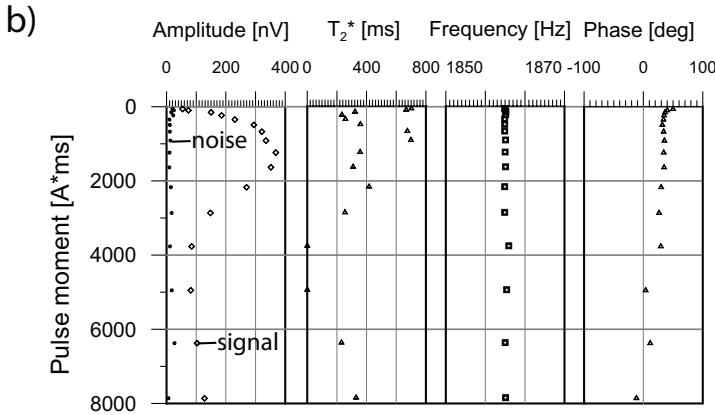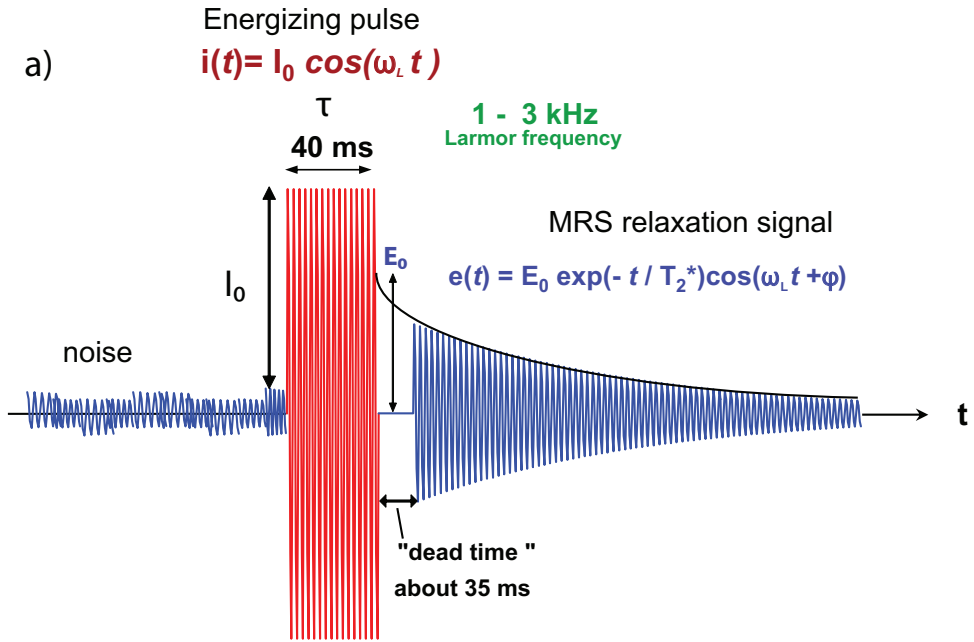
Fig. 3.3 a) Time sequence of the MRS signal: (1) noise is measured, (2) energizing pulse at the larmor frequency (f_L) and (3) relaxation of the signal, where parameters like the initial amplitude (E_0) and decay time (T_2^*) are recorded. b) Measured (from Site 16, Laos) parameters like initial amplitude (E_0) and noise, decay time (T_2^*), frequency (f) and phase (ϕ) are plotted against the pulse moment (q).

boundary. Also, (2) as water molecules due to diffusion collide with the grain walls they will automatically receive a new arbitrary magnetic moment. This leads to differences in larmor frequency and therefore a loss of phase coherency in the spin rotation (Legchenko and Valla, 2002). The relaxation time (both T_1 and T_2^*) is related to the mean pore size of the aquifer (Kenyon, 1997) according to

$$T_{1,2} \sim \frac{V_{pore}}{\rho \cdot S_{pore}} \qquad (3.8)$$

where S_{pore} and V_{pore} are the surface area and volume of the pore respectively. The surface relaxivity (ρ) is a material-fluid constant different for T_1 and T_2^*. Typical values of T_2^* are presented in Table 1.1. T_1 is less influenced by magnetic inhomogeneities compared to T_2 and
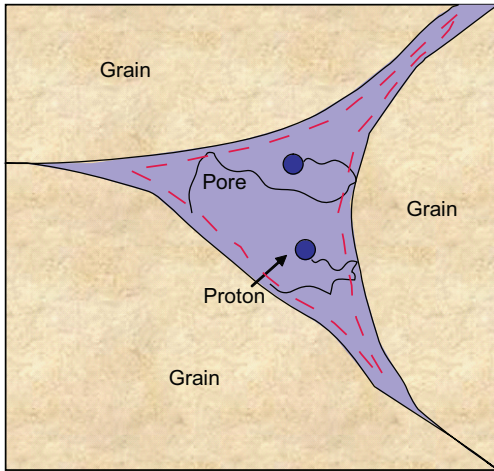
Fig. 3.4 The relaxation of the signal (T_2*) depends on the ratio of the volume (V_{pore}) to surface area (S_{pore}) of the pore according to Equation 3.8. The surface relaxivity (ρ) is affected by the magnetic mineral grains in the grain-pore boundary, inducing a magnetic field, different from the larmor frequency (indicated by dotted line in the figure), but also from diffusion of water molecules.

Table 1.1 Values of T_2* for different geological materials (Shirov et al., 1991; Allen et al., 1997)

Relaxation time	Petrophysical Information	MRS
T_2* < 3 ms	Clay bound water	Undetectable
T_2* < 30 ms	Sandy clays	
30< T_2* <60	Clay sands, very fine sands	Detectable
60< T_2* <120	Fine sands	
120< T_2* <180	Medium sands	
180< T_2* <300	Coarse and gravely sands	
300< T_2* <600	Gravel deposits	
600< T_2* <1500	Surface water bodies	

will hence give more reliable estimations of pore size. T_1 is longer than T_2* (usually $T_1 \approx 1.5 * T_2$*), and can therefore be determined, using a double pulse technique, known as saturation recovery (Fig. 3.5a) (Dunn et al. 2002). The first pulse is followed by a second pulse with a short delay. In the end of the first pulse, the relaxation of the component of the magnetization (M) in direction of $B_{1\perp}$ is completed (T_2*), but not the component aligned with B_0 (T_1). Consequently, M_0 is not fully recovered (Fig. 3.5b) and the initial amplitude of the second pulse will be lower than the first pulse. The initial amplitudes of the first and second pulse as a function of pulse delay makes it possible to determine T_1 (Fig. 3.5c).
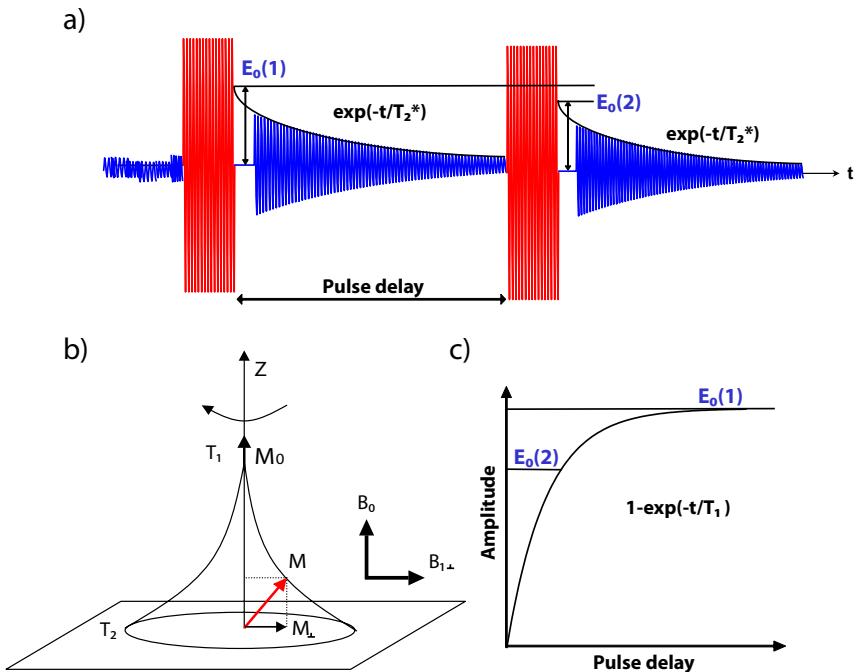
Fig. 3.5 a) A two pulse sequence, where the initial amplitude (E_0) is recorded for both pulses. b) T_1 can then be estimated from the E_0 from the first and second pulse as a function of pulse delay.

3.2 Factors Influencing the Signal

Several factors influence the MRS signal. The maximum amplitude and shape of the $E_0(q)$ curve depends among other things, on depth, thickness and number of water bearing layer within the subsurface. From a qualitative point of view, the shape, amount of water and location of the aquifer can be indicated from examining the sounding curve. Two aquifers with equal thickness positioned on the same depth but with different water content (Fig. 3.6a) will have a peak at the same pulse moment. However, the aquifer with higher water content will have a curve with higher amplitude. Analogous to this, two aquifers with equal water content with their centre point located on the same depth, but with different thicknesses will also have the same shape of the sounding curves but the thicker aquifer will have higher signal amplitude (Fig. 3.6b). For a two layer aquifer, with equal water content and thickness, the sounding curve will have two peaks, where the second peak will be smaller in amplitude but more extensive in pulse moment (Fig. 3.6c). Comparing Fig. 3.6d and Fig. 3.6a, it is obvious that the maximum amplitude of
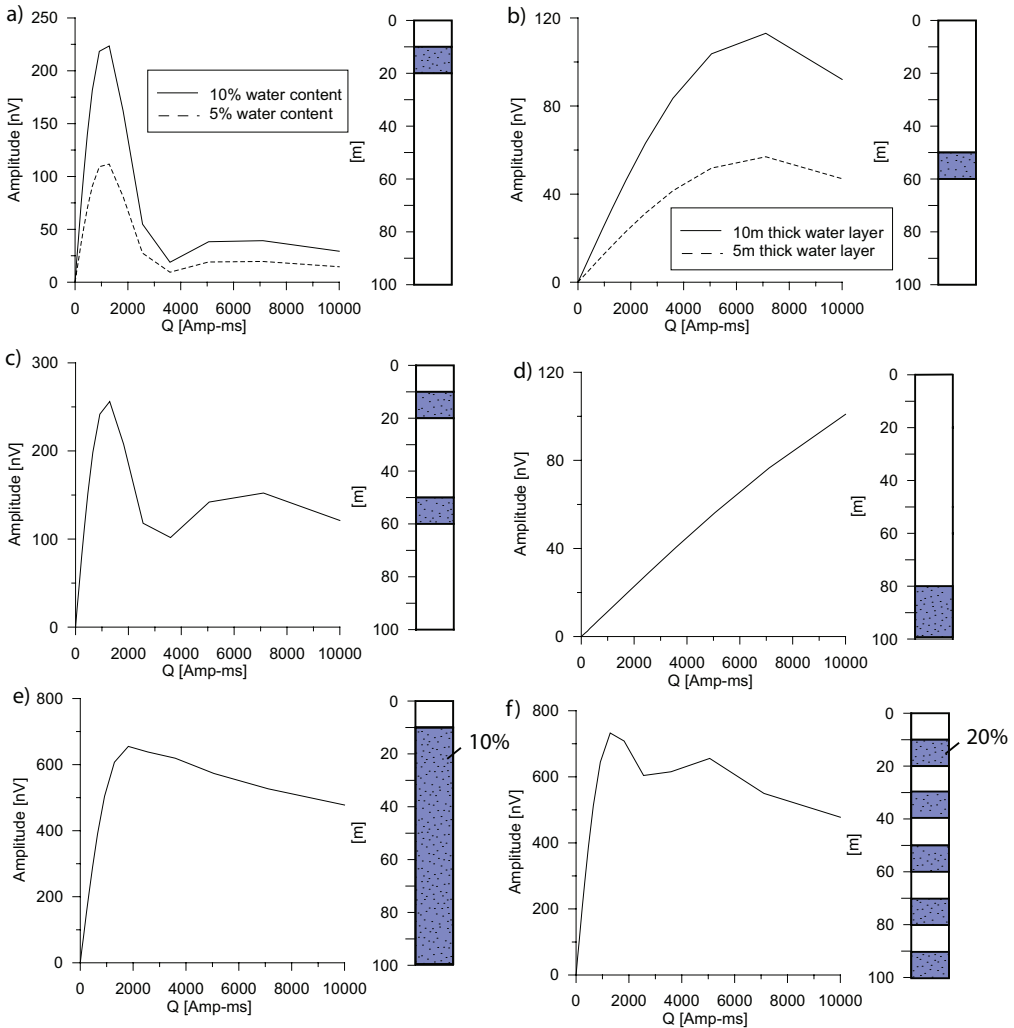
Fig. 3.6 The response on the sounding curve for a) different water contents for a single water layer, b) different layer thickness for a single water layer, c) two water layers at different depths, d) one deep water layer, e) one water layer extending from 10 m depth to 100 m depth and f) a multi layer aquifer.

the signal decreases for deeper positioned water layers. For aquifers with multiple layers, it might be difficult to differentiate several water bearing layers from one thick layer, since the resolution decreases with depth (Fig. 3.6e and f). Modelling results has shown that MRS is able to determine accurately the geometry of the aquifer down to a depth equivalent to roughly half the loop size (Legchenko et al., 2002).

The resistivity of the subsurface controls the depth of investigation, which can be estimated with the skin depth (δ),

$$\delta = 503 \cdot \sqrt{\rho / f} \qquad (3.9)$$

where the amplitude of the signal has been reduced to 37 %, ρ is the resistivity of the medium and f is the frequency of the transmitted signal. Modelling results for a 100 m square loop (Fig. 3.7) using the numerical modelling software Samogon (Legchenko, 2001) for a 10 m thick water layer with 10% water content, T_2^*=150 ms, at different depths illustrates the detection limit for different resistive half spaces. The geomagnetic field is set to 43800 nT, with an inclination of 24° corresponding to the conditions in the Vientiane basin. The noise threshold is set
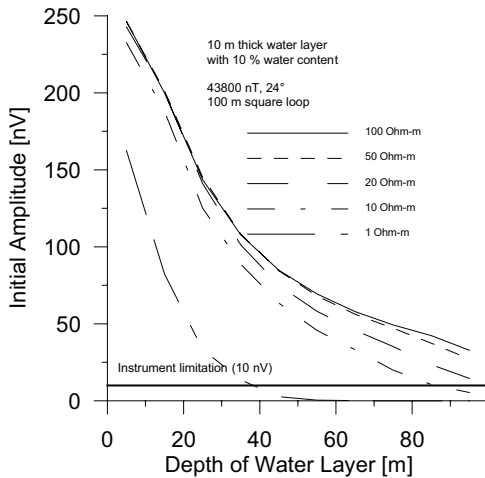
Fig. 3.7 Modelled initial amplitudes (E_0) for a 10 m thick water layer with a water content of 10%, with geomagnetic field conditions as in the Vientiane basin. The water layer is plotted at different depths for different resistivity curves. The signal is almost the same for the 50 ohm-m and 100 ohm-m curves but is more effected by lower resistivities.

to 10 nV. The 100 ohm-m and 50 ohm-m curves follow one another closely, indicating there is only a small effect on the amplitude of the signal. The difference becomes more significant for lower resistivities. For a 1 Ohm-m halfspace, water can only be detected down to a depth of about 35 m. The noise level is however often higher than 10 nV and the amount of water in many cases less than 10%, which reduces the detection depth.

The signal of the water varies also with the intensity and inclination of the field. The earth magnetic field (Fig. 3.8a) is strongest at the poles (B_0= 60000nT ~ f_L 2500 Hz) and weakest around the equator (30000 nT ~ 1200 Hz). With lower larmor frequency, the penetration depth increases according to the skin depth formula (Equation 3.9). However, the initial amplitude of the signal (E_0) is proportional to the square of the geomagnetic field ($E_0 \sim B_0^2$). For low B_0, the investigation depth is more affected by the amplitude of B_0, than the skin depth. The effect of B_0 on the signal is illustrated in Fig. 3.8, where the signal response of an aquifer positioned between 10-20 m (Fig. 3.8b) and 50-60 m (Fig 3.8c) is plotted for local earth magnetic conditions in Luleå, Sweden; Vientiane, Laos and Beira, Mozambique. There is a substantial difference in signal amplitude between Luleå and Beira, where the signal in Beira is reduced to 1/3 compared to Luleå. The inclination of the geomagnetic field affects the perpendicular component of the excitation field, and must be accounted for in the interpretation.

One of the main limitations of the MRS method is electromagnetic (EM) noise, since the signal of the water generally is lower than the amplitude of noise. Noise can be natural and uncorrelated, caused by magnetic storms, thunderstorms etc. Man made EM noise are commonly generated by power lines, radio transmitters, cars, electrical fences etc. Industrial noise is considered to be a superposition of harmonics of the industrial frequency 50 or 60 Hz. The MRS signal is severely affected by noise and different approaches can be applied to remove or at least decrease the noise during acquisition or inversion. In order to improve the signal to noise (S/N) ratio a stacking procedure is utilized during acquisition. In case of non correlated noise the
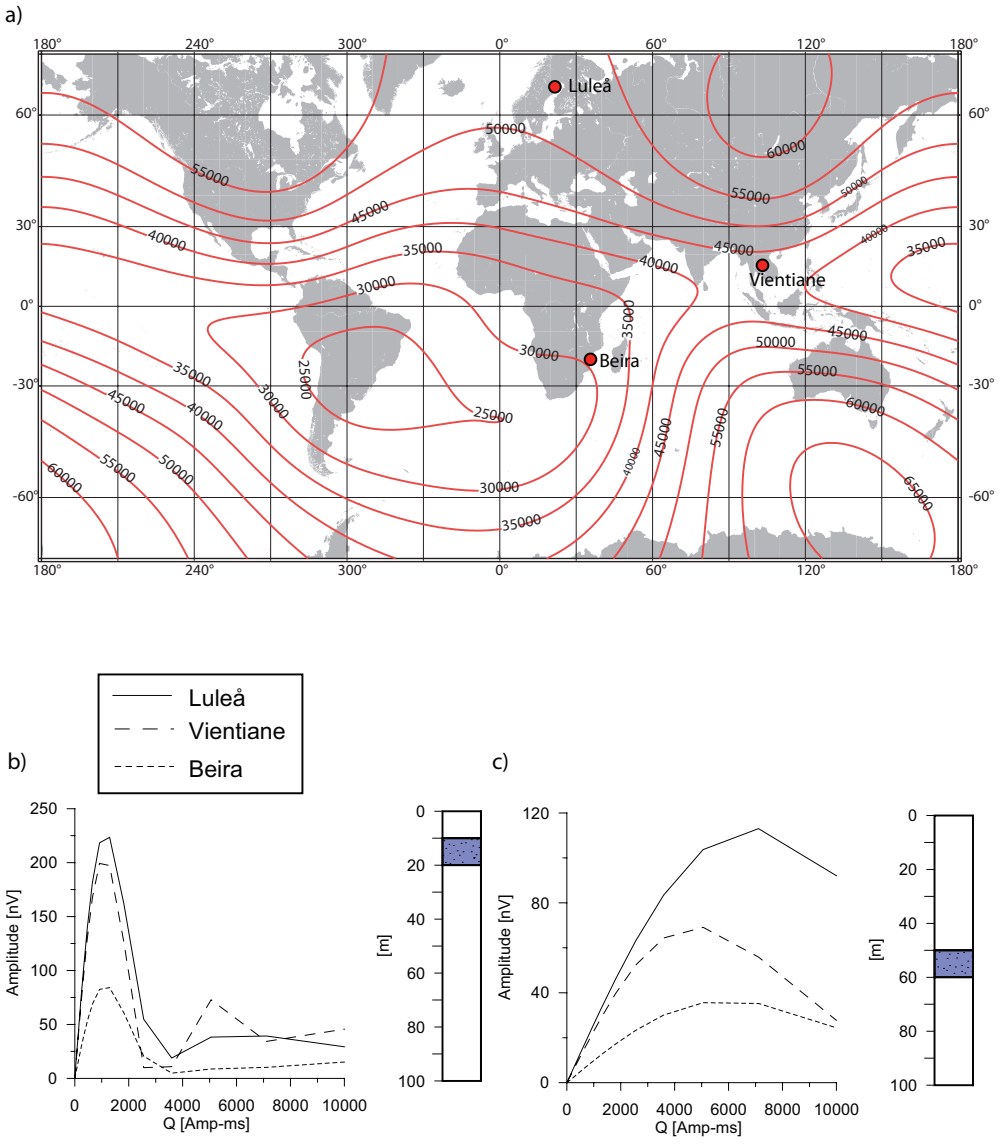
Fig. 3.8 a) US/UK world magnetic model for the main field (B_0) intensity. Luleå, Vientiane (Laos) and Beira (Mozambique) is marked with circles. Response from b) a shallow aquifer and c) a deep aquifer from Luleå (─), Vientiane (--) and Beira (⋯). The amplitude of the water layer is almost decreased to 1/3 in Beira compared to Luleå.

S/N-ratio should increase √n times, where n is the number of stacks. If the noise is much larger than the signal and time-varying, i.e. not constant during the measurement, a specific algorithm can be used, "weighted average", to weight the readings by a coefficient. This coefficient is inversely proportional to the noise and signal. When the noise suddenly increases during the measurement, the coefficient determined during

the measurement must be low and the quality of the already stacked readings is left unaltered. By default, the Numis system applies a high cut filter (Fig. 3.9) centred at the excitation pulse frequency, with a ±100 Hz bandwidth. In addition, in presence of industrial EM noise, a notch filter can be applied according to Fig. 3.9. The notch filter is centred at the harmonics of the power line frequency and ±1 Hz of the bandwidth

12
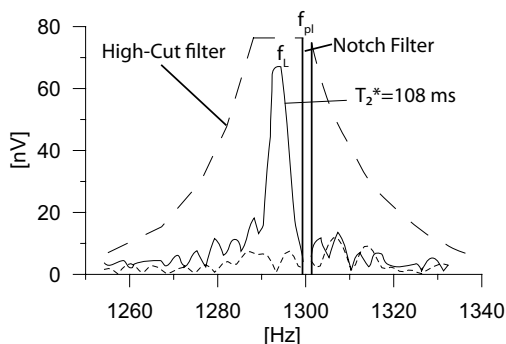
Fig. 3.9 Fourier spectra showing the response of a MRS signal with an initial amplitude (E_0) of 65 nV and decay time (T_2^*) of 108 ms at the larmor frequency f_L. The Numis system uses by default a high cut filter (--) and the optional notch filter (−) centred at the harmonic of the power line frequency (f_{pl}).

is cut. Notch filters are very effective to remove industrial noise, but should be handled with care. If the larmor frequency is close to one of the power line frequency harmonics, the signal can suppress important information in the signal. Fig. 3.10, illustrates two measurements conducted with a 100 square loop, using 64 stacks, in a small village outside Maputo, Mozambique. One measurement was conducted with notch filter and the other without. Here, it is obvious that the notch filter increases the signal to noise (S/N) ratio and hence the quality of the measurement but also that acquisition time can be decreased since the number of stacks can be reduced. Legchenko and Valla (2003) summarize the use of notch filter as follows: when the frequency offset (ΔF) between the power line harmonics (f_{pl}) and the larmor frequency (f_L) is greater than 8 Hz the notch filter is most effective. When $\Delta F < 8$ Hz, the notch filter can distort signals for $T_2^* > 200$ ms. Another method to suppress noise is changing the 100 m square loop to a eight shape loop (2*50 m) (Fig. 3.11). Here, the noise (n_1 and n_2) cancel each other since wires are crossed and therefore their corresponding surfaces have opposite signs. The signal on the other hand add each other, since the current circulates in opposite sense to one another in the small squares, reversing the effect of the opposite signs of the two surfaces (Bernard, 2007). The signal to noise (S/N) ratio can in this manner increase substantially compared to the 100 square loop, depending on the local noise condition. The negative side

is that the penetration depth decreases to half of the penetration depth of the 100 square loop. Sometimes the loop size is changed due to lack of room, e.g. a 50 m, 2 turn square side loop. This decreases the signal, since the excited volume of water decreases and in addition the penetration depth decreases as well.

3.3 Inversion of MRS Data

At the moment, only the inversion software Samovar, based on the least square solution with regularization is commercially available (Legchenko and Shushakov, 1998). Assuming a stratified earth for each pulse moment (q), the parameters e(t) and E_0 are inverted using a modified form of Equation 6 and 7 into θ_{MRS} [%]and $T_{1,2}^*$ [ms] versus depth according to Fig. 3.12. A geoelectrical model is needed to account for the effect of a conductive subsurface through the MS-DOS based software, Nmr. Different filters, like notch-, band pass- and running average filter can be used to improve S/N-ratio. Due to equivalence, several models can fit the data. The parameter of regularization (pr) controls the smoothness of the interpreted water content distribution with depth, where a high regularization (pr=1000) spreads the water in thick layers, and a low regularization (pr=1) concentrates the water in thin layers. The number of layers, can be altered to gain a more "blocky" or "smooth" model.
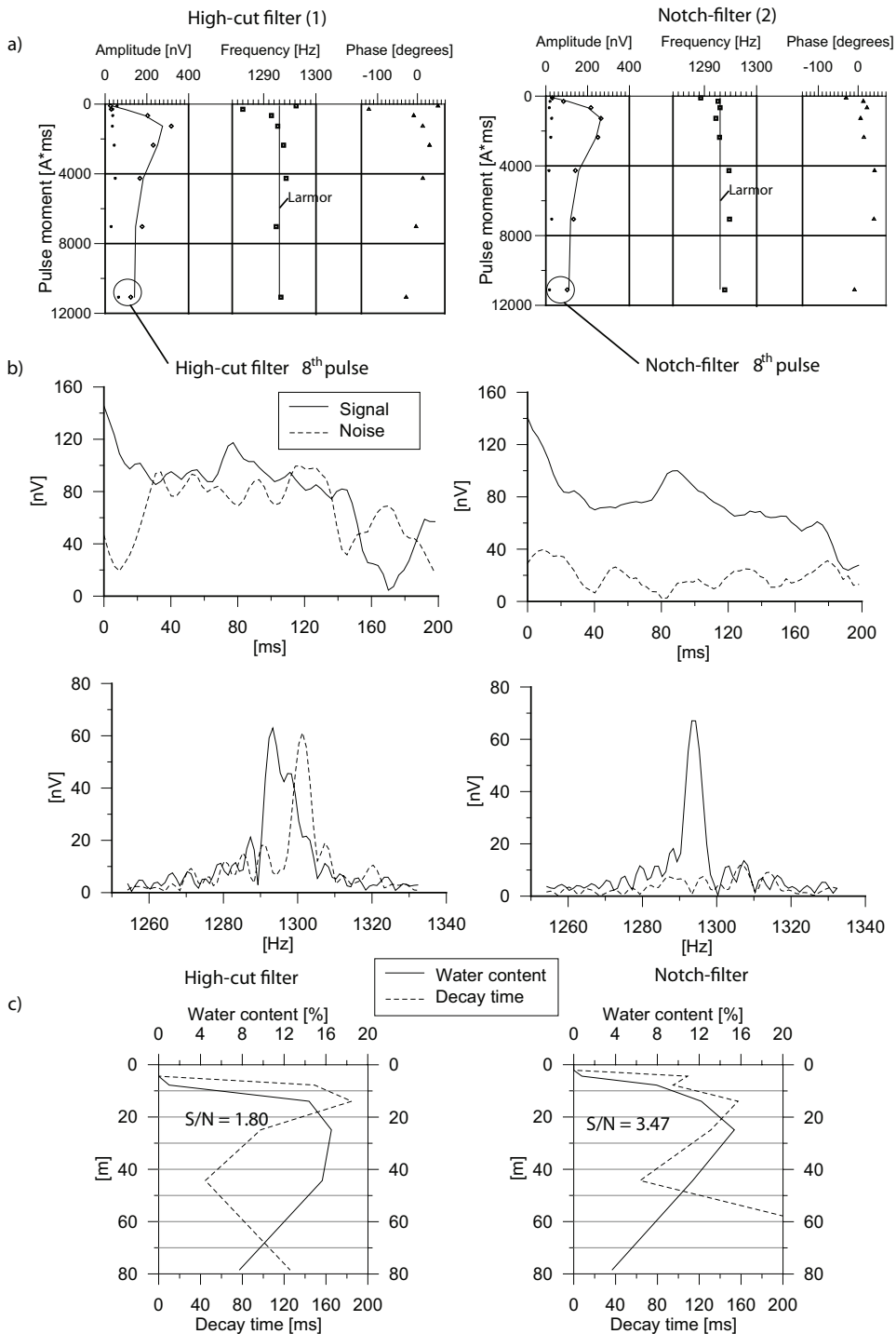
Fig. 3.10 a) Comparison of two MRS 8 pulse and 64 stacks measurement on the same location outside Maputo, Mozambique, using (1) high cut filter and (2) notch filter. b) The relaxation of the signal with corresponding Fourier spectra from the 8th pulse showing that the signal is less corrupted for the notch-measurement. c) The final model with a 1.8 signal to noise (S/N) ratio for the high cut-measurement and a S/N of 3.5 for the notch-measurement.
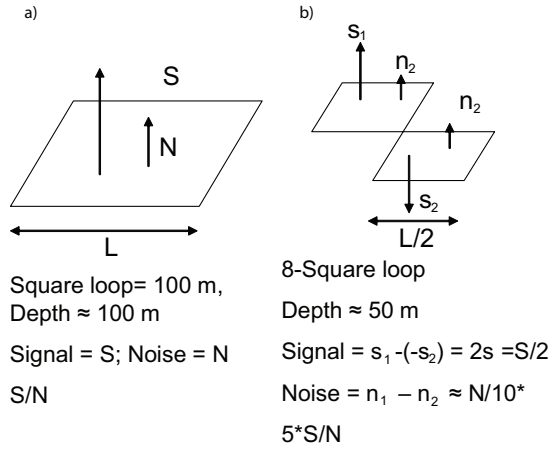
Fig. 3.11 a) 100 square and b) 8-shape loop configuration.
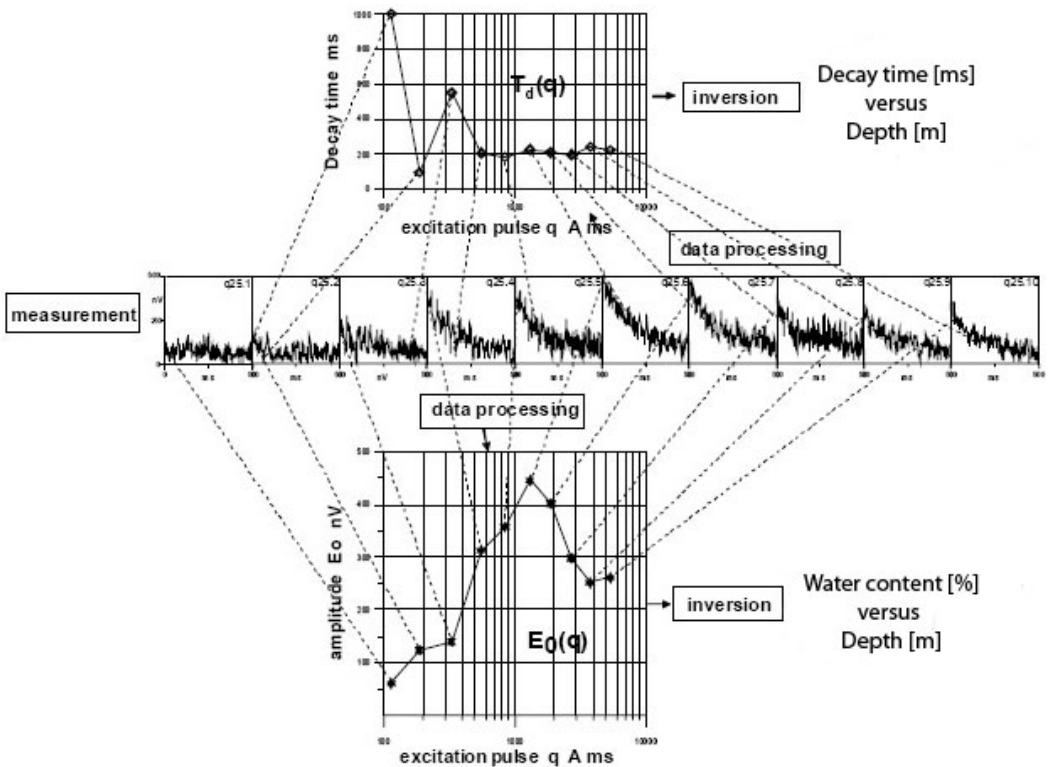
Fig. 3.12 Inversion of MRS data, (modified from Plata and Rubio, 2001). The initial amplitude (E_0) and decay time (T_2^*) for each curve e(t) is calculated, generating the functions of $E_0(q)$ and $T_2^*(q)$, where q denotes the pulse moment. Inversion of these functions returns the water content (θ_{MRS}) and T_2^* with depth (z).

3.4 Instruments and Fieldwork

The Numis$_{plus}$ equipment (Fig. 3.13) utilizes a DC/DC converter to increase the voltage from the 24 V parallel connected batteries to 400 V. This will generate pulses up to 4000 V and current intensities up to 600 A by the main unit (Bernard, 2007). The maximum current (I_0) that the equipment can transmit into the loop is given by ratio of the voltage (V) and the impedance (Z) of the loop

$$I_0 = V / Z \qquad (3.9)$$

with

$$Z = \sqrt{\left(R^2 + L^2\omega_L^2\right)} \qquad (3.11)$$

where $\omega_L = 2\pi f_L$ is the angular larmor frequency. R is the resistance and L is the inductance of the loop, respectively. In order to maximize the current (Iris instrument, 2005) the following conditions should be met

$$L \cdot C \cdot \omega_L^2 = 1 \qquad (3.12)$$

where the capacitance (C) is tuned by the capacitors tuning unit to meet the criteria in Equation 3.12.

Before conducting a measurement a couple of tests must be conducted to ensure MRS compatibility; (1) The noise-level at the specific site must be measured with the accompanying noise analyzer. (2) The earth magnetic field measured with a proton magnetometer, should not vary more than ±20 nT within the loop (corresponding to ±1 Hz). When the fluctuations are greater than this the signal from the water can be difficult to detect, since the signal originate from multiple frequencies. The magnetic susceptibility of the surrounding sediments and rock should be as low as possible (3) as high magnetic susceptibility creates a non homogenous magnetic field.

When starting an acquisition, the choice of antenna and the static magnetic field is entered into the acquisition software, ProDiviner, which in turn returns the configuration of the tuning capacitors. The number of pulse moments is usually a compromise between resolution of the subsurface aquifer and acquisition time. Usually a 16 pulse moment measurement is a good compromise. When measuring in a new environment, a 5 pulse moment measurement could give an idea of the noise in the area and if water is detectable. The number of stackings and the optional notch filter is selected according
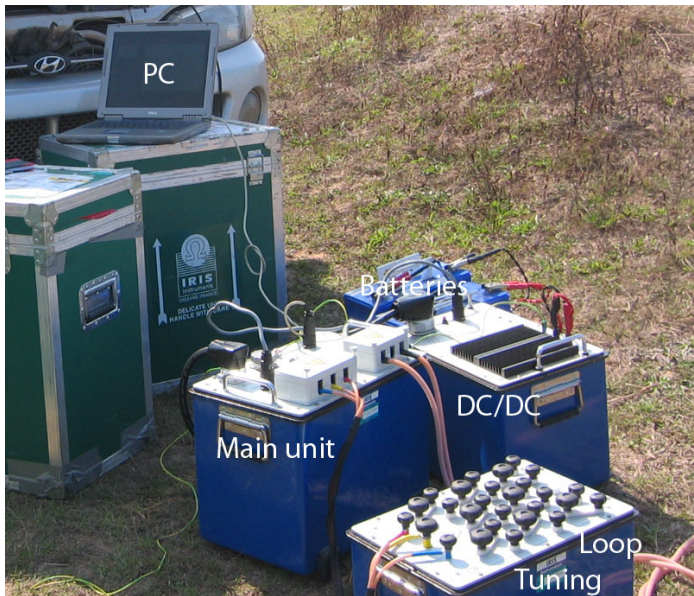
Fig. 3.13 Numis Plus equipment, consisting of a main unit, a DC/DC converter, a capacitor tuning unit, a PC, two batteries and 400 m of cable.

to the noise condition. The number of stacking can also be altered during measurement. Finally, signal and noise acquisition time can be changed from default (240 ms) if longer decay times are expected, but this will increase the duration of the sounding. For better permeability estimates, the longitudinal decay time (T_1) can be measured using a double pulse. This will increase the time of the sounding by 30% and require more power from the batteries. Normally, it is possible to achieve 2 soundings a day.

The main criteria to confirm that the signal measured is actually reflecting water (Fig. 3.14) are: (1) the stacked signal should be on top of the noise and (2) decaying; (3) The frequency of the signal should be ±1Hz from the transmitted excitation frequency. The Numis system has an instrument noise (IN), which can be stacked down to 3-5 nV. Signal to Noise ratio (S/N) should be >2 for a reliable quantitative interpretation (Legchenko, 2006), which means that the lower threshold for detecting and quantitatively interpret a signal is 10 nV. If the S/N=1 and ratio of external noise (EN) to instrument noise equals one (EN/IN=1), the quality of the sounding is good, although no signal is obtained and the only conclusion is that the volume of free water in the subsurface is smaller than the threshold of the instrument. If EN/IN>1 and S/N=1, the sounding is of bad quality and the only conclusion is that the signal is lower than the noise level. Furthermore, a smooth transition of phase and frequency insures that the data are of good quality (Fig. 3.3b).
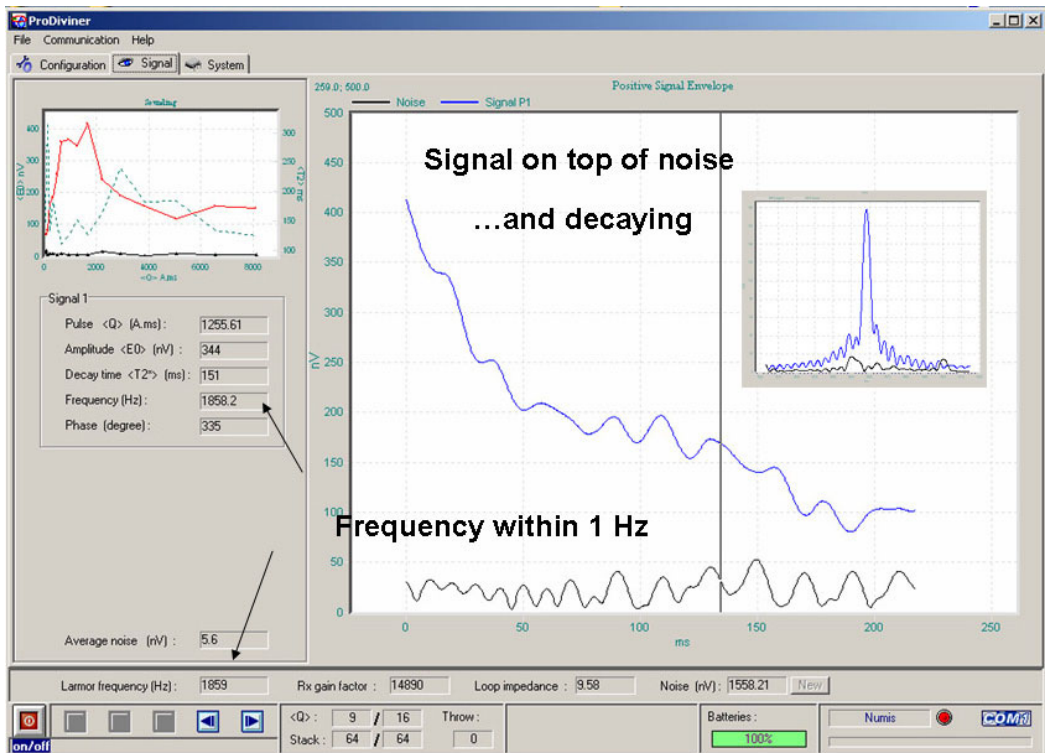
Fig. 3.14 Criteria for validating a MRS signal. The stacked signal should be on top of the noise (1) and decaying (2). The frequency of the received signal should not differ more than ±1 Hz (3) from the transmitted frequency.

3.5 MRS Related to Hydrogeological Parameters

The occurrence and movement of groundwater depends on the subsurface characteristics, like lithology, texture and structure. An aquifer is a geological formation that contains sufficient amount of water and permeable material to yield a significant amount of water to wells or springs. Geological formations that serve as aquifers are gravel and sand deposits, fractured granite etc. Aquifers can be either unconfined (Fig. 3.15a) or confined (Fig. 3.15b). In unconfined aquifers the water table is in direct contact with the air of the unsaturated zone and is hence at atmospheric pressure. A confined aquifer is overlain by a confining layer, usually clay, where the water pressure is higher than the atmospheric pressure. The piezometric surface is here an imaginary surface for which water would rise if a well was drilled into the aquifer.

3.5.1. Classification of Groundwater

Subsurface water can be divided into two zones. In the saturated zone, the pores are completely filled with water. In the unsaturated zone, the voids contain a mixture of water, moisture and air (Fig. 3.16). The part of the water that is attached to the grain walls due to molecular forces is called bound water (θ_b). The remaining
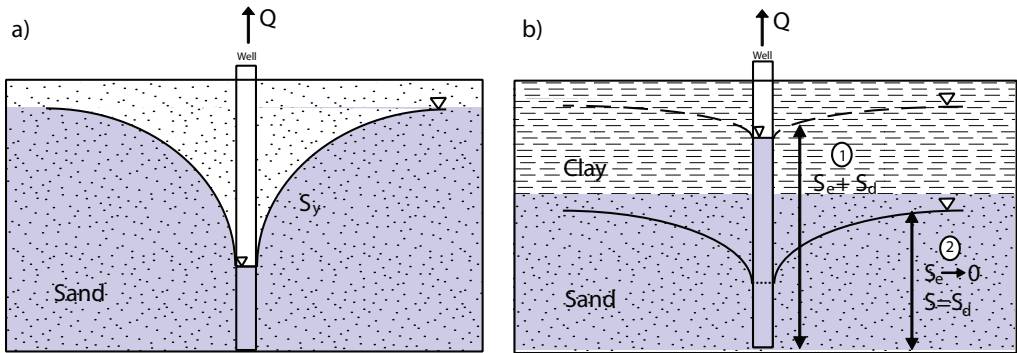
Fig. 3.15 a) In an unconfined aquifer the water table is in direct contact with the atmospheric pressure and the amount of extractable water due to gravitation is given by the specific yield (S_y). b) In a confined aquifer, the water pressure is higher than the atmospheric pressure and the extractable water (1) is partly released due to gravitation given by the specific drainage (S_d) and partly due to the compressibility of the aquifer represented by the elastic storage (S_e). When the water level reaches below the confining layer (2) $S_e \rightarrow 0$.
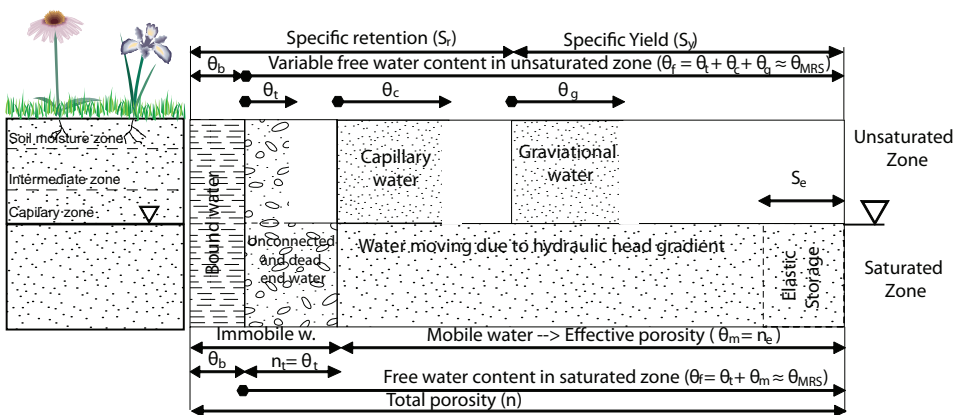
Fig. 3.16 Aquifer storage concepts in the unsaturated and the saturated zone (modified from Lubczyniski and Roy, 2005; Sen, 1995)

part is called free water (θ_f). The unsaturated zone can further be divided into three different zones. The soil moisture zone (1) which differs in thickness depending on soil type and climate is the top layer. The movement of water can be either upwards or downwards depending on suction or gravity. In the intermediate zone (2), water is held due to intermolecular forces against the pull of gravity (θ_g). The capillarity zone (3) is located above the water table and the water here is held by the capillarity forces (θ_c) acting against gravity (Sen, 1995). In the saturated zone water can either be trapped (θ_t) or mobile water (θ_m). MRS (θ_{MRS}) is believed to only measure θ_f, since θ_b with its short decay time is undetectable with current instrument limitation (40 ms dead time). This implies that in the saturated zone:

$$\theta_{MRS} \approx \theta_f = \theta_m + \theta_t = \eta - \theta_b \qquad (3.13)$$

where η is the total porosity, and in the unsaturated zone:

$$\theta_{MRS} \approx \theta_f = \theta_t + \theta_c + \theta_g < \eta - \theta_b \qquad (3.14)$$

The total porosity (η) is a measure of voids in the rock formation. It is defined as the ratio between pore volume V_{pore} and total volume V. Porosity is of two types. Primary porosity is governed from the rock formation and secondary porosity is developed through weathering (Sen, 1995). In the saturated zone η corresponds to the volume of free water (θ_f) and bound water (θ_b). In a coarse grained aquifer, θ_b tends be negligible, and hence $\eta \approx \theta_f \approx \theta_{MRS}$. Since some voids are unconnected or trapped (θ_t) preventing fluid flow, a more useful term for hydrogeological applications is the effective porosity (η_e), which only includes the porosity available for transportation of liquids. It is defined as the difference between η and θ_t, where θ_t does not contribute to the water flow but still contributes to the measured θ_{MRS}. However, in a rock formation where θ_t can be neglected, $\theta_{MRS} \approx \eta_e$.

3.5.2 Storage Related Parameters

The total porosity (η) and the free water (θ_f) are not good measures of the extractable water from the aquifer, since some part of the water can be bound or trapped. Effective porosity (η_e) is more

related to this concept but lacks good methods for determination. The ability of an aquifer to store water is called storativity. It is defined as the volume of water which a vertical column of the aquifer of unit cross-sectional area releases from storage as the average head within this column declines by a unit distance. In unconfined aquifers the specific yield, S_y is defined as the volume fraction of water that is drainable due to gravity forces (Fig. 3.15a). In the same way, water held by molecular and surface tension forces is called specific retention, S_r. Together they form the total porosity. Assuming, $\theta_{MRS} \approx \eta$, S_y can be approximately estimated for unconfined aquifers

$$S_y = \theta_{MRS} - S_R \qquad (3.15)$$

where S_R is the specific retention which can be determined from other methods (Lubczynski and Roy, 2003). Vouillamoz et al., (2006) proposed that S_y could be determined from $S_y = C_y * \theta_{MRS}$, where C_y is a proportionality factor determined from comparing S_y and θ_{MRS} from pumping tests and MRS, respectively.

In confined aquifers, where the potentiometric surface remain above the bottom of the groundwater table (1) the storativity depends on the elastic storage (S_e) (Fig. 3.15b), which is the water that can be released due to the compressibility of the rock matrix and the pore water. When the potentiometric surface falls below the bottom of the confining layer, creating local unconfined conditions, water is released due to gravity forces (2), according to the specific drainage (S_d)

In confined aquifers, again assuming $\theta_{MRS} \approx \eta$, the elastic storage ($S_e$) can be calculated from

$$S_e = \rho g(\alpha + \theta_{MRS}\beta) \cdot \Delta z = S_s \cdot \Delta z \qquad (3.16)$$

where S_s is the specific storage (aquifer specific coefficient), ρ is the density of water, g the gravity the acceleration, α and β compressibility of the aquifer and water respectively, which can all be estimated from tabled data or other methods. Δz is the water layer thickness determined with MRS. The S_d is determined in the same manner as S_y.

The hydrostatic column (H_w) [m³/m²] gives a direct volumetric estimate of the free water content with depth. Although, not widely used, this is the most reliable MRS parameter since it is insensitive to equivalence. It can be estimated for the targeted aquifer of the arbitrary depth intervals, e.g. maximum MRS investigation depth (Lubczynski and Roy, 2003).

$$H_W = \theta_{MRS} \cdot \Delta z \qquad (3.17)$$

3.5.3. Hydraulic Conductivity and Transmissivity

Permeability (k) is a measure of the ability for a rock formation to transmit fluids and is governed from Darcy's law (Darcy, 1856). It is defined as the amount of water (Q) that will flow through a unit cross section area (A) under a unit gradient of hydraulic head ($\Delta h/\Delta l$) (Fig. 3.17).
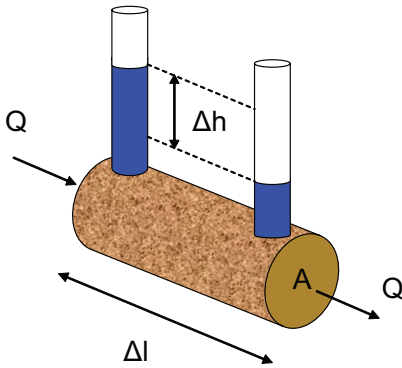
Fig. 3.17 Hydraulic flow through a cylinder, illustrating the terms in the Darcy equation. A=cross section area, $\Delta h/\Delta l$ the hydraulic gradient, and Q the flow rate.

$$k = -\frac{Q * \Delta l}{A * \Delta h}; \left[L^2 \right] \qquad (3.18)$$

Hydraulic conductivity (K) is a measure of the ability of the medium to transmit water. It depends not only on soil/rock characteristics but on fluid properties described below

$$K = k \left(\frac{\rho g}{\mu} \right); \left[L/T \right] \qquad (3.19)$$

where μ is the dynamic viscosity and ρ is the density of the fluid, g is the acceleration of gravity.

Transmissivity is the ability of the aquifer to transmit water. It is defined as product of the average hydraulic conductivity (K) and the saturated thickness of the aquifer (Δz)

$$T = K \cdot \Delta z \qquad (3.20)$$

There is a direct relation between the decay time ($T_{1,2}$) and k and it has been found from Nuclear Magnetic Resonance (NMR) logging that

$$k = C_p \cdot \theta_{NMR}^a \cdot T_{1,2}^b \qquad (3.21)$$

Several different values for the parameters a and b have been suggested. Among other Kenyon (1989) proposed a=4 and b=2, which has proven to be particularly suitable for sandstone media, whereas Seevers (1966) proposed a=1 and b=2, which proved to correlate better with secondary porosity media like diorite, gneiss and karstic limestone (Legchenko et al., 2002). The constant C_p, depends on the surface relaxivity of the mineral grains in rock matrix and is highly site specific. This means that NMR or MRS must be correlated to hydraulic data for a precise estimation of permeability. In large scale measurement, it is more accurate to estimate the aquifer transmissivity. MRS is correlated to pumping test data, for which:

$$T_{MRS} = C_T \sum_{i=1}^{n} \left(\Delta z_{MRS} \theta_{MRS}^a \cdot T *_{1,2}^b \right) \qquad (3.22)$$

where C_T is an area specific constant derived from pumping test transmissivity T_P:

$$C_T = \sum_{i=1}^{n} T_{P\_i} / \sum_{i=1}^{n} \Delta z_{MRS} \theta_{MRS}^a \cdot T *_{1,2}^b \qquad (3.23)$$

Using T_1, with a=1 and b=2 has proved to correlate best with pumping test transmissivity. If only T_2* has been measured a better correlation is gained from a= 4 and b=2 (Vouillamoz et al., 2007)

4. Vertical Electrical Sounding (VES)

The DC resistivity method has its origin in the 1920's work of the Schlumberger brothers and has been used for many decades in hydrogeological, mining, geotechnical and environmental investigations.

4.1 Theory of Method

Resistivity (ρ) [ohm-m] is a bulk property of a material and describes how well that material inhibits current flow and should not be confused with the term resistance (R) (Fig. 4.1). The inverse of resistivity is called conductivity, σ [S/m] and is also used in geophysical literature. The purpose of Vertical Electrical Soundings (VES) is to determine the variations in resistivity with depth. VES measurements are carried out by injecting current into the ground through two current electrodes (A and B) and then measure the resultant potential difference (ΔV) between two potential electrodes (M and N) (Fig. 4.2).

$$R = \rho \frac{l}{A}$$
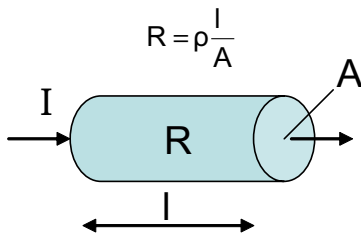
Fig. 4.1 The resistance (R) for a cylinder with the resistivity (ρ), where A is the cross section area and *l* is the length of the cylinder.
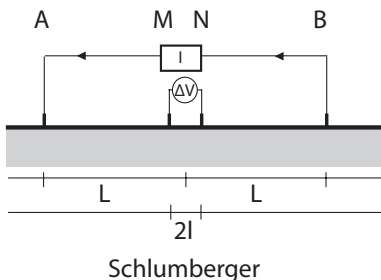
Schlumberger

Fig. 4.2 Outline of a Schlumberger array for Vertical Electrical Soundings (VES). A and B are current electrodes and M and N are potential electrodes.

The centre point of the electrode array remains fixed but the spacing of the electrodes is increased and information from deeper sections of the subsurface can be retrieved. Different types of electrode configurations are used, depending on the type of investigation, field condition and the sensitivity of the resistivity meter. This study has been carried out using a Schlumberger array.

4.1.1. Resistivity Measurement

The electric current flow (I) in a unit cylinder (Fig. 4.1), with the length *l*, cross-section A, is given by Ohm's law:

$$I = -\Delta V / R \tag{4.1}$$

where ΔV (volt) is the potential difference between the ends of a conductor and R (ohm) is the resistance of the conductor. The negative sign indicates that the current flow goes from high to low potential. R is directly proportional to the length (l) of the conductor and inversely proportional to the cross-section (A), which leads to

$$R = \rho \frac{l}{A} \tag{4.2}$$

where ρ (Ω-m) is the resistivity. Equation 4.1 and 4.2 results in

$$\frac{I}{A} = -\frac{1}{\rho} * \frac{\Delta V}{l} \tag{4.3}$$

Where l/A is equal to the current density j (Am⁻¹) and $\Delta V/l$ is equal to electric field E (Vm⁻¹).

In a homogeneous, isotropic half-space the current spreads radially through a hemisphere of equipotentials (Fig. 4.3), and the current density can hence be determined by

$$j = \frac{I}{2\pi r^2} \tag{4.4}$$

Using Equation 4.4 the potential drop dV across a shell dr at the distance r from the point current source is shown to be

$$dV = -\frac{I * \rho * dr}{2\pi r^2} \tag{4.5}$$

a)

b)
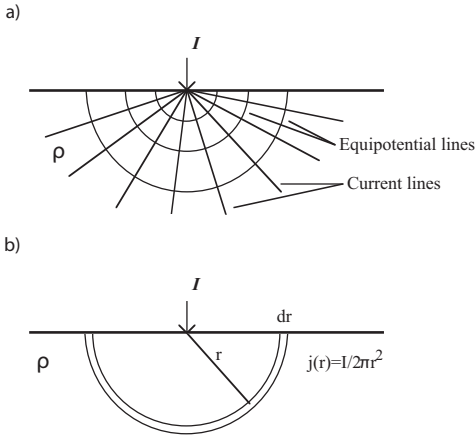
Fig. 4.3 a) Distribution of the current flow in a homogenous halfspace. b) Geometry for calculation of the potential (V) at the distance r.

The potential is assumed to be zero at an infinitive distance from the current electrode and integrating, the potential V at a distance r from the current source, is given by

$$V = \frac{-I\rho}{2\pi r} \qquad (4.6)$$

In practice it is necessary to use four electrodes. Two current electrodes (A and B) and two potential electrodes (M and N), the resistivity is then calculated from the measured potential difference

$$\Delta V = V_M - V_N \qquad (4.7)$$

where

$$V_M = \frac{\rho \cdot I}{2\pi} \left(\frac{1}{AM} - \frac{1}{BM} \right) \qquad (4.8)$$

$$V_N = \frac{\rho \cdot I}{2\pi} \left(\frac{1}{AN} - \frac{1}{BN} \right) \qquad (4.9)$$

thus

$$\Delta V = \frac{\rho \cdot I}{2\pi} \left(\frac{1}{AM} - \frac{1}{BM} - \frac{1}{AN} + \frac{1}{BN} \right) \quad (4.10)$$

where AM, BM, AN and BN represents the geometrical distances between the different electrodes and is together called the geometric factor, K. The resistivity is then given by

$$\rho = 2\pi * \frac{\Delta V}{I} * K \qquad (4.11)$$

4.1.2. Apparent Resistivity

Equation 4.11 is only true for a homogenous earth. In reality, the ρ varies with different resistivities at different depths in the subsurface and also different electrode configurations, thus, Equation 4.11 yields the apparent resistivity ρ_a and can be considered to be some kind of average of the different subsurface resistivities. To determine the true subsurface resistivity, an inversion of the measured apparent resistivity values must be carried out.

4.2. Data Processing

When interpreting VES-data the simplification of an infinite layer earth model is used.
The data from this study were interpreted with the inversion software RESIST87 (Velpen, 1988), by the use of linear filters. The apparent resistivity (ρ_a) of a layered earth can be expressed by

$$\rho_a = \sum_{k_{MIN}}^{k_{MAX}} T(\lambda) f_k \qquad (4.12)$$

where $T(\lambda)$ is the resistivity transform and f_k represent the coefficient of a linear filter of Ghosh type, which have been calculated once and for all. A first guess is made of the number of layers, together with the corresponding thickness (T_i) and resistivity (ρ_i) for the different layers denoted by i. The calculated curve is then matched against the measured curve in an iterative process, where the model parameters are updated until a given error criteria is met (Parasnis, 1997; Sharma, 1997).

When geological borehole data is present, it can be used to constrain layer geometry. Some interpretation problems for VES can occur when mapping subsurface salinity, since resistivities for salt water, saturated clay and sand overlaps. Furthermore, due to the high resistivity contrasts between an often high resistive, dry top soil and a low resistive saline aquifer, interjacent freshwater layers with medium resistivities are difficult to detect on the sounding curve (Kirsch, 2006). These problems can be accounted for if using a first MRS model in the VES interpretation to identify and constrain water layers in the apparent resistivity curve (Vouillamoz et al, 2007).

4.3. VES Related to Water Quality and Hydrogeological Parameters

The resistivity varies greatly for different geological materials, as can be seen in Fig. 4.4. Most rocks and minerals are insulators in their dry state. However, in nature, they usually contain some water with different quantity of dissolved salts within their pores and cracks. The degree of interconnected and water filled pores together with the concentration of dissolved salts are major factors affecting the resistivity. The resistivity of fresh groundwater varies usually from 7-100 ohm-m, depending on the degree of salt. Seawater or saline water has resistivities down to 0.2 Ohm-m, which makes resistivity method the ideal technique to distinguish the interface between salt and fresh water. As can be seen from Fig. 4.4, the resistivity of of different earth materials is not exclusive, e.g. clay overlaps with both freshwater and brackish water.

The value of n and m depends mostly on the wettability and cementation, respectively. If the mineral grains are insulator, then a = 1, which is the main condition for Archie's formula. To a certain degree of decreasing resistivity of the mineral grains, the constant a decreases too (Worthington, 1993). If working in a geological environment without conducting grains (a = 1) and assuming that bound water, dead-end unconnected porosity is negligible, the MRS water content (θ_{MRS}) ≈ porosity (η), ρ is then deduced from VES resistivity and ρ_0 can be determined from the EC of water from the wells. Together they form the formation factor F= ρ/ρ_0. If the aquifer is assumed to be saturated (s=1), the cementation factor (m) for a specific geological material can be determined using regression analysis of the formation factor (F=ρ/ρ_0) and θ_{MRS} on a bilogarithmic cross plot, where m is the slope of the curve. Vouillamoz (2007) argue that in an environment where aquifers are not
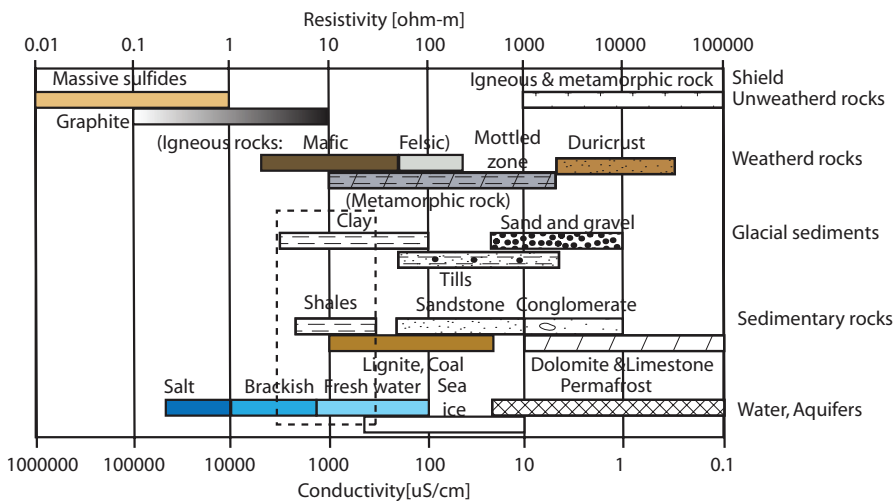
Fig. 4.4 Typical ranges of resistivities for different earth materials (modified from Palacky, 1987). Note the overlapping resistivities of clays, freshwater and brackish water indicated by the dotted rectangle.

The resistivity ρ, of a porous, water-bearing material, free of clay minerals can be expressed with Archie's law (Archie, 1942), which is an empirically determined formula that expresses the resistivity as a function of the water resistivity ρ_0, the porosity (η) and the water saturation s.

$$\rho = a \cdot \rho_0 \cdot \eta^{-m} \cdot s^{-n} \tag{4.13}$$

free of low resistive clayey material, a "rough estimator" for the water EC can still be made using a linear relationship between ρ determined from VES and water EC measured from water wells. Other approaches to describe current flow through porous media is described by Waxman and Smits, 1968; De Lima and Sharma, 1990; Johnson and Sen, 1988.

The conductivity of a fluid is strongly dependent on the concentration and mobility of ions, where mobility is highly temperature dependent. Conductivity of water is usually standardized at 25°C. When comparing EC of water with aquifer conductivity it is important to correct for the true temperature of the water. The conductivity of most groundwater varies with about 2% per °C (Clesceri et al. 1998).

Transverse resistance is also known as the Dar-Zarrouk variable (Maillet, 1947). It is defined for a specific layer as:

$$TR_i = \rho_i \cdot T_i \qquad (4.14)$$

Where T_i is the thickness for layer i. TR_i is free from the ambiguity of VES interpretation while T_i and ρ are subject to principle of equivalence. Attempts have been made to correlate TR with aquifer transmissivity (Niwas and Singhal , 1981; Ponzini et al, 1984; Salem, 1999), with good results in homogenous geological environment where aquifer resistivity is insensitive to variations in water conductivity (Niwas and Singhal , 1981)

Salinity is measured in Total Dissolved Solids (TDS), which is the total sum of cations and anions and the undissociated dissolved species after evaporation and filtration of a sample. TDS however, can also be determined by multiplying the electrical conductivity (EC) in µS/cm at 25°C with the TDS-factor (C_{TDS}) (usually between 0.55-0.90), which depends upon the types of salt present (Reynold and Richards, 1996).

$$TDS\,[mg/l] = C_{TDS} * EC \qquad (4.15)$$

TDS is often used for evaluating the water quality for domestic usage. TDS less than 600 mg/l is considered to be of good quality (Table 4.1).

Table 4.1 *Palatability of drinking water (WHO, 1996)*

Class	TDS (mg/l)
Excellent	<300
Good	300-600
Fair	600-900
Poor	900-1200
Unacceptable	>1200

The main source of cations and anions in groundwater is the slow dissolution of minerals in rocks, and soils when the groundwater moves through the strata (Reynolds and Richards, 1996). Shoeller (1959) identified three types of sources that contribute to the variation in chemical characteristics: (1) Variation in mineralogy of the aquifer; (2) Vertical and lateral variations in groundwater flow, i.e. increasing dissolution and hence more ions in solution along the path of the groundwater flow and (3) Difference in climatic factors like rainfall and evaporation, which results in groundwater in arid environments to generally be more saline than groundwater in humid regions.

The European drinking water standards (directive 80/778EEC) have for an acceptable quality suggested a level of no more than 400 µS/cm at 20°C for electrical conductivity (EC) and defines the upper limit of EC to 1500 µS/cm at 20°C (Brassington, 2007). The salt content is sometimes measured with reference to the level of chloride, which can also be directly related to EC. According to the Swedish National Food Administration, chloride concentrations >100 mg/l can have a corrosive effect on metal pipes and concentrations >300 mg/l can cause taste differences (SEPA, 2007). The major source of natural chloride in groundwater comes from dissolution of halite. Water with a high mineral content, primarily of Calcium (Ca^{2+}) and Magnesium (Mg^{2+}) ions, is considered as hard. Hardness of water is an important criterion for technical and esthetical reasons (Table 4.2), since hardness can produce a scale in hot water pipes, heaters and boilers. It also requires considerable amounts of soap before lather can be produced and it causes taste differences. Hard water can be expected in regions with large amounts of limestone ($CaCO_3$) or dolomite ($CaMg(CO_3)_2$) (Reynolds and Richards, 1996). Hardness of the water with its polyvalent ions directly contributes to conductivity (Krawczyk and Ford, 2007).

Table 4.2 *Hardness of water (Reynolds and Richards, 1996).*

Hardness [mg/l] as Ca-HCO$_3$	Degree of Hardness
1-75	Soft
75-150	Moderately soft
150-300	Hard
300 or more	Very hard

Total hardness (H_T) can be calculated from the Ca^{2+} and Mg^{2+} content in the water using the equation:

$$H_T\left[mg/l\,as\,CaCO_3\right] = \\ 2.497\left[Ca^{2+},mg/l\right]+4.118\left[Mg^{2+},mg/l\right]$$

(4.16)

as described in Standard Methods 2340 B (Clesceri et al. 1998).

5. Summary of Research

Three areas were selected for geophysical studies (Fig. 2.1), where MRS and VES measurements have been performed in 32 and 18 sites, respectively. The most important geophysical site characteristics have been summarized in Appendix A. Water chemistry data have been collected from 13 deep and 15 shallow wells in near vicinity of the measuring sites. The most important water quality parameters are summarized in Appendix B. MRS measurements have been carried out, depending on the noise, with a 100 m square loop or an 8 shaped loop, together with 64 to 100 stacks and notch filter when needed. The decay time (T_2*) values matching the highest water content in a water bearing layer have been used to characterize that specific aquifer. The grain size indicated by T_2* usually agrees well with borehole petrophysical information. VES measurements have been carried out using a Schlumberger configuration and $AB/2$ distances usually up to 200 m.

Examples of measurements from the sites 20, 19 and 22 are presented in Fig. 5.1. The Signal to noise (S/N) ratios for the different sites is presented in Appendix A. The general trend is that the inverted MRS data seems to fit the raw data quite well for low pulse moments but looses coherency for high pulse moments (Fig. 5.2). Regularizations between 300 and 700 usually results in a smooth aquifer model geometry, which corresponds quite well with the lithology mapped in adjacent boreholes. T_2* can vary significantly for different regularization (eg. Site19). VES measurements are generally of good quality with RMS varying between 2 and 6% (Fig. 5.2).

5.1 Identification and Characterization of Geological Structures

In area 1 (Figs. 2.1 and 5.3a), the K_2cp is the dominant formation in the western part of the basin, whereas N_2Q_{1-3} is dominant in the central part and the K_2tn in the eastern part. In the geological cross section FE (Long et al., 1986) (Fig. 5.3b) in area 1, the different characteristics of the N_2Q_{1-3} and the K_2tn (see also Paper I) are illustrated. The N_2Q_{1-3} holds in most parts coarser materials like sand and gravel but also comprises finer sediments like clay and silt. K_2tn on the other hand, contain materials such as clay and breccia overlying rock salt, all with poor potential for hosting aquifers. MRS usually identifies one shallow and one deep aquifer in the N_2Q_{1-3} (e.g. Site 31, Fig. 5.3c). The deep, main aquifer generally starts at around 10 to 15 m depth with maximum water content at around 20 to 25 m and the aquifer floor positioned from 30 to 50 m depth. The maximum water content varies between 4 and 12%, but is usually about 6 to 8 %. The T_2* -values range from 100 ms (Site 24, and 31) to 300 ms (Site 3) corresponding to medium to coarse sand and gravel sands. The resistivity for these water layers ranges between 20 and 600 ohm-m. The K_2tn is located below the N_2Q_{1-3} with the exception for the south-eastern part where it is found from the surface and down. It is characterized by very low water contents and resistivities lower than 5 ohm-m (Site 31 and 24; Figs. 5.3c and d). Area 2 includes the sites 5 to 11 and has similar MRS and VES characteristics as those in Area 1 (see Paper I). The aquifer floor is usually situated at depth of 20 to 30 m.

The knowledge of the depth to the halite layers is very important hence the shallower they are situated the greater the risk of increased salinity in the groundwater. Fig. 5.4 illustrate the distribution of MRS and VES measuring points and borehole data in area 1 together with an interpolated map of halite depths (Long et al, 1986) and the Bouguer gravity anomaly map (Na Wetcharin, 2007). Rock salt can here be found as shallow as at 52 m depth. With reference to the clay layer deposited on top of the halite layer, the depth to the halite is also an estimate of the maximum depth of the aquifer, which is defined by MRS. The gravity
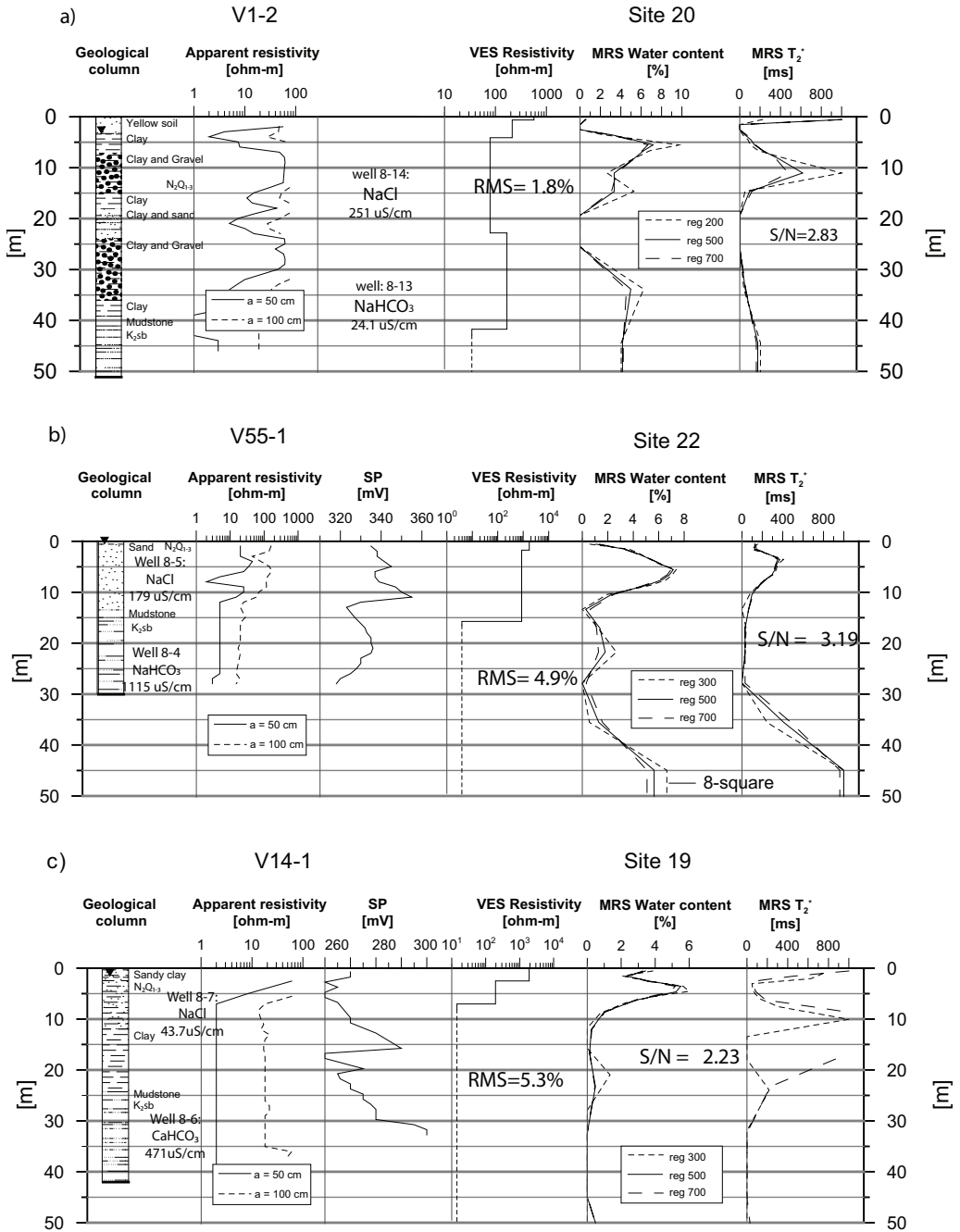
Fig. 5.1 MRS models illustrating the effect of regularization and VES models together with borehole data in area 3 from a) Site 20, b) Site 19 and c) Site 22.
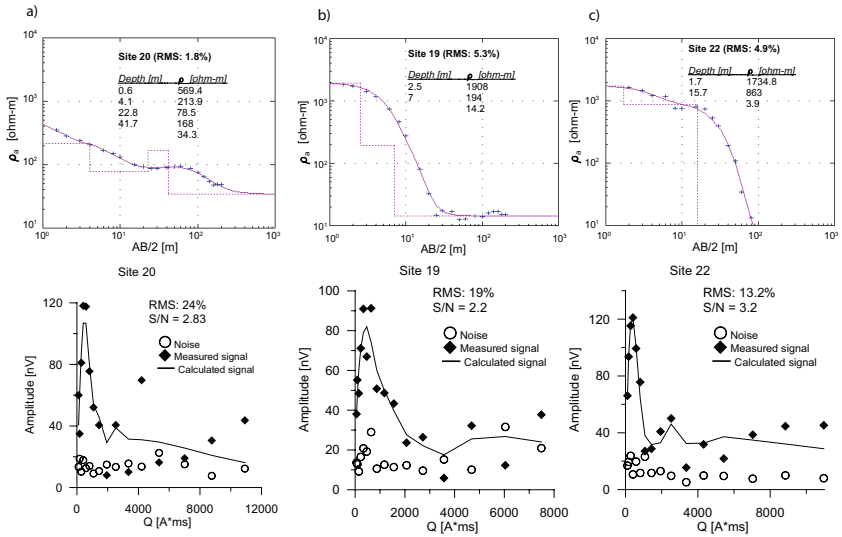
Fig. 5.2 VES and MRS raw data and model from a) Site 20, b) Site 19 and c) Site 22. Note the poor fit on the MRS model for high pulse moment with low initial amplitudes.
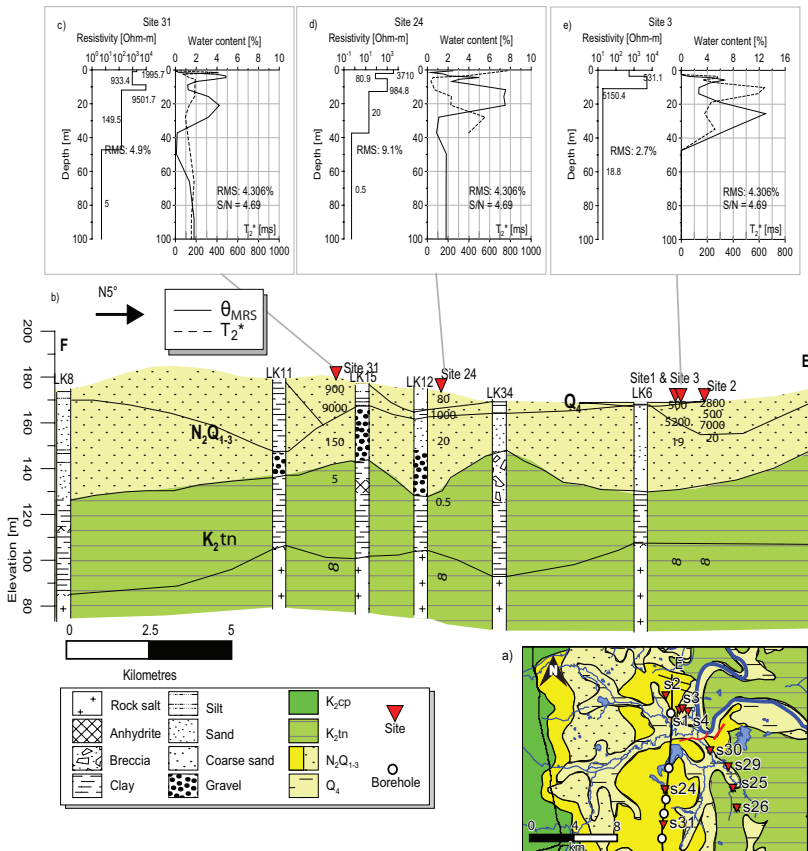
Fig. 5.3 a) Geological map of Area 1, illustrating the relative position of sites and boreholes along the profile. b) Modified geological cross sections EF (profile 2) after Long et al. (1986). Inverted MRS data presenting θ_{MRS} and T_2^* together with the VES result from c) site 31, d) site 24 and e) site 3.

anomaly map shows that the regional gravity field generally decreases from west to east. However, there is a local maximum, which correlates well with the shallow halite depths. This is probably an indication of an uplift of the higher density basement rock, where the upper part of K_2tn has undergone erosion and been replaced by younger sediments of N_2Q_{1-3}. This supports a shallower halite layer here as compared with the eastern part of the area. The shape of the halite structure is difficult to determine due to the sparse gravity data.

(Fig. 5.5c) and MRS (Fig. 5.5d) data collected in this study, illustrates the geophysical soil and rock characteristics of the area. The stratigraphic unit, N_2Q_{1-3} comprises two water bearing layers (Site 20 and Site 16) in the western part with a thickness of up 40 m, which transcends to one thinner layer, with significantly lower water content in the middle of the cross section. The maximum water content is varying between 4 and 16%, and the T_2* generally varies between 100 and 400 ms, with longer T_2* in the western part of the basin. The resistivity for the main water
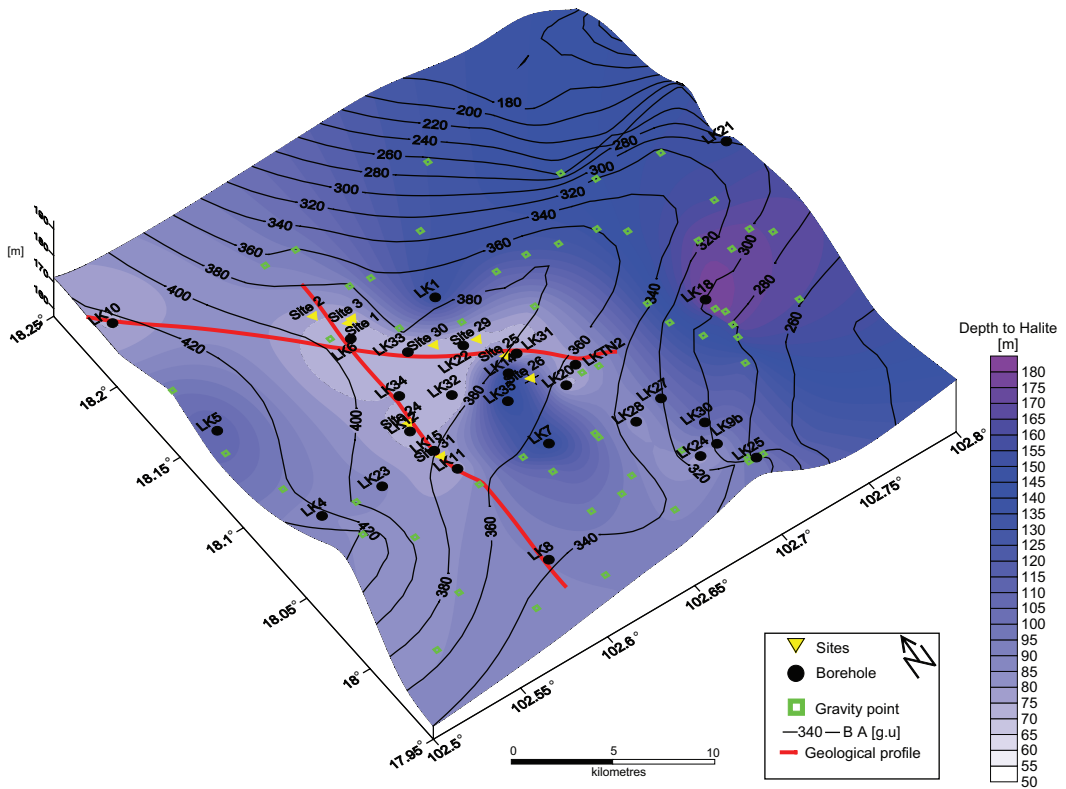
Fig. 5.4 Interpolated map of the depths down to the halite layer obtained from borehole data (Long et al., 1986) in the southern part of the Vientiane basin (see Fig. 2.2) together with gravity data collected by Na Wetcharin (2007). The depths agree well with MRS and VES interpreted depths from area 1.

The area 3 is located in the narrowing upper part of the Vientiane Basin (Figs. 2.1 and 5.5a) with the K_2cp in the western and eastern border of the basin, the K_2tn in the north and N_2Q_{1-3} in the central part. The geological cross section GH (Fig. 5.5b) compiled from lithology borehole data (JICA, 1994), shown together with VES

bearing layer varies considerably from site to site but usually ranges between 10 to 250 ohm-m. In the eastern part, the composition of the N_2Q_{1-3} changes to more clayey material and the water content is lower than 4% and T_2* lower than 100 ms. The K_2sb underlying N_2Q_{1-3}, consists of mudstone or siltstone (Fig. 5.5b). It has a fairly

low water content (<2%), and T_2* around 50 to 200 ms. The resistivity varies between 10 to 25 ohm-m (e.g. site 23). Rocks from the K_2tn has not been observed in any boreholes here, but VES measurement from the sites 15, 16 in the middle of the basin, show resistivities (< 5 ohm-m) that may indicate the existence of this formation as characterized in area 1.

Rock salt has a relatively high resistivity compared to the overlaying materials (ρ=1.1*10[6] ohm-m; Paper I), but it would be difficult to identify it with VES since the current probably will not be able to penetrate through the superimposed conductive clay. However, the low resistive clay layer, sometimes lower than 1 ohm-m, could work as an indicator of halite
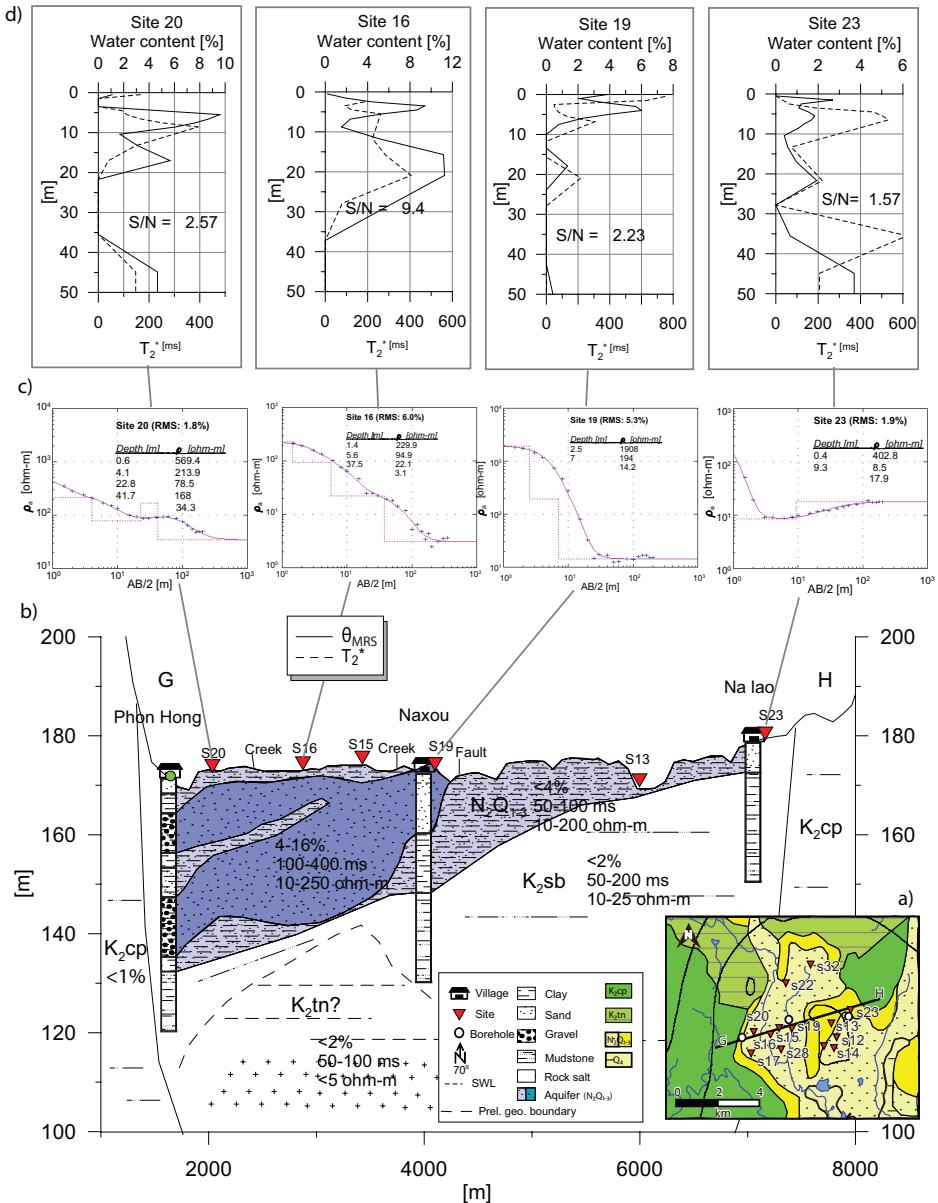
Fig. 5.5 a) Geological map of area 3 showing the locations of measuring sites together with boreholes relative the profile GH. b) The cross section GH summarizes existing geological information from borehole data, water content, T_2* and resistivity based on the geophysical measurement with c) VES models and d) θ_{MRS} and T_2* models from site 20, site 16, site 19 and site 23.

or at least an indicator of the Thangon formation (K_2tn). These low resistivities can be found in all three areas at depths of 20 to 50 m, and they are always related with very low water contents. Table 5.1 roughly summarizes the geophysical characteristics obtained in our study for some of the geological formations and stratigraphic units in the region.

gradient, with the length of the arrows denoting the gradient amplitudes correlates well with increasing T_{MRS} and H_w in the western part. Transverse resistance (TR) has been calculated for the main aquifer layer in area 3 (Equation 4.14) and compared to T_{MRS} with a best fit (R^2=0.41) obtained using TR=644.63*$T_{MRS}^{0.3591}$ (Paper I). Transverse resistance is probably not a good

Table 5.1 *A rough summery of typical geophysical parameter like water content (θ_{MRS}), decay time (T_2^*) and resistivity (ρ) for different water bearing units in the Vientiane basin.*

Formation	Rock Material	θ_{MRS} [%]	T_2^* [ms]	ρ [ohm-m]	Comment
Q_4	Sand			450 - 4500	Dry top layer, with a thickness of ca 0.5 m
	Silt				
N_2Q_{1-3}	Silt				Main aquifer in the area, usually between 10 and 50 m thick, with highly varying water content.
	Sand	4-16	100 - 400	10-250	
	Coarse Sand				
	Gravel				
K_2sb	Claystone	<2	100	10-25	Impervious layer with little or no water. Mostly found in area 2 and 3.
	Siltstone				
K_2tn	Breccia	1 - 2.5		0.5 - 8	Impervious layer with little or no water. Find throughout the whole study area. Lower resistivity and water content than K_2sb.
	Clay			0.3 - 0.6	
	Anhydrite				
	Halite			10^6	
K_2cp	Sandstone	<1			Little or no water. Mostly found in outer border of the basin

5.2 MRS and VES Related to Hydrogeological Parameters

The hydrostatic column (H_w) has been estimated from the MRS (Equation 3.17) for different sites (Appendix A), and gives a direct volumetric estimate of the free water content of the aquifer within N_2Q_{1-3}. This is the most reliable MRS parameter since it is insensitive to equivalence. MRS Transmissivity (T_{MRS}) has also been determined using Equation 3.22 for the aquifer of N_2Q_{1-3} at different sites (Appendix A) where the site specific constant C_T= 1.81*10^{-13} (Equation 3.23; Paper I) is derived from MRS data from site 17 and 20 and pumping test transmissivity from well 8-13. Interpolated maps of H_w values (Fig. 5.6a) and T_{MRS} values (Fig. 5.6b) from area 3 illustrates that high T_{MRS} and H_w values are found in the western part where N_2Q_{1-3} is thick. The transgression to low T_{MRS} and H_w values are found within the thin sediments deposited on top of the K_2sb in the eastern part. The topographic

parameter to determine aquifer transmissivity in the Vientiane Basin, since the aquifer resistivity differs a lot from one site to another. Specific yield (S_y) and specific storage (S_s) have been estimated using Equation 3.15 and 3.16, respectively. The vertical compressibility (α) and specific retention (S_R) have been estimated from tabled values for different kinds of sediments indicated by T_2^* (Paper 1; Table 1). S_y varies between 3 and 13% (S_r = 3) and S_s is roughly estimated to around 10^{-4} for coarse grained aquifers. These values corresponds quite well to area specific values obtained in Thailand, S_y = 0.15 and S_s = 2 to 3*10^{-3} (Srisuk et al., 1999), although α and S_R varies significantly for the same type of sediments.
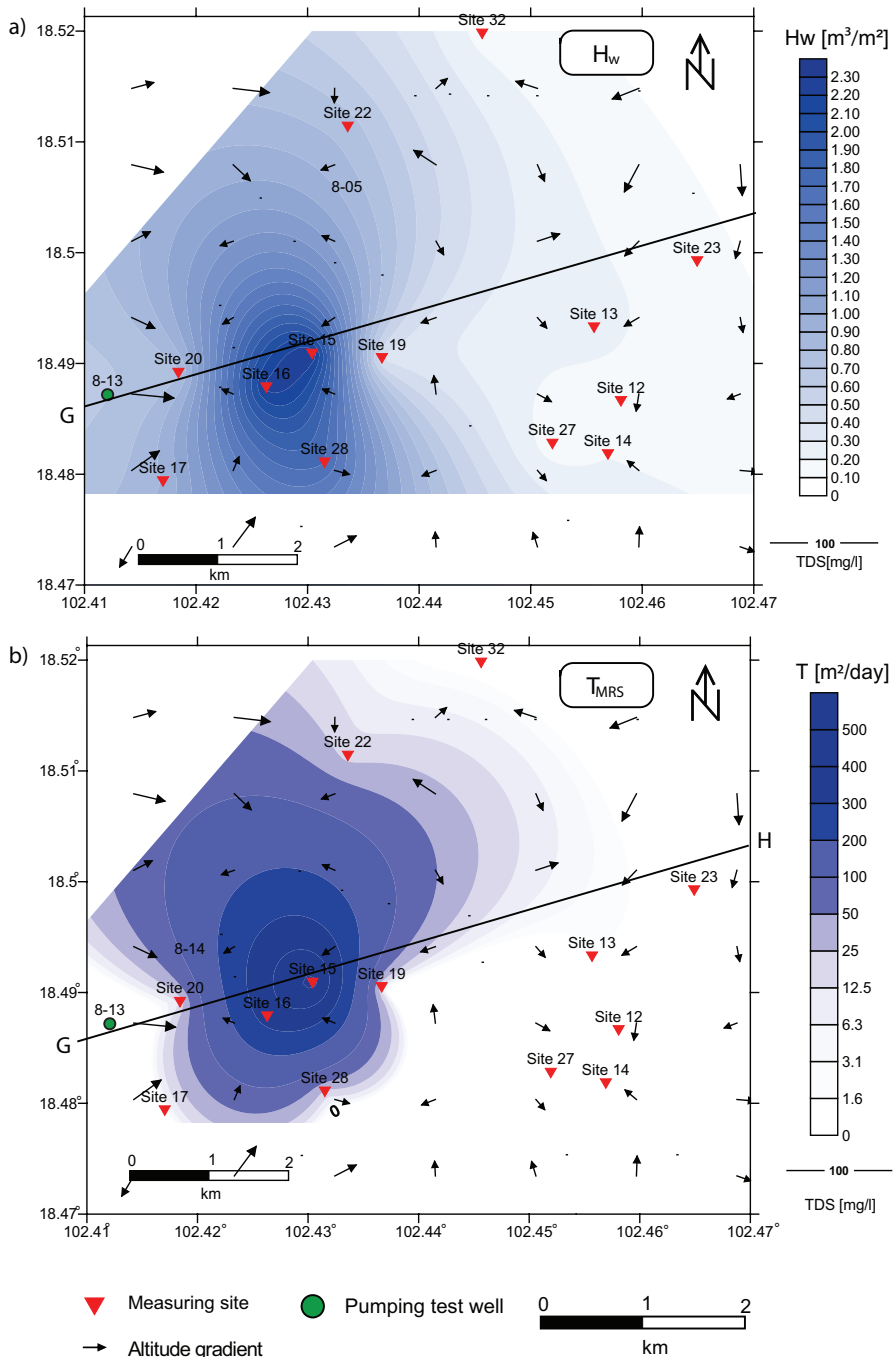
Fig. 5.6 Interpolated maps of a) H_w and b) T_{MRS} values in area 3. T_{MRS} and H_w values are high in the western part of the map and decreases towards east. The topographic gradient, expressed by the arrows, where the length denotes gradient amplitude, correlates well with T_{MRS} and H_w in the western part of the basin. The full drawn line refers to the cross section GH in Fig 8b.

5.3 Estimation of Water Conductivity from Geophysical data

The measured water EC (25°C) corrected for temperature has been compared to the modelled VES conductivity. The best fit is obtained using EC[μS/cm]= 0.3821VES[μS/cm], R^2=0.81 for water from deep wells (Fig. 5.7a), although the data is quite scattered. A good fit is also achieved with the double squared method: EC[μS/cm]= $\sqrt{(17972,8 + 0,16538*VES[\mu S/cm]^2)}$, R^2=0.78. For shallow wells the coefficient of determination is very low (R^2<0.1). This is because the data is very scattered for low VES conductivity (<200 μS/cm or >50 ohm-m) (Fig. 5.7b). The often higher water conductivity in deeper wells, probably contribute more to the VES conductivity. Shallow wells (shallow aquifer) are also more vulnerable to local anthropogenic activities whereas deeper wells (deeper aquifer) are more homogenous. This model does not take the aquifer material into consideration. In a recharge area, composed of fine grained material with soluble minerals, one could expect the water to have more dissolved solids, than in a recharge area containing coarser, less soluble material (Back and Hanshaw, 1966). Waxman and Smits (1968) provided a model for electric current flow in porous media, where one part of the current is conveyed through the pore water, and the other part is associated with the electrical double layer (i.e. clay), and the total resistivity is the sum of the two. Analogous to this, it should be possible to roughly estimate the contribution from the finer sediments/clay using the petrophysical information from T_2*. The EC-estimator for deep wells would then transform to *EC[μS/cm]= 0,345*VES[μS/cm]- 0,221* T_2*[ms]*, with an unchanged R^2 of 0.81 using the least squares method. Since, the P-value = 0.76 > 0.05 (operating at the 0.05 significance level) for T_2*, there is no indication of serial autocorrelation and T_2* should be removed from the model. This implies that the conductivity of the deeper aquifer is more controlled by the conductivity of water than by the aquifer material, but also that T_2* is probably not a good parameter to estimate the conductivity contribution from finer sediments. The cementation factor (*m*) for different grain sizes indicated by the decay time from MRS (Paper II; Table 6), has been determined from Archie's law (Equation 4.13) with poor results. This is because high conductive sediments are present in the N_2Q_{1-3}, which invalids Archie's law. Moreover, the porosity estimation from MRS water content (θ_{MRS}) is probably underestimated, since MRS can not detect bound water in finer sediments.
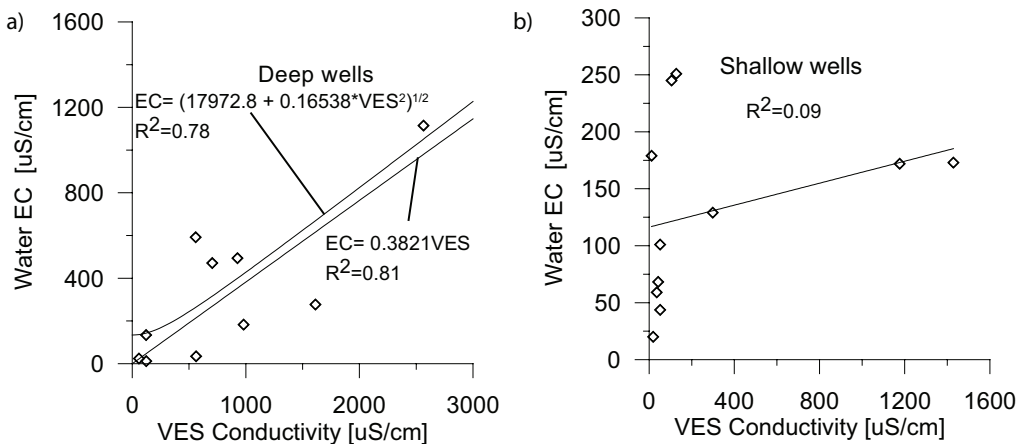
Fig. 5.7 a) Conductivity of aquifers (VES) against water EC from a) deep and b) shallow wells. The best fit for deep wells is obtained using EC[μS/cm]= 0.3821VES[μS/cm] , R^2=0.81. For shallow wells the R^2 <0.1, and the data is very scattered for low aquifer conductivity.

5.3.1 Water Quality Parameters Related to Water Conductivity

Water sample for chemical analysis were collected in January 2007 and 2008, from altogether 15 shallow and 13 deep wells (4 wells in area 1, 7 wells in area 2 and 17 wells in area 3). Chemical analysis for the most common ions together with EC, TDS and alkalinity was made by the Department of Irrigation in Vientiane.

With reference to the analyzed TDS values (Appendix B), the groundwater from most wells can be classified of excellent quality (<300 mg/l) or at least of good quality (<600 mg/l) according to WHO's international standard. Neither, does any water samples exceed the limit of electrical conductivity (EC>1500 µS/cm) for unacceptable quality according to the European water quality standard (directive 80/778EEC). Chloride concentrations are also generally low. Only one sample exceeds the risk of pipe corrosion (>100 mg/l; well 8-4) according to SEPA, and no sample exceeds the limits of taste effects (>300 mg/l, SEPA or >250 mg/l, WHO) (Paper II).

The correlation matrix, including all 28 sampled wells for 9 variables is presented in Table 5.2, where each cell provides the correlation coefficient for two sets of analytes.

that the chloride concentration can be directly related to halite. Magnesium and calcium show a strong positive correlation to one another and to alkalinity.

The analyzed TDS-factor determined from Equation 4.15 has an average value of $C_{TDS} \approx 0.5$ and is constant in all the three areas (Appendix B).

Salt (NaCl) from the salt factory of Ban Bo has been diluted using de-ionized water and then measured in the laboratory at Luleå University of Technology for EC for a wide range of concentrations. This analyze show an almost perfect linear fit (EC = 2.5841*Cl⁻; R^2=0.998). Chloride concentrations from water samples in different wells in the three areas are here plotted against EC (Fig. 5.8). The EC of the chloride concentrations is quite scattered and exceeds the EC of the diluted chloride graph defined here, which could be explained by other ions contributing to the EC. However, the gradient of the diluted chloride curve and the water samples from wells seems to be about the same.

Table 5.2 Correlation coefficients determined for different water chemistry parameters. EC show a high correlation to TDS, chloride, sodium and alkalinity.

	EC	TDS	Cl	SO₄	Ca	Mg	Na	K	Alkalinity
EC	1								
TDS	1.00	1							
Cl	0.76	0.76	1						
SO₄	0.36	0.36	0.42	1					
Ca	0.70	0.70	0.25	0.24	1				
Mg	0.73	0.73	0.33	0.23	0.96	1			
Na	0.88	0.88	0.93	0.29	0.30	0.34	1		
K	0.22	0.22	0.25	0.32	0.05	0.17	0.18	1	
Alkalinity	0.85	0.85	0.40	0.11	0.89	0.88	0.56	0.12	1

EC and TDS have correlation of 1, which suggests that the measured TDS reflects the change is conductivity perfectly. EC and TDS also show a strong and positive correlation to Na, Cl and alkalinity and also to Ca and Mg, which suggest that EC can be directly related to hardness. Furthermore, chloride shows a significant correlation to sodium, which indicates

Total hardness (H_T) can be calculated from the Ca^{2+} and Mg^{2+} content in the water from the Equation 4.16 and plotted against EC (Fig. 5.9) with a best fit using H_T=0.43*EC-11.07 (R^2=0.90).

This analysis shows that the main water quality parameters influencing EC within the Vientiane basin are TDS, hardness and chloride.
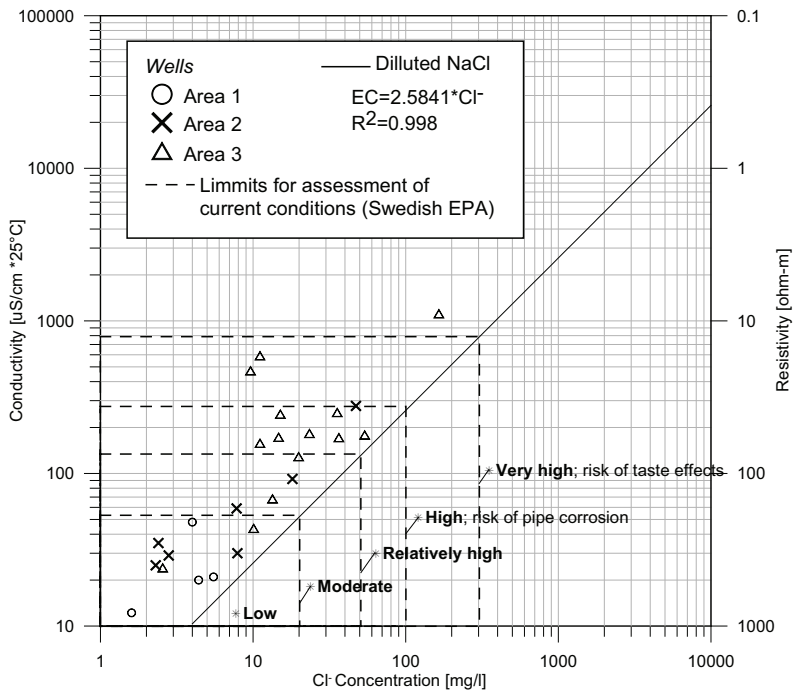
Fig. 5.8 Salt (NaCl) from the Ban Bo salt factory has been diluted for different concentration and measured for EC at 25°C (–), with an almost perfect linear fit. Chloride data from sampled wells in area 1 (O), area 2 (X) and area 3 (Δ) plotted against EC are quite scattered but the overall gradient is the same as the diluted salt curve.
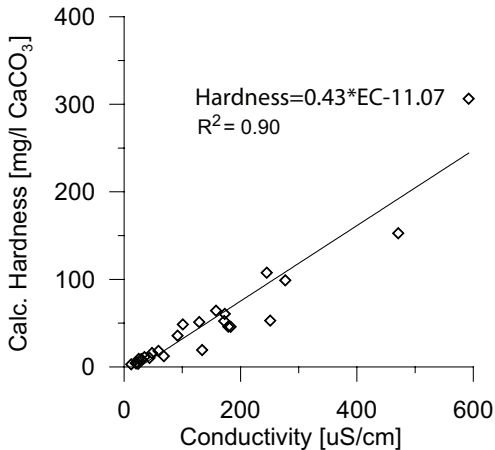
Fig. 5.9 Measured EC plotted against calculated hardness. Best fit is obtained from $H_T = 0.43*EC-11.07$ ($R^2 = 0.90$).

4.4 Comparison of TDS to Aquifer Conductivity and Hydrogeological Parameters

The Salinity (TDS) is caused by differences in mineralogy, topography, flow paths of the groundwater and climate factors. Therefore, the spatial distribution of TDS [mg/l] from area 3 is here plotted together with the VES conductivities of the bottom confining layer (Fig. 5.10a) and of the main aquifer layer (Fig. 5.10b). TDS is also plotted together with hydrogeological parameters like transmissivity (T_{MRS}) (Fig. 5.10c) and hydrostatic column (H_w) (Fig. 5.10d).

TDS determined on water from 7 deep wells in area 3 has a maximum in the northern central part of the basin, with the highest value of 558 mg/l in well 8-4. The TDS decreases towards the south, but also to the east in area 3. This agrees fairly well with the conductivity of the bottom layer located beneath the main aquifer on depths of 20

to 40 m in the western part and at about 10 m in the eastern part. It has also a maximum in the central part of the basin, although shifted more to the south part (Fig. 5.10a). The main aquifer conductivity has a similar relation with the TDS, although the conductivity seems to be high in the eastern part of the basin as well (Fig. 5.10b). This might be an indication that the salinity of deep wells is more affected by the bottom layer than the main aquifer. The topographic gradient correlates well with increasing T_{MRS} and H_w in the western part, and the maximum T_{MRS} (Fig. 5.10c) and H_w (Fig. 5.10d) correlates very well with the conductivity of the bottom layer and

the aquifer and is thus also located somewhat different compared to the TDS maximum. This could imply that the amount of water and the rate of circulation could have an impact on the salinity of the underlying layer and the aquifer layer. It could also be an indication that salt in the northern part of area 3 is diluted and transported southward, where it contributes to the higher conductivity in the main aquifer layer and the underlying layer. Still the number of data is too small and scattered spatially to make a more quantitative interpretation possible.
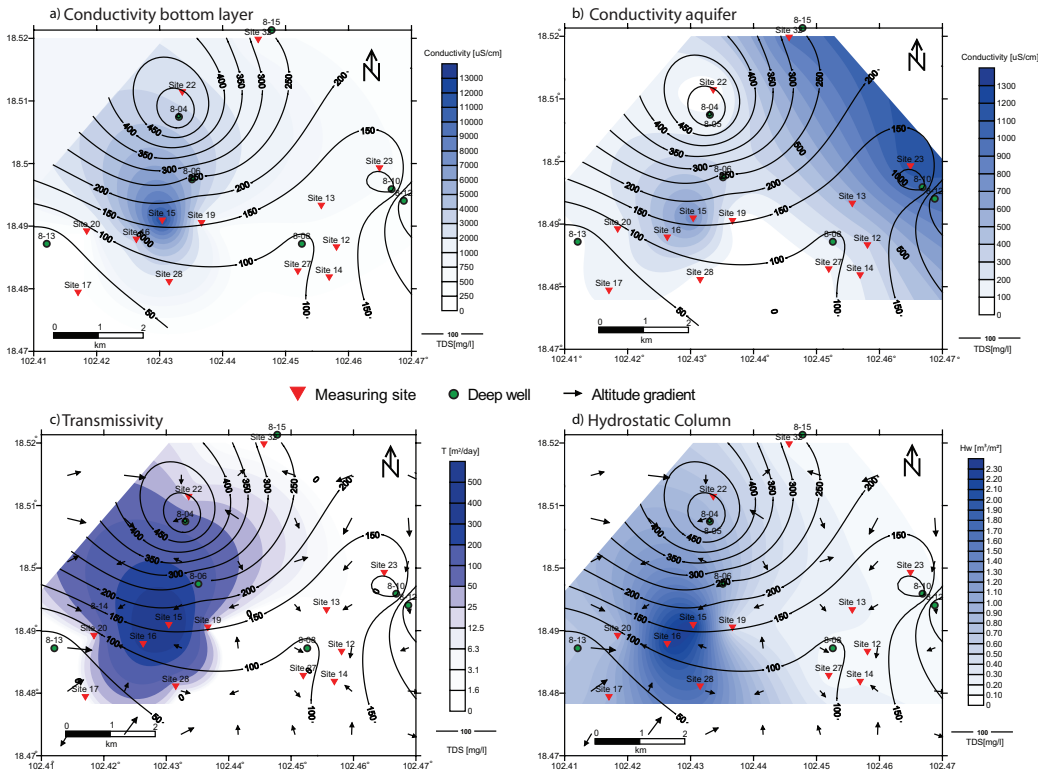
Fig. 5.10 TDS contours together with maps of VES conductivity a) of the bottom layer and the b) aquifer layer, c) transmissivity (T_{MRS}) and d) hydrostatic column (H_w), together with topographic gradients expressed by arrows, where the length denotes gradient amplitude. The maximum conductivity of the bottom layer and the aquifer layer correlates well to the maximum H_w and T_{MRS} but is shifted to the south compared to the maximum TDS.

6. Conclusions and Recommendations

The physical conditions in the Vientiane basin, Laos, with small variations in the magnetic field, low magnetic susceptibility of the rocks and sediments and fairly low noise, make MRS a suitable method for groundwater exploration here. MRS demonstrated to be a good tool to identify and characterize aquifers in different geological environments. Where the MRS Signal to noise ratio was too low for a reliable interpretation, MRS and VES together proved to decrease the uncertainty in the interpretation. Moreover MRS has also shown to be a powerful tool in constraining layer thickness and to identify water layers with medium resistivity in between high and low resistive structures in the VES interpretation (e.g. site 9 and site 16). MRS also helps distinguishing between medium resistive layers of impermeable rock from what could have been interpreted as water if only VES measurements had been carried out.

MRS and VES recognizes the stratigraphic unit N_2Q_{1-3}, consisting of alluvial unconsolidated sediments, as the main water bearing unit. The results from the MRS measurements show that within the region there is usually one to two water bearing layers. The aquifer thickness varies between 10 to 40 m and the depth to the main aquifer range from 5 to 15 m. The water content is here relatively high, up to 16 % and decay times varying between 100 and 400 ms, suggesting a mean pore size equivalent to medium sand to gravel. The resistivity of the water layers is usually between 10 to 100 ohm-m suggest that the water is fresh, which is supported by conductivity measurement on water from wells. MRS and VES also identify an underlying confining clay layer usually situated between 20 to 50 m depth. Since this clay is most probably related to halite layers and has a resistivity as low as 0.5 ohm-m, it is likely that it is affected by the salt. The clay layer might serve as an indicator of halite, and it probably works as a salinity barrier for the overlying aquifers. Hence, as a future drilling guidance in the Vientiane Basin, one should not drill deeper than 30 to 40 m in area1, 20 to 30 m in area 2 and 20 to 30 m in area 3.

Several approaches have been used to establish the relationship between the water EC and the aquifer conductivity, including Archie's law and a model where the total conductivity is the sum of the water EC and the conductivity contribution from finer sediments indicated by T_2^*. However, both with poor results. There is still a strong relationship between water EC from deep wells and VES conductivity, where the best fit is obtained using: EC[µS/cm]= 0.3821VES[µS/cm], R^2=0.81. No relation is found between conductivity from shallow wells and VES conductivity (R^2=0.09). This is probably because the often higher water conductivity in deeper wells contributes more to the VES conductivity. Interpolated maps of TDS from deeps wells together with maps of the conductivity of the bottom layer, aquifer layer, MRS transmissivity and MRS hydrostatic column indicates that the salt originate from the underlying layer situated beneath the main aquifer, but could also be transported from the northern part southward where it is trapped in the bottom of the thicker part of the aquifer. No wells in the investigated areas have water chemistry parameters exceeding the limit for unacceptable drinking water according to WHO or the European water quality standard. The main water quality parameters influencing the water conductivity in the Vientiane Basin are TDS, hardness and chloride, which all have high correlation to the water EC and thus VES conductivity. This makes MRS and VES a very promising tool for guidance of future drillings and water quality estimation.

References

Allen, D., Andreani, M., Badry, R., Flaum, C., Gossenberg, P., Horkowitz, J., Singer, J., White, J. 1997. How to use borehole NMR. Schlumberger's Oilfield Review summer, 34–57

Archie, G.E., 1942. The electrical resistivity as an aid in determining some reservoir characteristics. Metallurgical and Petroleum Engineers 146, 54–62.

Arunin, S., 1987. Management of Saline Soil and Alkaline Soils in Thailand, Paper presented at the Regional Expert Consultant on the Management of Saline/Alkaline Soils, FAO Regional Office for Asian and the Pacific, August 25-29, 1987, Bangkok, Thailand, 15 p.

Back, W., Hanshaw B., 1965. Chemical geohydrology. Advances in hydroscience, V. 2. Academic press, New York, pp. 49-109

Bates, B.C., Z.W. Kundzewicz, S. Wu and J.P. Palutikof, Eds., 2008. Climate Change and Water. Technical Paper of the Intergovernmental Panel on Climate Change, IPCC Secretariat, Geneva, 210 pp.

Bernard, J. 2007. Instruments and field work to measure a Magnetic Resonance Sounding. Bóletin Geológico y Minero, 118(3), 459-472.

Brassington, R. 2007. Field Hydrogeology. 3rd edition. West Sussex, England, pp. 264.

Clesceri, L. S.(Editor), Greenberg, A. E. (Editor), Eaton, A. D. (Editor), 1998. Standard Methods for the Examination of Water and Wastewater, 20th Edition. American Public Health Association (Washington), American Water Works Association (Denver), and Water Environment Federation (Alexandria, VA), pp.1220.

Darcy, H. 1856. Les Fontaines Publiques de la Ville de Dijon, Dalmont, Paris.

De Lima, O. A. and Sharma, M. M., 1990. A Grain Conductivity Approach to Shaly Sandstone, Geophysics 55(10), 1347-1358. Directive 80/778/EEC. 1980.

Directive of 15 July 1980 relating to the quality of water intended for human consumption. European water quality standards.

Dunn, K.J., Bergman, D.J., La Torraca, G.A., 2002. Nuclear Magnetic Resonance Petrophysical and Logging Applications. St. Lois, Missouri: Elsevier Science.

Iris instruments. 2005. NUMIS, MRS (Magnetic Resonance Sounding) SYSTEM, User's manual. URL: http://www.iris-instruments.com/ (read: 2007-05-10)

Japan International Cooperation Agency (JICA), 1994. Drilling logs from the "Vientiane Province Groundwater Development Project". JICA local office in Phon Hong, Vientiane Province, Laos.

Japan International Cooperation Agency (JICA), 2000. The study on rural water supply and sanitation improvement in the northwest region in the Lao People´s Democratic Republic, Ministry of health, National center for environmental health and water supply, Progress report 2, 14 pp

Johnson , D. L. and Sen, P. N., 1988. Dependence of the Conductivity of a Porous Medium on Electrolyte Conductivity, Phys. Rev. B 37.

Kenyon, W.E., Howard, J.J., Sezginer, A., Straley, C., Matteson, A., Horkowitz, K., Ehrlich, R., 1989. Pore-size distribution and NMR in microporous cherty sandstones. SPWLA 13th Annual Logging Symposium, Paper LL.

Kenyon, W.E., 1997. Petrophysical principles of application of NMR logging. The Log Analyst March–April, 21–43.

Kirsh Reinhard (Editor). 2006. Groundwater Geophysics: a Tool for Hydrogeology. Springer –Verlag Berlin Heidelberg 2006, pp. 493.

Krawczyk W.E., and Derek C. Ford, DC, 2007. Correlating specific conductivity with total hardnessin gypsum karst waters. Earth Surface Processes and Landforms, Earth Surf. Process. Landforms 32, 612–620 (2007).

Legchenko A., 2001 –Samogon, v4.041. Program of numerical modeling of surface magnetic resonance sounding.

Legchenko, A. 2006. MRS Measurements and Inversion in Presence of EM noise. In: 3rd Magnetic Resonance Sounding Workshop, Spain, Madrid 25-27 October 2006.

Legchenko, A., Baltassat, J.M., Beauce, A., Bernard, J., 2002. Nuclear magnetic resonance as a geophysical tool for hydrogeologists. Journal of Applied Geophysics 50 (1–2), 21–46.

Legchenko A., Shushakov O. (1998). Inversion of surface NMR data Geophysics, Volume 63, Issue 1, pp. 75-84

Legchenko A., Valla P. 2002, A review of the basic principles for proton magnetic resonance sounding measurements. Journal of Applied Geophysics 50, 3 – 19

Legchenko A., Valla P. 2003. Removal of power-line harmonics from proton magnetic resonance measurements, Journal of Applied Geophysics 53 (2003) 103– 120.

Long, N. X., Lam N. X., Canh, N. D. 1986. Report on Geological data for Potassium and Manganese in Thangon Region, Dong Bang, Vientiane, 1986. Department of Geology and Mining, Vientiane, Laos.

Lovatt Smith, P. F., Stokes, R B., Bristow, C., Carter, A. 1996. Mid-Cretaceous inversion in the northern Khorat Plateau of Lao PDR and Thailand. Tectonic evolution of Southeast Asia ; Geological Society Special Publications, vol.106, pp.233-247.

Lubczynski M., Roy J. 2003. Hydrogeological interpretation and potential of the new magnetic resonance sounding (MRS) method. Journal of Hydrology Volume 283, Issues 1-4, 10 December 2003, Pages 19-40

Lubczynski M., Roy J. 2003. Hydrogeological interpretation and potential of the new magnetic resonance sounding (MRS) method. Journal of Hydrology Volume 283, Issues 1-4, 10 December 2003, Pages 19-40

Lubczynski M., Roy J. 2005. MRS contributing to hydrogeological system parameterization. Near Surface Geophysics 3, 131-139.

Löffler, E. & Kubiniok, J., 1988. Soil Salinization in North-East Thailand, Erdkunde, Band 42, Heft 2, s. 89-100.

Maillet, R. 1947. The fundamental equations of electrical prospecting. Geophysics, vol.12, no.4, pp.529-556, Oct 1947

Na wetcharin, S. 2007. Gravity Anomalies in Vientiane Capital, Lao PDR. 2007. Department of Physics, Faculty of Science, Prince of Songkla University, Hatyai, Thailand, pp. 85.

Niwas, S. and Singhal, D.C., 1981. Estimation of aquifer transmissivity from Dar-Zarrouk parameters in porous media. J. Hydrol., 50: 393--399.

Palacky, G. J., 1987. Clay mapping using electromagnetic methods. First break, 5, pp. 295-306.

Parasnis, D.S. 1997. Principles of Applied Geophysics. 5th edition. Chapman and Hall, London, UK, p.429.

Plata J.L., and Rubio, F.M. 2001. Condiciones para la utilazación de kos Sonderos de Resonancia Magnética (SRM) en la prospección y gestíon de las aguas subterráneas. Congreso Internacional Las Caras del Agua. Libro de Comunicaciones tomo II, 807-813.

Ponzini, G., Ostroman, A. and Molinari, M., 1984. Empirical relation between electrical transverse resistance and hydraulic transmissivity. Geoexploration, 22: l-15.

Reynolds, T. and Richards, P. 1996. Unit operations and processes in Environmental Engineering, 2nd edition. PWS Publishing Company. Boston, USA, pp 798.

Salem H.S. 1999. Determination of fluid transmissivity and electric transverse resistance for shallow aquifers and deep reservoirs from surface and well-log electric measurements. Hydrology and Earth System Sciences, vol.3, no.3, pp.421-427, Sep 1999.

Seevers, D.O., 1966. A nuclear magnetic method for determining the permeability of sandstones. Paper L in Annual Logging Symposium Transactions. Society of Professional Well Log Analysts.

Sen, Z. 1995. Applied Hydrogeology For Scientists And Engineers. Taylor & Francis Ltd, 1995. pp. 460.

Sharma, P.V., 1997. Environmental and Engineering Geophysics. Cambridge University Press, UK, 1997. pp. 499.

Shiklomanov, Igor A., State Hydrological Institute (SHI, St. Petersburg) and United Naitons Educational, Scientific and Cultural Organisation (UNESCO, Paris), 1999.

Shirov, M., Legchenko, A., Creer, G. 1991. New direct non-invasive ground water detection technology for Australia. Explor.Geophys. 22, 333–338.

Shoeller. H. 1959. Arid Zone Hydrology: Recent Developments, UNESCO, Paris, p.125.

Srisuk, K., Sriboonlue, V., and Buaphan, C. 1999. Groundwater flow, saline water and saline soils in the Central Khorat Basin, northeast Thailand. Symposium on Mineral, Energy and Water Resources of Thailand: Towards the year 2000. 238-251.

Srisuk, K., Toth, K. 1994. Groundwater Salinity and Three-Dimensional Groundwater Flow Model at Ban Nong Khai Nun, Khon Kaen, 186 p.

Stuart-Fox, M., Rooney, D.F. 2006. Microsoft Encarta 2006.

Velpen, V. 1988. Resist87: a computer prcessing packaged for dc Resistivity interpretation. M.sc. thesis, ITC-Delft, The Netherlands.

Swedish Environmental Protection Agency (SEPA) 2007. URL: http://www.internat.naturvardsverket.se/ (read: 2007-04-11)

Tabakh El. M., Utha-Aroon C., Schreiber B.C. 1999. Sedimentology of the Cretaceous Maha Sarakham evaporites in the Khorat Plateau of northeastern Thailand. Sedimentary Geology, Volume 123, Number 1, January 1999 , pp. 31-62(32).

Takayanagi, K. 1993. Basic Design Study Report on the Project for Groundwater Development in Vientiane Province in Lao People's Democratic republic.

UNESCO. 2003. "Water for People, Water for Life" United Nations World Water Development Report, Part II: Alook at the world's freshwater resources. UNESCO, 2003, www.unesco.org

UNEP/GRID-Arendal. 2002a. Freshwater availability: groundwater and river flow [Internet]. UNEP/GRID-Arendal Maps and Graphics Library; 2002 [cited 2008 Oct 4]. Available from: http://maps.grida.no/go/graphic/freshwater-availability-groundwater-and-river-flow

UNEP/GRID-Arendal. 2002b. Trends and forecasts in water use, by sector [Internet]. UNEP/GRID-Arendal Maps and Graphics Library; 2002 [cited 2008 Oct 4]. Available from: http://maps.grida.no/go/graphic/trends-and-forecasts-in-water-use-by-sector

Velpen, V. 1988. Resist87: a computer prcessing packaged for dc Resistivity interpretation. M.sc. thesis, ITC-Delft, The Netherlands.

Vouillamoz, J.M., Favreau,G., Massuel S., Boucher M., Nazoumou, Y., Legchenko, A. 2006. Contribution of MRS to better understanding aquifer recharge: preliminary results. Proceedings 3rd Magnetic Resonance Sounding Workshop. Madrid-Tres Cantos, 97-100

Vouillamoz, J.M., Baltassat, J.M., Girard, J.F., Plata, J., Legchenko, A. 2007. Hydrogeological experience in the use of MRS. Bóletin Geológico y Minero, 118(3), 531-550.

Wannakomol, A. 2005. Soil and Groundwater Salinization Problems in the Khorat Plateau, NE Thailand, Integrated Study of Remote Sensing, Geophysical and Field Data. Fachbereich Geowissenschaften, Freie Universität Berlin. http://www.diss.fu-berlin.de/2005/210/indexe.html

Waxman, M. H. and Smits, L. J. H. Electrical conductivities in oil-bearing shale sands. Soc. Petrol. Eng. J. June 1968, pp. 107-122; Trans. AIME, vol 243.

WHO. 1996. Guidelines for drinking-water quality, 2nd ed. Vol. 2. Health criteria and other supporting information. World Health Organization, Geneva, 1996.

WHO. 2004. Water, Sanitation and Hygiene Links to Health, Facts and Figures, WHO, updated November 2004, www.who.int

Williamson, D. R., Peck, A J.Turner, J. V., Arunin, S. 1989. Groundwater hydrology and salinity in a valley in Northeast Thailand. Groundwater contamination
IAHS-AISH Publication, vol.185, pp.147-154

Worthington, P.F., 1993. The uses and abuses of the Archie equations, 1: The formation factor-porosity relationship. J.Appl. Geophys., 30:215-228.

WRI. 2000. World Resources 2000-2001, People and Ecosystems: The Fraying Web of Life, World Resources Institute (WRI), Washington DC, 2000.

Yaramanci, U., 2004. New technologies in groundwater exploration. Surface Nuclear Magnetic Resonance. Geologica Acta, 2, No 2, 109-120.

Appendix A

Summary of the most important site characteristics for the sites 1 to 32 with coordinates expressed in WGS84 (Lat/Long). Geology unit, choice of MRS loop design: 100 square, 8-shape or 50 square 2turn, MRS signal to noise (S/N) ratio, resistivity of the main aquifer (ρ), transverse resistance (TR), hydrostatic column (H_w), MRS transmissivity (T_{MRS}), specific yield (S_y), specific storage (S_s) and depth to the aquifer floor.

Name	North [°]	East [°]	Geology	Loop	MRS S/N	ρ [aquifer]	VES TR	H_w	T_{MRS}	S_y	S_s [*10^-4]	Aq. Floor [m]
Area 1												
Site 1	18.15149	102.59822	N_2Q_{1-3}	100	10.77			1.83	29			42.5
Site 2	18.16318	102.58663	N_2Q_{1-3}	100	4.31	600	x	2.72	214	6.44	1.42	42.5
Site 3	18.15233	102.6011	N_2Q_{1-3}	100	6.27	19	x	2.58	157	9.97	1.59	40.1
Site 4	18.14991	102.60523	N_2Q_{1-3}	100	<2							
Site 24	18.08789	102.5862	N_2Q_{1-3}	100	2.15	20	492	1.52	28			31.9
Site 25	18.08951	102.64348	K_2tn	100	<2							
Site 26	18.07345	102.64638	K_2tn	100	<2							
Site 29	18.10662	102.63969	K_2tn	100	<2							
Site 30	18.11939	102.62428	N_2Q_{1-3}	100	4.95			1.18	19			31.9
Site 31	18.05997	102.58526	N_2Q_{1-3}	100	2.19	150	5277	0.95	1			31.9
Area 2												
Site 5	18.32905	102.65276	N_2Q_{1-3}	100	9.75	6	97	1.18	17			29.5
Site 6	18.34009	102.64332	N_2Q_{1-3}	100	<2							
Site 7	18.34072	102.6558	N_2Q_{1-3}	100	<2							
Site 8	18.28359	102.67604	N_2Q_{1-3}	100	9.94			1.31	72	3.13	1.26	23.9
Site 9	18.2799	102.67656	N_2Q_{1-3}	100	5.38	13	233	0.55	5		1.18	17.9
Site 10	18.27501	102.67675	N_2Q_{1-3}	100	7.6			2.44	342	11.47	1.66	27
Site 11	18.28401	102.6701	N_2Q_{1-3}	100	8.89			1.06	33	4.69	1.34	23.9
Area 3												
Site 12	18.48658	102.45809	N_2Q_{1-3}	100	2.06	34	131	0.15	0			6
Site 13	18.49323	102.45568	N_2Q_{1-3}	100	<2							
Site 14	18.48178	102.45693	N_2Q_{1-3}	100	2.02			0.20	0			13.4
Site 15	18.49086	102.43041	N_2Q_{1-3}	100	3.26	13	255	2.29	533	12.82	1.72	23.9
Site 16	18.48782	102.4263	N_2Q_{1-3}	100	9.44	22	705	2.23	341	8.27	1.51	31.9
Site 17	18.47934	102.41704	N_2Q_{1-3}	8	2.56	76	2292	0.91	0			31.2
Site 18	18.4388	102.39045	K_2cp	2*50	<2							
Site 19	18.49046	102.43666	N_2Q_{1-3}	100	2.63	194	873	0.38	2			10
Site 20	18.48913	102.41842	N_2Q_{1-3}	8	2.57	79	1468	0.77	11			19.1
Site 21	18.56654	102.38577	N_2Q_{1-3}	8/100	2.3	82		0.74	2			30.2
Site 22	18.51135	102.4336	N_2Q_{1-3}	8	3.19	863	12082	0.75	18	4.70	1.34	24.4
Site 23	18.4992	102.46492	N_2Q_{1-3}	8	<2	9	76	0.13				9.1
Site 27	18.48273	102.45195	N_2Q_{1-3}	100	2.07	103	405	0.14	0			6
Site 28	18.48104	102.43152	N_2Q_{1-3}	100	2.82	267	5201	1.70	18			31.9
Site 32	18.51975	102.44565	N_2Q_{1-3}	8	<2	11	113	0.16				8

Appendix B

Summery of the groundwater chemistry analysis. Grey marked samples exceed limits of water quality standards according to WHO or SEPA. Measured Total Dissolved Solids (TDS), electrical conductivity (EC) TDS-factor (C_{TDS}), passed quality control parameters according to section 4.2.1. S and D denote shallow and deep well, respectively.

| Sample ID | TDS | EC | TDS-factor | Chloride | Water Type | Calc. Hardness | Quality control | East [°] | North [°] | Area | Well | | Geology | |
	mg/L	µS/cm		mg/L		mg/L CaCO$_3$	1,2,3,4,5,6	Long (WGS84)	Lat (WGS84)	1,2,3	Shall./Deep	Layer 1	Layer 2	Layer 3
7-1	11	21	0,53	5,5	Na-Cl	4,14	1,4,5	102,61163	18,15464	1	S	N₂Q₁₋₃	K₂tn	
7-3	24	48	0,50	4	Ca-HCO₃	15,84	1,4	102,60747	18,16647	1	S	N₂Q₁₋₃	K₂tn	
7-4	10	20	0,50	4,4	Na-Cl	4,32	1,4,5	102,5993	18,1575	1	S	N₂Q₁₋₃	K₂tn	
7-5	12	25	0,48	2,3	Ca-HCO₃	9,13	1,4	102,68113	18,27853	2	S	N₂Q₁₋₃	K₂tn	
7-6	15	29	0,52	2,8	Ca-HCO₃	8,63	1,3,4	102,67916	18,28564	2	S	N₂Q₁₋₃	K₂tn	
7-7	17	35	0,49	2,4	Ca-SO₄	11,11	1,4	102,67304	18,28525	2	D	N₂Q₁₋₃	K₂tn	
7-8	29	59	0,49	7,8	Ca-Cl	18,41	1,4,5	102,67325	18,28467	2	S	N₂Q₁₋₃	K₂tn	
7-9	46	92	0,50	18,1	Ca-Cl	35,75	1,4	102,65963	18,34006	2	D	N₂Q₁₋₃	K₂tn	
7-10	139	277	0,50	47,2	Ca-Cl	98,90	1,3,4,5	102,65621	18,33047	2	D	N₂Q₁₋₃	K₂tn	
7-11	15	30	0,50	7,9	Ca-Cl	8,88	1,4	102,66138	18,33774	2	D	N₂Q₁₋₃	K₂tn	
7-12	64	129	0,50	19,9	Ca-Cl	51,29	1,3,4	102,45911	18,48735	3	S	N₂Q₁₋₃	K₂sb	
7-13	50	101	0,50	1	Ca-HCO₃	48,57	1,3,4	102,43498	18,48783	3	S	N₂Q₁₋₃	K₂sb	
7-14	123	245	0,50	15,1	Ca-HCO₃	107,65	1,3,4	102,42404	18,49725	3	S	N₂Q₁₋₃	K₂sb	
8-1	6	12,2	0,49	1,6	K-Cl	2,99	1,4	102,58786	18,0913	1	D	N₂Q₁₋₃	K₂sb	
8-2	67	134	0,50	0,85	Na-HCO₃	19,28		102,39073	18,56783	3	D	N₂Q₁₋₃	K₂sb	
8-3	86	173	0,50	14,7	Ca-HCO₃	60,65	1,3,4	102,39073	18,56783	3	S	N₂Q₁₋₃	K₂sb	
8-4	558	1115	0,50	165	Na-HCO₃	117,23	1	102,43307	18,50745	3	D	N₂Q₁₋₃	K₂sb	K₂tn?
8-5	90	179	0,50	53,9	Na-Cl	46,04	1,4,5	102,43353	18,50472	3	S	N₂Q₁₋₃	K₂sb	
8-6	236	471	0,50	9,62	Ca-HCO₃	152,77	3,4	102,43515	18,49747	3	D	N₂Q₁₋₃	K₂sb	K₂tn?
8-7	22	43,7	0,51	10,1	Na-Cl	10,33	1,4	102,43515	18,49747	3	S	N₂Q₁₋₃	K₂sb	
8-8	91	183	0,50	23,4	Ca-HCO₃	45,91	1,3,5	102,45259	18,48718	3	D	N₂Q₁₋₃	K₂sb	
8-9	34	68,2	0,50	13,4	Na-Cl	12,35	1,3,5	102,45259	18,48718	3	S	N₂Q₁₋₃	K₂sb	
8-10	79	158	0,50	11,1	Ca-HCO₃	64,21	1,3,4	102,46684	18,4959	3	D	N₂Q₁₋₃	K₂sb	
8-11	86	172	0,50	36,5	Ca-Cl	52,48	1,3,4,5	102,46652	18,49545	3	S	N₂Q₁₋₃	K₂sb	
8-12	296	592	0,50	11,1	Ca-HCO₃	306,30	1,3	102,46878	18,49405	3	D	N₂Q₁₋₃	K₂sb	
8-13	12	24,1	0,50	2,56	Na-HCO₃	3,73	1,4	102,41207	18,48718	3	D	N₂Q₁₋₃	K₂sb	
8-14	126	251	0,50	35,6	Na-Cl	52,91	1,3,4	102,41932	18,49265	3	S	N₂Q₁₋₃	K₂sb	
8-15	247	494	0,50	0,084	Na-Cl			102,44778	18,52132	3	D	N₂Q₁₋₃	K₂sb	

I

Perttu N., Wattanasen K., Elming S-Å., Phommasone K. 2008.

**Characterization of Aquifers in the Vientiane Basin, Laos,
Using Magnetic Resonance Sounding and
Vertical Electrical Sounding**

(Manuscript).

Characterization of Aquifers in the Vientiane Basin, Laos, Using Magnetic Resonance Sounding and Vertical Electrical Sounding

Nils Perttu[1,*], Kamhaeng Wattanasen[1,2], Sten-Åke Elming[1], Khamphouth Phommasone[3]

[1]*Division of Ore Geology and Applied Geophysics, Luleå University of Technology, SE-971 87 Luleå, Sweden*

[2]*Department of Physics, Faculty of Science, Prince of Songka University, HatYai, 90112 Thailand*

[3]*Department of Physics, National University of Laos, P.O. Box 7322, DongDok Campus Vientiane, Lao PDR*

*Corresponding author: Nils.Perttu@ltu.se, Tel: +46-920-491884, Fax: +46-920-491199

Abstract

The aim of this study is to define and characterize water bearing geological formation and to test the possibility of using geophysical techniques to determine hydrogeological parameters in three areas in the Vientiane basin, Laos. The investigation area is part of the Khorat Plateau where halite is naturally occurring as shallow as 50 m in depth in the Thangon Formation. Magnetic Resonance Sounding (MRS) has been used in combination with Vertical Electrical Sounding (VES) in different geological environments. In total, 32 sites located in three different areas were investigated and MRS and VES recognized the stratigraphic unit N_2Q_{1-3}, consisting of alluvial unconsolidated sediments, as the main water bearing unit. The aquifer thickness varies between 10 to 40 m and the depth to the main aquifer range from 5 to 15 m. The water content is here relatively high, up to 16 % and decay times varying between 100 and 400 ms, suggesting a mean pore size equivalent to medium sand to gravel. The resistivity is highly variable, but usually around 10-100 ohm-m. Hydraulic and storage related parameters such as transmissivity, hydraulic column, specific yield and specific storage have been estimated from MRS and transverse resistance estimated from VES. MRS together with VES has also shown to be a useful and important tool in identifying the salt related clay layer of the Thangon Formation. This layer is characterized by a very low water content and a resistivity lower than 5 ohm-m. This formation can be found in all 3 areas on depth of 20 to 50 m.

Keywords: magnetic resonance sounding; vertical electrical sounding; resistivity; transmissivity; transverse resistance; hydrostatic column; storativity; Vientiane basin, Laos; Khorat Plateau.

1. Introduction

Lao People's Democratic Republic (Laos) is located in the middle south-east Asia bordering to Thailand, China, Burma (Myanmar), Vietnam and Cambodia (Fig. 1).

current demand of 228 m³/person (STEA, 2000). This makes Laos the richest country in Asia of renewable freshwater per capita. Still, according to WRI (1998), only 60% of the urban and 51% of the rural population had direct access to water supply in 1998 (STEA, 2000). The Vientiane Basin is located in the central part of Laos on the
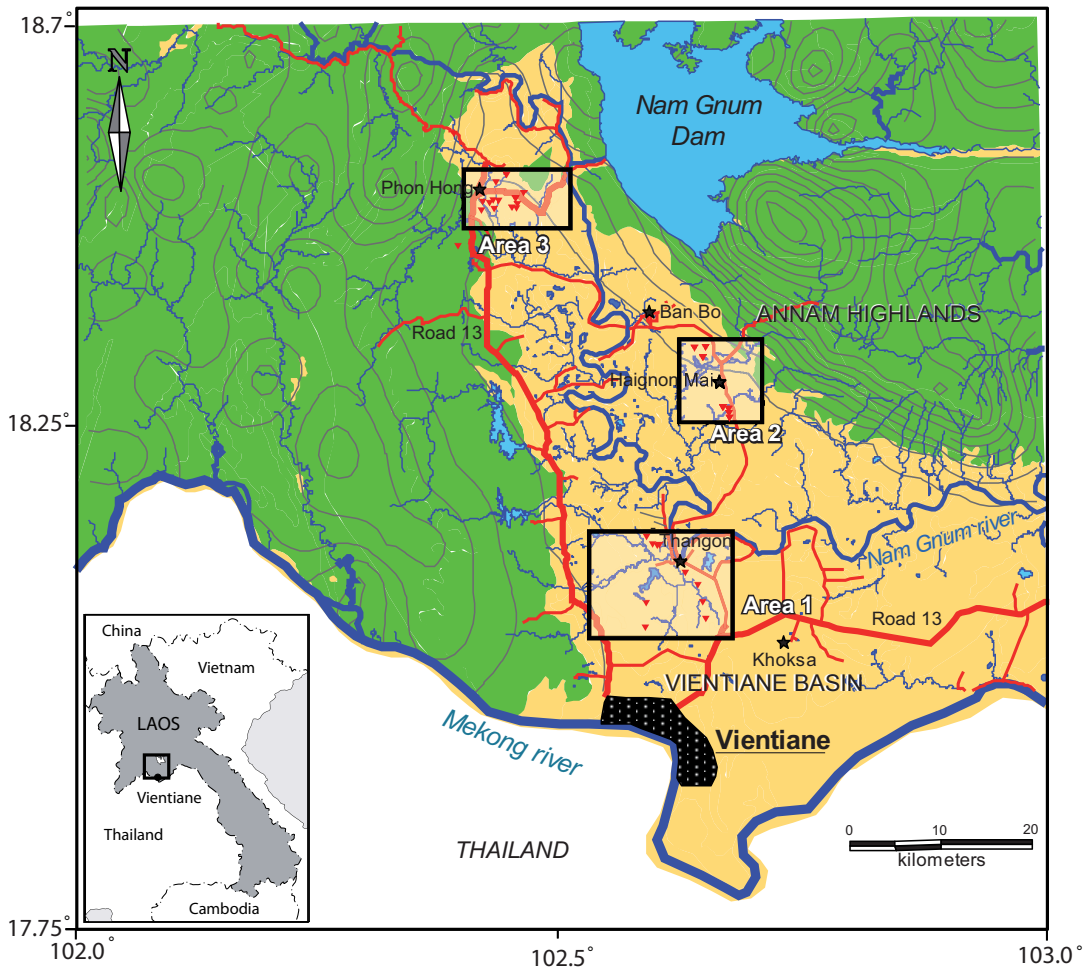
Fig. 1. The Vientiane Province, with the Vientiane Basin in the drainage basin of Nam Gnum and Mekong river. The three study areas defined with rectangles.

Laos possesses great water resources as estimated 35% of all water in the Mekong River originates from watersheds in Laos. Approximately 80% of the precipitation arises in the rainy season. The two most important socio economic sectors to take advantage of this natural resource are irrigation and hydropower (STEA, 2000). The annual renewable fresh water supply per capita amounts to 54 000 m³/person, compared to the

outer border of the Khorat Plateau. In the basin, natural salt layers are found in the Thangon Formation. This affects the groundwater quality in some deep wells (JICA, 2000). Salinity problems are common in central Laos and north-east Thailand and have been studied by among others Wannakomol, (2005); Srisuk et al. (1999) and Williamson et al. (1989).

Most Lao people live on the country side and are heavily dependent on dug wells as their main water source, but also deep wells, river water and rainwater are used (Medlicot, 2001). Dug wells usually dry out during the dry period and in addition, water-borne diseases caused by infiltrations of domestic waste and excreta from farm animals, has lead to a high morbidity rate (Medlicot, 2001; Takayanagi, 1993). Deep groundwater has many advantages compared to surface water and shallow groundwater, since it demand little or no treatment and the access is secured against temporary droughts. However, for exploration the small topography difference in the Vientiane Basin makes it difficult to evaluate the groundwater potential from the visible physical environment. Deep wells are expensive and unprofitable if drilling is made without knowing the groundwater potential and the location of salt affected groundwater. Therefore, basic information that can guide drilling is essential.

The aim of this study is to define and characterize water bearing geological formation according to their relative hydraulic and storage related properties. Furthermore, we want to explore the possibility to distinguish freshwater aquifers from salt affected groundwater. This we do by combining Magnetic Resonance Sounding (MRS) and Vertical Electrical Sounding (VES) in different geological environment in the Vientiane basin. Resistivity methods have been widely used to characterize aquifers as there is a direct relationship between hydraulic and electric parameters governed by electric conduction through porous media and fluid flow (Sundberg, 1932; Archie, 1942; Worthington, 1992). However, resistivity methods only give an indirect image of the water content and high conductive sediments can easily be mistaken for an aquifer. MRS is based on the application of Nuclear Magnetic Resonance (NMR) and gives a direct image of the water content in the ground and hence the vertical distribution of an aquifer. Similar MRS investigations have been made in Cambodia and in Burma (Vouillamoz et al., 2002 and 2007).

2. Study Area

The Vientiane Province is located in central Laos (Fig. 1), between latitude 18° and 18.67° and longitude 102° and 103°. The central part of the province is situated in the Vientiane Basin with an average elevation of 170 to 190 m. This fertile flat low-land is mainly used for agriculture with big irrigation systems. The surrounding mountain area is covered by forests with elevations ranging up to 1600 m. The whole region is within the drainage basin of Nam Gnum and Mekong Rivers. Laos has a tropical monsoon climate with a rainy season from May to October, followed by a cool dry season from November to February and a hot dry period from March to April. The average rainfall is about 1 780 mm, but it varies regionally. Temperature ranges from as high as 40°C in the Mekong lowlands during the hot months to as low as 5°C in the mountain area in the winter (Stuart-Fox and Rooney, 2006).

2.1 Geology and Hydrogeology

The Vientiane Basin is located on the very northern part of the Sakhon Nakhon Basin in the Khorat Plateau (Fig. 2).The Khorat Plateau covers an area of 170 000 km^2 between latitudes 101° and 106° and longitudes 14° and 19° in the region of north-eastern Thailand and central Laos. During the Cretaceous, due to relative sea-level rise, the plateau underwent periods of marine influx but was sporadically isolated from the oceans. This created the Maha Sarakham Formation, a three layer salt unit separated by red-coloured siliciclastics of fluvial origin. Tectonics during the early Tertiary lead to severe folding and deformation of the salt beds, creating a variety of different salt structures such as domes, anticlines, synclines and ridges as shallow as 50 m below the surface. The upper and middle parts of the salt beds are often missing due to dissolution from groundwater percolation. The evaporites include thick successions of halite, anhydrite and potassic minerals like sylvite and carnalite (Tabakh et al., 1999).

The geology (Fig. 2) and stratigraphy (Fig. 3) are summarized in the section below using Lao nomenclature proposed by Long et al. (1986)

Fig. 2. Geology of Vientiane province (Long et al. 1986). Keymap showing the extent of the Khorat Plateau after Tabakh et al. (1999). The rectangle defines the area where halite depths have been determined from borehole data. A and B, E and F, G and H defines profiles along which geophysical and geological data are presented.

Fig. 3. Stratigraphy of the Vientiane Basin after Long (1986) and Lovatt Smith et al. (1996).

with modifications based on Thai stratigraphy (Lovatt Smith et al., 1996) and hydrogeological data (Srisuk et al., 1999; Takayanagi, 1993).

The equivalent to the Maha Sarakham Formation in the Vientiane Basin is the middle Cretaceous Thangon formation (K_2tn). It is most easily found in the south-eastern part of the Vientiane basin, where the salt beds have been mobilized into pillows and small diapirs. It is mainly composed of salt-layer bearing anhydrite interbedded with claystone with a thickness lower than 550 m and a maximum halite thickness of of 340 m (Lovatt Smith et al., 1996). The depth to the salt layer generally ranges between 50 to 200 m in the

southern part of the province (Long et al., 1986). The hydraulic conductivity (K) ranges between 10^{-8} to 10^{-14} m/s, the specific yield is in the range of (S_y) 10^{-7} and the average specific storage (S_s) is $2*10^{-9}$, which makes K_2tn an aquiclude or non water bearing formation (Srisuk et al., 1999).

The Thangon formation is overlain by the Saysomboun Formation (K_2sb) (not in map). This formation originates from upper Cretaceous and constitutes of red-brown claystone that gradually change to siltstone. The maximum thickness of K_2sb is 150 m. K_2sb is found in the middle and northern part of the basin with a relative low K ranging from 10^{-8} to 10^{-5} m/s, a S_y of around 0.01 and a S_s 10^{-6}. The Neogene to Quaternary Vientiane Formation (N_2Q_1vc) has a thickness lower than 70 m. This formation is overlain by the stratigraphic units: Q_{2-3} (<25 m) and Q_4 (<0.5 m) of Quaternary origin. The N_2Q_1vc and Q_{2-3} are alluvial deposits found in abandoned river channels, and contain mostly gravel, sand and clay. Since they share the same characteristics they will be referred to as the N_2Q_{1-3} unit in this paper. The equivalent Thai units has K ranging from 10^{-6} to 10^{-4} m/s, with S_y around 0.15 and S_s around 2 to $3*10^{-3}$. The possibility for developing groundwater in this unit is regarded as high (Takayanagi, 1993). The above mentioned units are all part of the Phon Hong Group. Underlying the Thangon Formation is the Khorat Group, which among others consists of the Champa- (K_2cp) and Phu Pha Nang formations (J-Kpn). These up to 400 m and 350 m, respectively, thick units are found primarily in the western and eastern part of the basin on the border to the mountain area. They are largely composed of sandstone of Cretaceous and Jurassic age, with K ranging from 10^{-8} to 10^{-5} m/s, S_y of around 0.05 and S_s of about $5*10^{-6}$.

2.2 Investigation Areas

Three areas were selected for geophysical studies (Fig. 1), where area 1 is located about 20 km north of Vientiane in the district of Thangon, area 2 is located around 40 km northeast in the district of Tholakhom and area 3 is located about 60 km northwest of Vientiane in the district of Phon Hong. Data has been collected from 32 sites. The locations have been chosen according to differences in geology, where geological data was retrieved from JICA and Department of Geology and Mining in Vientiane. In an initial survey, noise level and accessibility was evaluated, which in most cases resulted in that dry rice paddies were chosen as measuring sites.

3 Geophysical Methods and Interpretation Techniques

The MRS measurements were carried out with the Numis_plus equipment manufactured by Iris instruments. The magnetic field was measured using a G 816 magnetometer (Geometrics) with a resolution of 1 nT. The VES measurements were conducted with a Terrameter SAS4000 (ABEM). Resistivity measurements of core samples were done in the geophysical laboratory at Luleå University of Technology.

3.1 Magnetic Resonance Sounding (MRS)

MRS is a non invasive geophysical technique that energizes the protons in groundwater by transmitting an electromagnetic pulse in the larmor frequency and then measures the resonance signal emitted by the protons. The method and principles are thoroughly described in Legchenko and Valla (2002); Yaramanci (2004); Lubczynski and Roy (2003). The initial amplitude (E_0) of the received signal is directly related to the free water content (θ_{MRS}) and the decay time (T_2^*) is related to mean pore size of the material. With current limitation of the Numis equipment, signals within the first 30 ms can not be detected. The water content (θ_{MRS}) is determined from the inversion of E_0 and is presented as a function of θ_{MRS}, together with T_2^* versus depth.

In coarse grained aquifers, parameters such as porosity (η) and effective porosity (η_e) can be roughly determined directly from the inversion of E_0. This is under the assumption that bound water and dead-end, unconnected porosity is negligible (Lubczynski and Roy, 2003). Assuming that θ_{MRS} reflects η, ($\theta_{MRS} \approx \eta$), the specific yield ($S_y$) can be approximately estimated for unconfined aquifers as:

$$S_y = \theta_{MRS} - S_R \qquad (1)$$

where S_R is the specific retention, which can be determined by other methods (Lubczynski and Roy, 2003) or retrieved from tabled values (Table 1). In confined aquifers, the specific storage (S_s) can be calculated from:

$$S_s = \rho g(\alpha + \theta_{MRS}\beta) \qquad (2)$$

where ρ is the density of water, g the gravity acceleration, α and β compressibility of the aquifer and water respectively (Table 1).

where C_T is an area specific constant derived from pumping test transmissivity (T_p) data:

$$C_T = \sum_{i=1}^{n} T_{P\_i} / \sum_{i=1}^{n} \Delta z_{MRS} \theta_{MRS}^4 \cdot T*_{1,2}^2 \qquad (5)$$

The MRS data was interpreted with the inversion software Samovar, based on the least square solution with regularization (Legchenko and Shushakov, 1998). Legchenko (2006) defines a lower limit of signal to noise ratio of 2 (S/N>2) for reliable interpretations. Due to equivalence, several models can fit the data. The parameter of regularization controls the smoothness of the interpreted water content distribution with

Table 1. *Typical values of decay time (T_2*) for different geological materials (Shirov et al, 1991; Allen et al (1997), Values of Specific retention (Sr) (after Morris and Johnson, 1967; Johnson, 1967 and Hamill and Bell, 1986). Vertical compressibility (α) for some geological materials and for water (β) (Domenico and Mifflin, 1965).*

Decay time	S_R [%]	α [m^2/N] *10^-8	Petrophysical Information
T_2* < 3 ms T_2* < 30 ms	25-45	6.9-200	Clay bound water Sandy clays
30< T_2* <60 60< T_2* <120 120< T_2* <180	5-15	1.3-10	Clay sands, very fine sands Fine sands Medium sands
180< T_2* <300 300< T_2* <600	3-12	0.52-1	Coarse and gravely sands Gravel deposits
600< T_2* <1500		β[25°C] = 4.8*10^{-10}	Surface water bodies

The hydrostatic column (H_W) [m³/m²] gives a direct volumetric estimate of the free water content with depth. This is the most reliable MRS parameter since it is insensitive to equivalence.It can be estimated for aquifers of arbitrary depth intervals, e.g. maximum MRS investigation depth (Lubczynski and Roy, 2003).

$$H_W = \theta_{MRS} \cdot \Delta z \qquad (3)$$

The transverse relaxation time T_2*, is the characteristic time for the loss of spin rotation coherency and is directly linked to the mean size of the water filled pores. Typical values of T_2* are presented in Table 1. Access to pumping test data makes it possible to relate T_2* and θ_{MRS} to transmissivity (Legchenko et al., 2002; Vouillamoz et al., 2002) according to:

$$T_{MRS} = C_T \int_{\Delta z} \theta^4 \cdot T_2^{*2} \cdot dz \qquad (4)$$

depth. Yaramanci et al. (2002) argues that a high regularization will not present sharp boundaries or changes in water content with depth in medium to coarse sand aquifers in an accurate way. A low regularization on the other hand could cause unrealistic variations in small depth ranges. As the subsurface conductivity influences the depth of penetration of the excitation field (Legchenko and Shushakov, 1998), the MRS interpretation also requires an electrical model of the subsurface.

3.2 Vertical Electrical Sounding (VES)

18 VES measurements were conducted on or in proximity of the MRS sites using a Schlumberger configuration and *AB/2* distances usually up to 200 m. The data were interpreted with the inversion software RESIST87 (Velpen, 1988).

5

When geological borehole data is present, it has been used to constrain layer geometry. Some interpretation problems for VES can occur when mapping subsurface salinity, since resistivities for salt water, saturated clay and sand overlaps. Furthermore, due to the high resistivity contrasts between an often high resistive, dry top soil and a low resistive saline aquifer, interjacent freshwater layers with medium resistivities are difficult to detect on the sounding curve (Kirsch, 2006). These problems can be accounted for if using a first MRS model in the VES interpretation to identify and constrain water layers in the apparent resistivity curve (Vouillamoz et al., 2007).

Transverse resistance is also known as the Dar-Zarrouk variable (Maillet, 1947). It is defined for a specific layer as:

$$TR_i = \rho_i \cdot T_i \qquad\qquad (6)$$

Where ρ_i and T_i are the resistivity and thickness, respectively, for layer i. TR_i is free from the ambiguity of VES interpretation where T_i and ρ are subject to principle of equivalence. Attempts have been made to correlate TR with aquifer transmissivity (Niwas and Singhal, 1981; Ponzini et al., 1984; Salem, 1999), with good results in homogenous geological environment where the aquifer resistivity is insensitive to variations in water conductivity (Niwas and Singhal , 1981)

5. Results

5.1 Laboratory Measurements

Laboratory measurements of the resistivity of the halite samples from the Thakhek area (central Laos) showed a resistivity around $1.1*10^6$ ohm-m to be compared with the resistivity of rock salt, of 10^6 to 10^7 ohm-m (Parasnis, 1997).

5.2 Field Measurements

The geomagnetic field in the area has an inclination of 24° and it varied between 43620 to 43850 nT equivalent to a larmor frequency (f_L) of 1859 to 1868 Hz. This allowed for notch filters to be used (F=50 Hz power line frequency), since there is little or no influence on the MRS signal when the harmonics of the power line frequency (F_H) closest to f_L is greater than 8 Hz for a T_2*=400 ms ($|F_H - f_L|$ >8Hz) (Legchenko and Valla, 2003) Depending on the noise amplitude, a 100 m square loop or a 8 square loop was used together with 64 to 100 stacks. The decay time value matching the highest water content in a water bearing layer have been used to characterize that specific aquifer. The grain size indicated by T_2* usually agrees well with borehole petrophysical information. However, borehole data can not always be related to the sites of measurements.

Examples of raw-data from the site 22 in area 3 are presented in Fig. 4. MRS S/N-ratios for the different sites are presented in Table 2. The general trend is that the inverted MRS data seems to fit the raw data quite well in the first pulse moments but looses coherency in the last pulse moments, where the initial amplitude usually is low. A regularization between 300 and 700 usually results in a smooth aquifer geometry which corresponded quite well with the lithology observed in adjacent boreholes. A 16 layer model has been used, corresponding to the number of pulse moment. Aquifer geometry retrieved from MRS measurements correlates roughly to the ground water table at different sites. VES measurements are generally of good quality with RMS varying between 2 and 6%. VES models with a low resistive last layer usually have more scattered apparent resistivity values in the end of the sounding and consequently higher RMS.
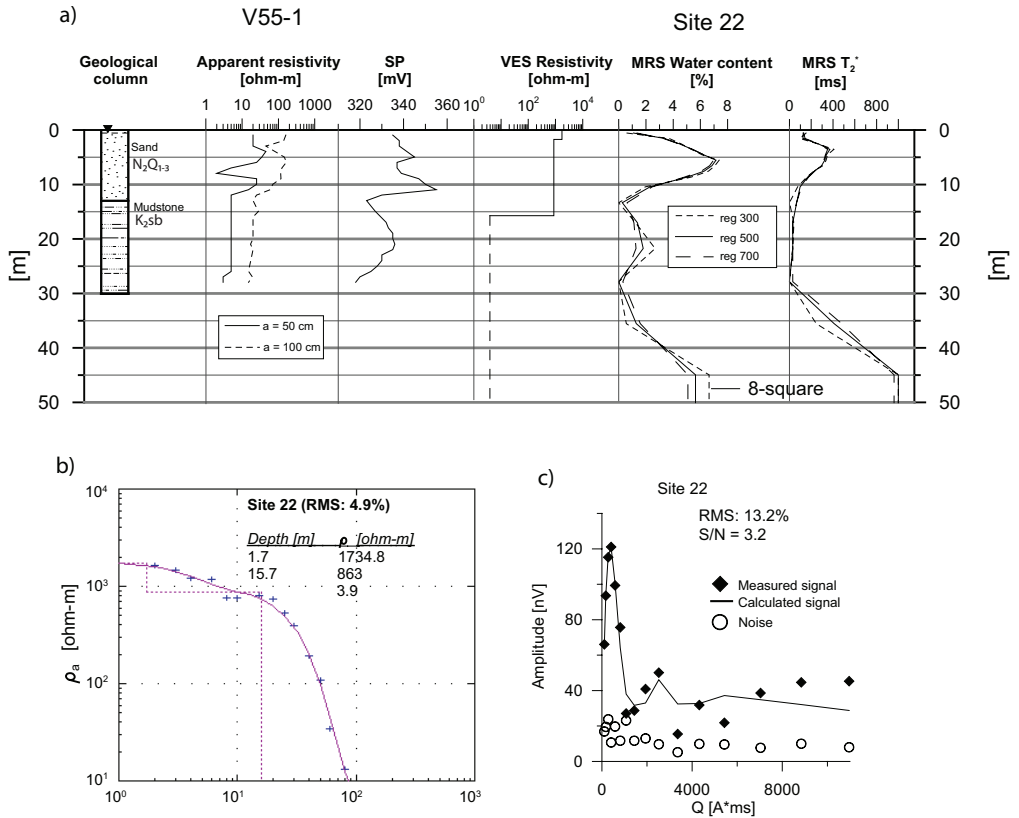
Fig. 4. Examples of raw data from site 22, showing a) the effect of regularization on the MRS model together-er with borehole data , b) VES model fit and c) MRS model fit. Note the poor fit on the MRS model for high pulsemoment.

5.2.1 Identification and Characterization of Geological Structures.

In area 1, the K_2cp is the dominant formation on the western border of the basin, whereas N_2Q_{1-3} is dominant in the central part and the K_2tn in the eastern part (Fig. 5a). The geological cross sections along profile 1 (Long et al., 1986) (Fig. 5) and profile 2 (Fig. 6) in area 1, show the N_2Q_{1-3} and the K_2tn. The N_2Q_{1-3} holds in most parts coarser materials like sand and gravel but also finer sediments like clay and silt. K_2tn on the other hand, is composed of clay and breccia overlying rock salt, with poor potential for hosting aquifers. MRS usually identifies one shallow and one deep aquifer in the N_2Q_{1-3} (Fig. 5 and 6). At some sites the boundary between the shallow and deep aquifer is vague, reflecting one thick aquifer with several peaks in water content (e.g. Site

1; Fig. 5d). The shallow aquifer usually starts a couple of meters below ground with a maximum water content of 4 to 6% at and a thickness of about 10 m. The deeper aquifer generally starts at depth of around 10 to 15 m. The maximum water content is found at 20 to 25 m and the thickness is generally 15 to 20 m. The water content maximum for deep wells varies between 4 and 12%, but is usually about 6 to 8 %. The T_2^* -values range from 100 ms (Site 24, 30 and 31) to 300 ms (Site 3), which corresponds to medium to coarse and gravely sands. The resistivities for these water bearing layers range between 20 and 600 ohm-m. The aquifer floor differs from site to site, but it is usually located around 30 to 50 m in depth, which corresponds well with borehole lithology. The K_2tn is located at depths of 40 to 50 m in the profile 1 (Fig. 5b) and at 30
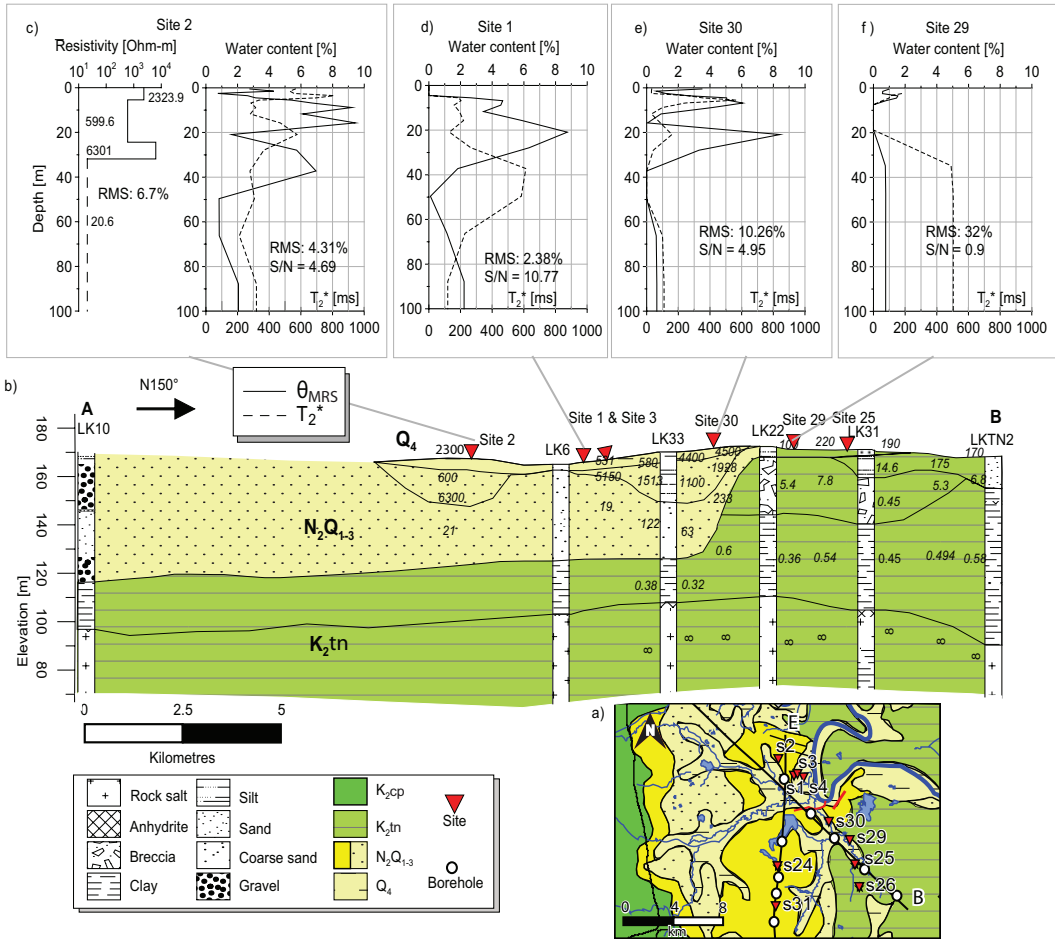
Fig. 5 a) Geological map of Area 1, illustrating the the relative position of sites and boreholes along the profiles. b) Modified geological cross sections AB (profile 1) after Long et al. (1986). VES model, water content and T_2^* data from c) site 2, d) site 1, e) site 30 and f) site 29.

to 50 m depth in the profile 2 (Fig. 6b), with the exception for the south-eastern part in profile 1 (Site 29) where it is found from the surface and downward. It is characterized by very low water contents (Site 29) and resistivities lower than 5 ohm-m (Site 31 and 24, Figs. 6c and d). This is supported by measurement conducted by Long et al. (1986). The K_2tn can not be identified in the VES measurements conducted in the sites 1, 2 and 3. The increase in water content defined from MRS data (>2%) at depth exceeding 50 m can not be explained from borehole lithology.

Area 2 is located in the eastern part of the basin, with the N_2Q_{1-3} as the dominating stratigraphic unit (Fig. 7a). Geological borehole data here is sparse, and no measurement has been conducted

in close proximity to a borehole. However, the compositional change in geology with depth is expressed in the borehole, B-6 (Fig.7a and b). Silt and sand from sedimentary deposits of the N_2Q_{1-3} is dominating in the upper part. At 10 m depth there is a change in composition to siltstone of the K_2sb. This agrees well with the shallow low water content layer in site 6 (Fig. 7b). Here, there is only one water bearing layer extending from the surface down to 10 m, with water content at its maximum of 2.5%. At about 45 meters the siltstone transcend into clay and anhydrite, which generally is associated with the K_2tn. The data from site 5 differs from that of site 6 regarding water content and thickness of the upper water bearing layer, although the distance from site 5 to sites 6 is only about 1.5 km, with no
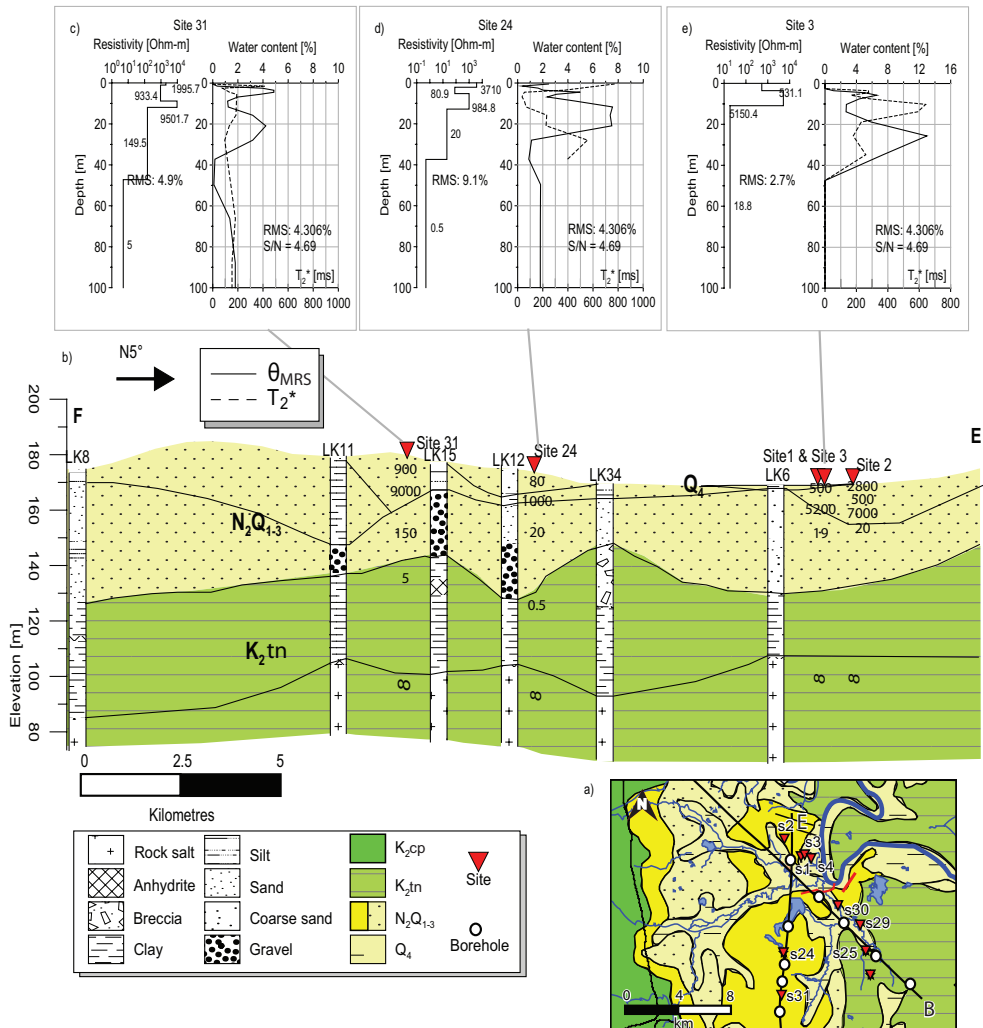
8

Fig. 6 a) Geological map of Area 1, illustrating the relative position of sites and boreholes along the profiles. b) Modified geological cross sections EF (profile 2) after Long et al. (1986). Inverted MRS data presenting θ_{MRS} and T_2^* together with the VES results from c) site 31, d) site 24 and e) site 3.

particular difference in elevation or vegetation. At site 5, a 3 layer aquifer starts at about 5 m depth and continues down to around 35 m with a water content varying between 4 to 8%. The T_2^* varies between 100 to 200 ms for the different peak water content and the aquifer is probably associated with the N_2Q_{1-3}. The resistivity of the two first layers is 6.2 ohm-m and the last water layer has a resistivity of 0.3 ohm-m, which could be an indication of salt affected water. The difference in water content and thickness of the aquifer between site 5 and site 6, could be an indication that the K_2sb becomes more prominent

in the northern part of the area. In the southern part of this area, four sites (8 to 11) (Fig. 7c) are located 500 m apart. The main aquifer extends from about 5 m down to around 20 m (site 9) and to 30 m (site 8, 10, 11). The water content varies between 4 to 8% with a T_2^* of 250 to 300 ms, with the exception of site 10 where the water content is as high as 15% in the main aquifer. The resistivity of the main aquifer in site 9 is modeled to 18 ohm-m. At depth of about 20 m, no water is detected and VES data indicate a low resistive layer of 0.6 ohm-m, which is equivalent to the low resistive clay of the K_2tn in area 1.
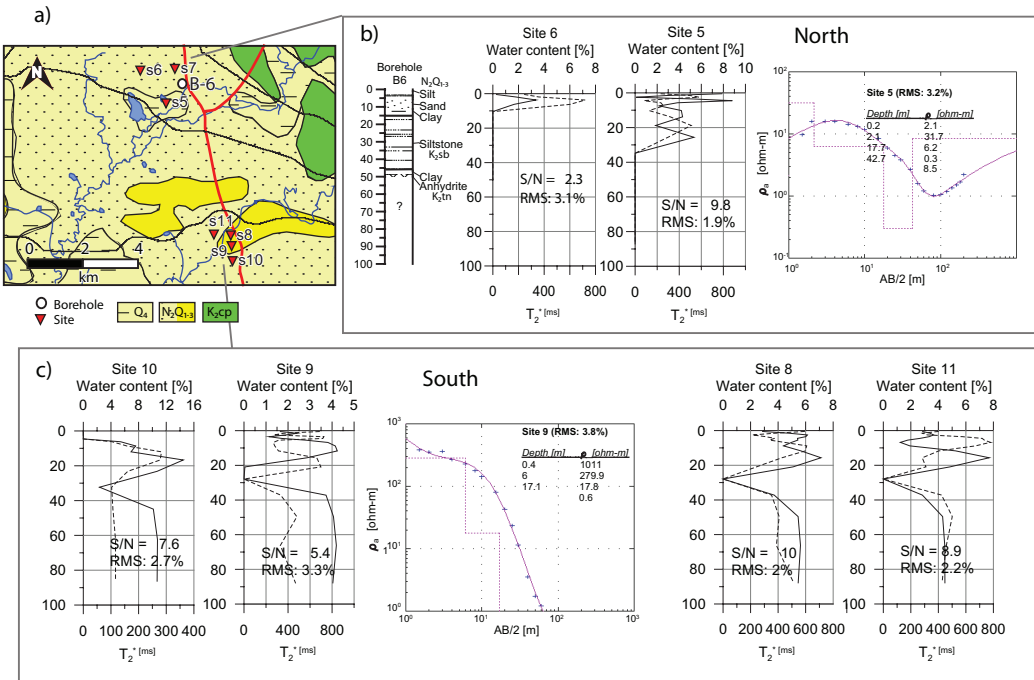
Fig. 7. a) Geological map of Area 2 showing the locations of sites and the location of borehole B-6. Sites 5 to 7 are located in the northern part, whereas sites 8 to 11 are situated in the southern part. **MRS data presenting** θ_{MRS} and T_2^* from b) site 6 and site 5 together with modeled VES and c) site 10, site 9 together with VES model, site 8 and site 11.

The water bearing layer situated beneath 30 m depths cannot be explained from borehole data and might be an artifact created from inversion of the MRS data.

Area 3 is located in the narrowing north part of the Vientiane basin (Figs. 1 and 8a) with the K_2cp in the western and eastern border of the basin, the K_2tn in the north and N_2Q_{1-3} in the central part. The cross section GH (Fig.2 and 8b), compiled from lithology of borehole data (JICA, 1994), together with VES (Fig. 8c) and MRS (Fig. 8d) data gathered from this study illustrates the geophysical soil characteristics of the area. The composition of N_2Q_{1-3}, also here varies from clay to gravel. There are commonly two water bearing layers (Site 20 and Site 16) in the western part, which transcends to one layer (e.g. Site 19; Fig 8d) in the middle of the cross section. The thickness of the N_2Q_{1-3} varies between 40 m in the western part to about 5 to 10 m in the eastern part. The first water bearing layer begins at 1 to 3 m below the ground surface, with a thickness

of 5 to 10 m. The second water bearing layer begins around 10 m with a maximum thickness of 25 m in site 16. The maximum water content is varying between 4 and 16% and T_2^* typically varies between 100 and 400 ms (Fig. 8d), with longer T_2^* in the middle of the basin (Site 15, 16 and 28). The resistivity for the main water bearing layer defined by the maximum water content, varies considerably from site to site but usually ranges between 10 to 250 ohm-m. In the eastern part, about 4000 m along the profile, the composition of the N_2Q_{1-3} changes to more clayey material and the water content is lower than 4% and T_2^* less than 100 ms. The K_2sb underlying N_2Q_{1-3}, consists of mudstone or siltstone and is found as shallow as 5 to 10 m in the eastern part. The water content is here fairly low (<2%), the T_2^* is around 50 to 200 ms and resistivities vary between 10 to 25 ohm-m (Site 12, 23 and 27; Fig 8a). Only one MRS measurement (Site 18; Table 2) has been conducted in the K_2cp where no water was found. Rocks or sediments from the K_2tn have not been observed in any boreholes in area
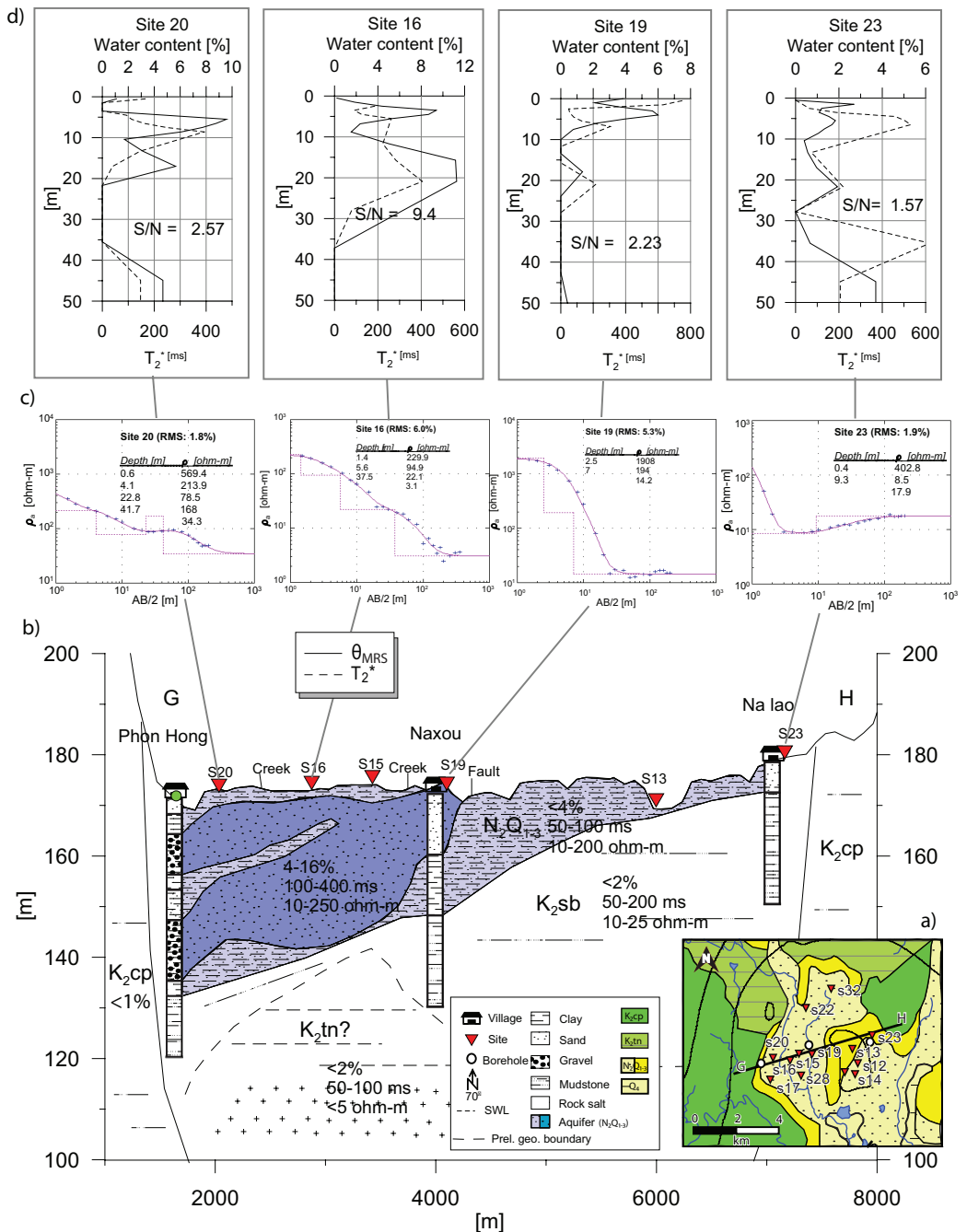
Fig. 8 a) Geological map of area 3 showing the locations of measuring sites together with boreholes relative the profile GH. b) The cross section GH summarizes existing geological information from borehole data, water content, T_2^* and resistivity based on the geophysical measurement with c) VES models and d) θ_{MRS} and T_2^* models from site 20, site 16, site 19 and site 23.

3, but VES measurement from site 15, 16 and 22 in the middle of the basin, show resistivities (<5 ohm-n) at depths of 20 (Site 22; Fig. 8c) to 40 m (Site 16; Fig 8c), that may indicate the existence of this formation as characterized from area 1.

5.2.2 MRS and VES Related to Hydrogeological Parameters

In one single well (in Phon Hong) a continuous pumping test with associated recovery test has been performed (Takayanagi, 1993). This well is located approximately 1000 m from site 17 and 700 m from site 20 (Fig. 11). We have estimated the transmissivity (T_p) using the Cooper-Jacob's method (Fig. 9a) for confined aquifers (Cooper and Jacob, 1946) and the Theis recovery method (Fig. 9b) for confined aquifers (Theis, 1935). T_p has been determined to $8.4*10^{-5}$ and $5.3*10^{-5}$ m²/s respectively, and using these results for site 17

and 20 (Equation 5), results in a C_T of $1.81*10^{-13}$, comparable to sands, clay and limestone (Legchenko et al., 2002). The MRS transmissivity (T_{MRS}) has been calculated using the above C_T for all sites (Table 2) within the same aquifer defined by N_2Q_{1-3}. The T_{MRS} varies usually between 1 and 350 m²/day, depending on site, but in the site 15 in Phon Hong, T_{MRS} reaches 530 m²/day. The transverse resistance (TR) has been calculated for different sites using Equation 6 (Table 2) and compared with the T_{MRS} for the main aquifer in area 3 (Fig.10). The best fit (R²=0.41) is achieved using TR=644.63*T$_{MRS}$$^{0.3591}$.

Fig. 9 Continues pumping test and recovery test from well 1-1, performed by Takayanagi (1993) and interpreted with a) the Cooper-Jacob and b) the Theis recovery method, respectively.

Fig. 10 MRS transmissivity T$_{MRS}$ [m²/day] plotted against transverse resistance, TR [ohm-m²]. The best fit is obtained with TR= 644.63*T$_{MRS}$$^{0.3591}$.
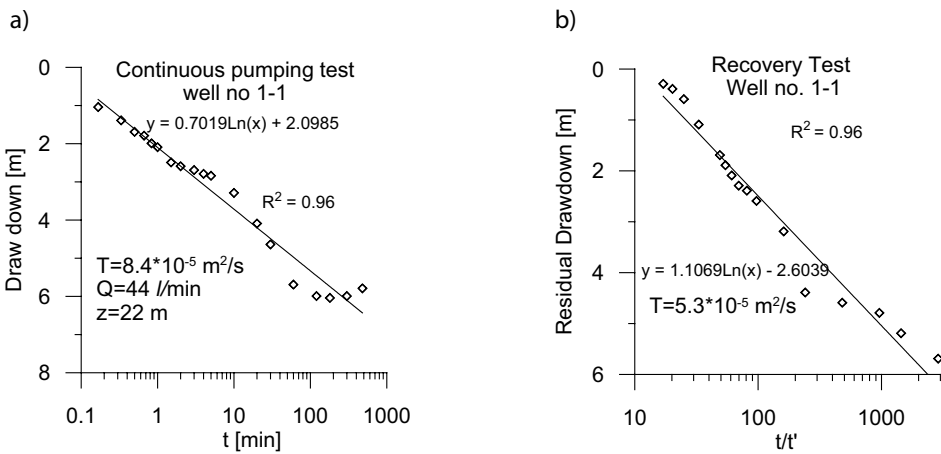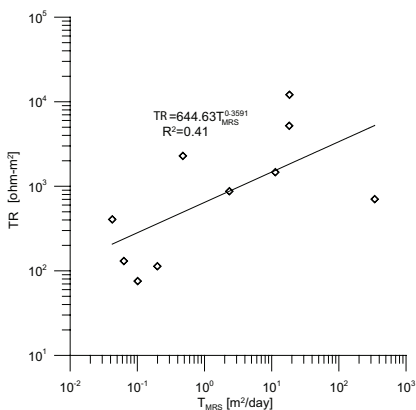
The hydrostatic column (H_w) has been calculated for all sites within the N_2Q_{1-3} (Table 2). It varies between 0.2 and 2.72 m³/m² and has a maximum of 2.72 m³/m² in area 1 (site 2), 2.44 m³/m² in area 2 (site 10) and 2.29 m³/m² in area 3 (site 15)

Interpolated maps of H_w values (Fig. 11a) and T_{MRS} values (Fig. 11b) from area 3 illustrates that high T_{MRS} and H_w values are found in the western part where N_2Q_{1-3} is thick. The transgression to low T_{MRS} and H_w values are found within the thin sediments deposited on top of the K_2sb in the eastern part. The topographic gradient, with the length of the arrows denoting the gradient amplitudes correlates well with increasing T_{MRS} and H_w in the western part. Specific yield (S_y) and specific storage (S_s) have been approximated for the more coarse grained aquifers within the N_2Q_{1-}
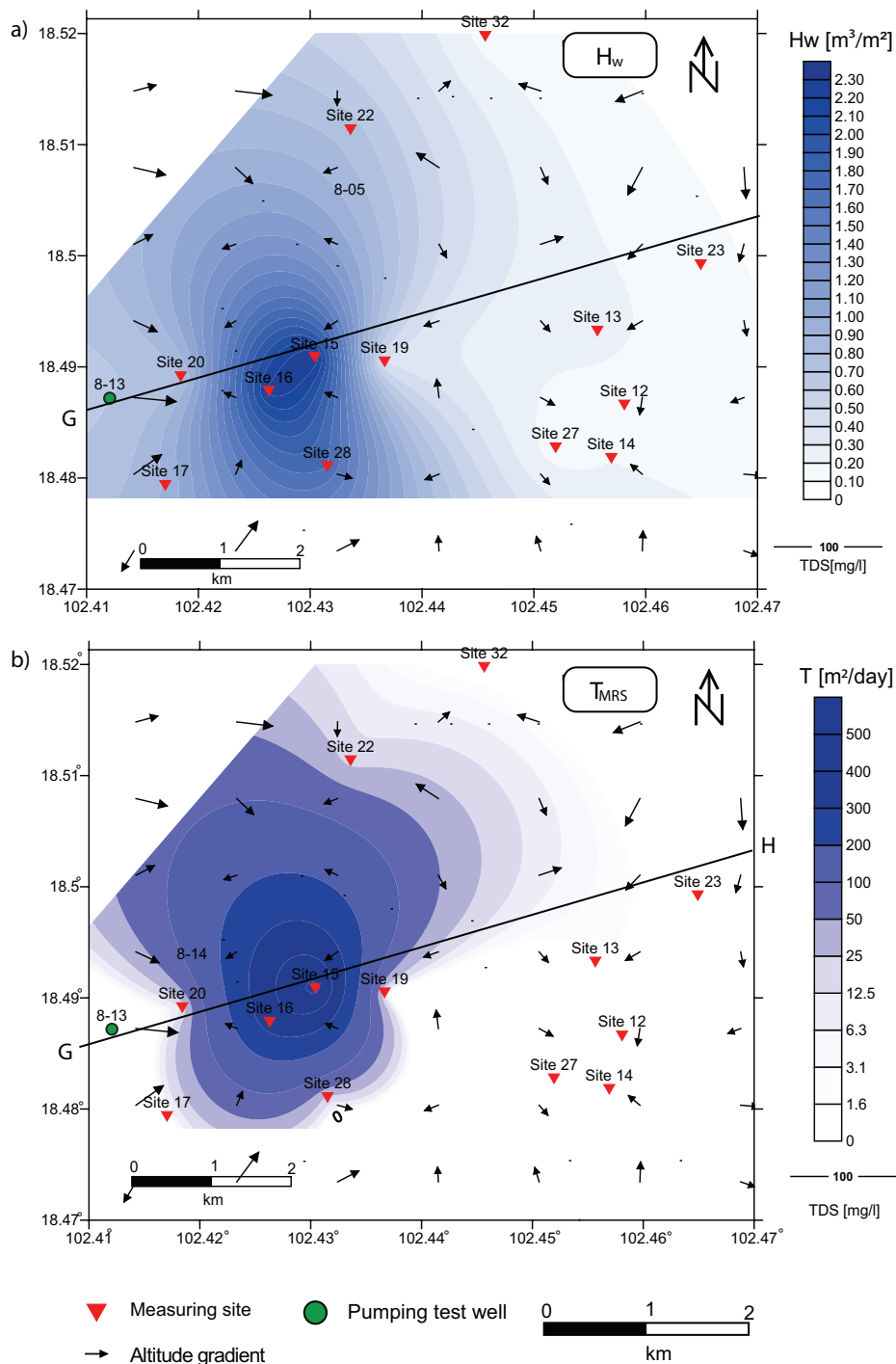
Fig. 11 Interpolated maps of a) H_w and b) T_{MRS} values in area 3. T_{MRS} and H_w values are high in the western part of the map and decreases towards east. The topographic gradient, expressed by the arrows. where the length denotes gradient amplitude, correlates well with T_{MRS} and H_w in the outer western border of the basin. The full drawn line refers to the cross section GH in Fig 8b.

Table 2. *Summary of the most important site characteristics for the sites 1 to 32 with coordinates expressed in WGS84 (Lat/Long). Geology unit, choice of MRS loop design: 100 square, 8-shape or 50 square 2turn, MRS signal to noise (S/N) ratio, resistivity of the main aquifer (ρ), transverse resistance (TR), hydrostatic column (H_w), MRS transmissivity (T_{MRS}), specific yield (S_y), specific storage (S_s) and depth to the aquifer floor.*

Name	North [°]	East [°]	Geology	Loop	MRS S/N	ρ [aquifer]	VES TR	H_w	T_{MRS}	S_y	S_s [*10^-4]	Aq. Floor [m]
Area 1												
Site 1	18.15149	102.59822	N_2Q_{1-3}	100	10.77			1.83	29			42.5
Site 2	18.16318	102.58663	N_2Q_{1-3}	100	4.31	600	x	2.72	214	6.44	1.42	42.5
Site 3	18.15233	102.6011	N_2Q_{1-3}	100	6.27	19	x	2.58	157	9.97	1.59	40.1
Site 4	18.14991	102.60523	N_2Q_{1-3}	100	<2							
Site 24	18.08789	102.5862	N_2Q_{1-3}	100	2.15	20	492	1.52	28			31.9
Site 25	18.08951	102.64348	K_2tn	100	<2							
Site 26	18.07345	102.64638	K_2tn	100	<2							
Site 29	18.10662	102.63969	K_2tn	100	<2							
Site 30	18.11939	102.62428	N_2Q_{1-3}	100	4.95			1.18	19			31.9
Site 31	18.05997	102.58526	N_2Q_{1-3}	100	2.19	150	5277	0.95	1			31.9
Area 2												
Site 5	18.32905	102.65276	N_2Q_{1-3}	100	9.75	6	97	1.18	17			29.5
Site 6	18.34009	102.64332	N_2Q_{1-3}	100	<2							
Site 7	18.34072	102.6558	N_2Q_{1-3}	100	<2							
Site 8	18.28359	102.67604	N_2Q_{1-3}	100	9.94			1.31	72	3.13	1.26	23.9
Site 9	18.2799	102.67656	N_2Q_{1-3}	100	5.38	13	233	0.55	5		1.18	17.9
Site 10	18.27501	102.67675	N_2Q_{1-3}	100	7.6			2.44	342	11.47	1.66	27
Site 11	18.28401	102.6701	N_2Q_{1-3}	100	8.89			1.06	33	4.69	1.34	23.9
Area 3												
Site 12	18.48658	102.45809	N_2Q_{1-3}	100	2.06	34	131	0.15	0			6
Site 13	18.49323	102.45568	N_2Q_{1-3}	100	<2							
Site 14	18.48178	102.45693	N_2Q_{1-3}	100	2.02			0.20	0			13.4
Site 15	18.49086	102.43041	N_2Q_{1-3}	100	3.26	13	255	2.29	533	12.82	1.72	23.9
Site 16	18.48782	102.4263	N_2Q_{1-3}	100	9.44	22	705	2.23	341	8.27	1.51	31.9
Site 17	18.47934	102.41704	N_2Q_{1-3}	8	2.56	76	2292	0.91	0			31.2
Site 18	18.4388	102.39045	K_2cp	2*50	<2							
Site 19	18.49046	102.43666	N_2Q_{1-3}	100	2.63	194	873	0.38	2			10
Site 20	18.48913	102.41842	N_2Q_{1-3}	8	2.57	79	1468	0.77	11			19.1
Site 21	18.56654	102.38577	N_2Q_{1-3}	8/100	2.3	82		0.74	2			30.2
Site 22	18.51135	102.4336	N_2Q_{1-3}	8	3.19	863	12082	0.75	18	4.70	1.34	24.4
Site 23	18.4992	102.46492	N_2Q_{1-3}	8	<2	9	76	0.13				9.1
Site 27	18.48273	102.45195	N_2Q_{1-3}	100	2.07	103	405	0.14	0			6
Site 28	18.48104	102.43152	N_2Q_{1-3}	100	2.82	267	5201	1.70	18			31.9
Site 32	18.51975	102.44565	N_2Q_{1-3}	8	<2	11	113	0.16				8

$_3$. Using Table 1, the specific retention (S_r) and the compressibility (α) can be roughly estimated for a specific water bearing layer according to its T_2^* (Table 1). S_y and S_s can then be estimated using Equation 1 and 2 respectively (Table 2). S_y varies between 3 and 13% ($S_r = 3$) for coarse grained aquifers within the N_2Q_{1-3}. The S_s for coarse grained aquifers is roughly estimated to around 10^{-4}. These values can be compared to area specific values obtained in Thailand, $S_y = 0.15$ and $S_s = 2$ to $3*10^{-3}$ (Srisuk et al., 1999).

6. Discussion

The knowledge of the depth to the halite layers is very important hence the shallower they are situated the greater the risk of increased salinity in the groundwater. Fig. 12 illustrate the distribution of MRS and VES measuring points and borehole data in area 1 together with an interpolated map of halite depths (Long et al, 1986) and the Bouguer gravity anomaly map (Na Wetcharin, 2007). Rock salt can here be found as shallow as at 52 m depth. With reference to the clay layer deposited on top of the halite layer, the depth to the halite is also an estimate of the maximum depth of the
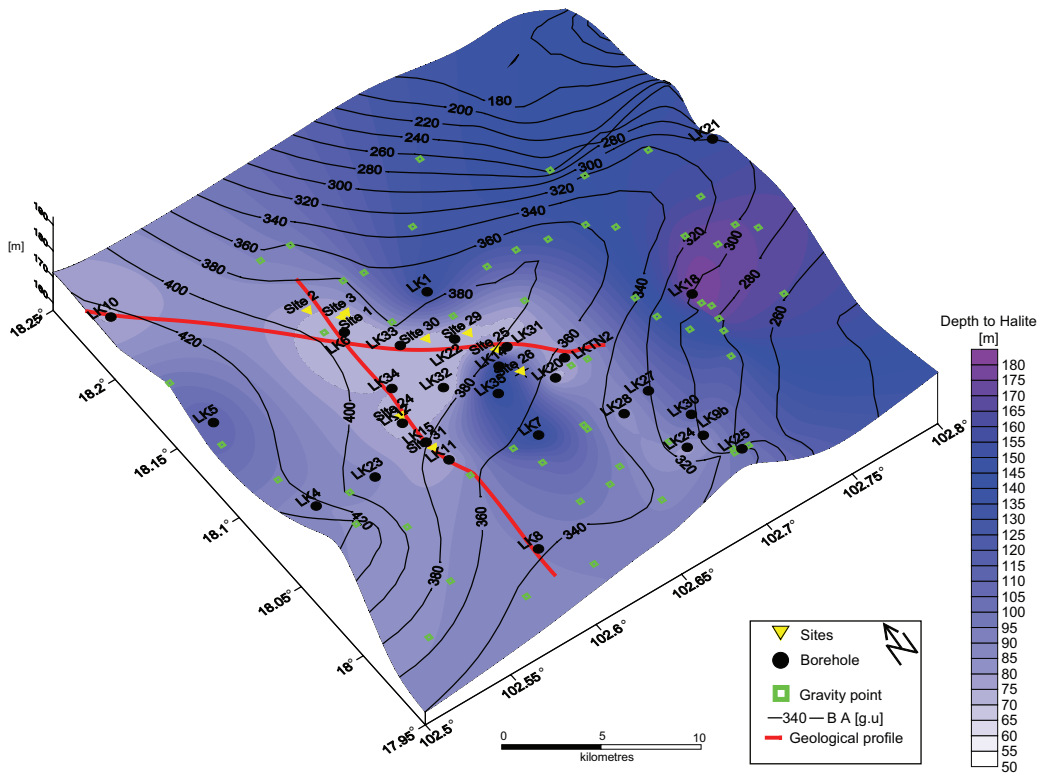
Fig. 12 Interpolated map of the depths down to the halite layer obtained from borehole data (Long et al., 1986) in the southern part of the Vientiane basin (see Fig. 2) together with gravity data collected by Na wetcharin (2007). The depths agree well with MRS and VES interpreted depths from area 1.

aquifer, which is defined by MRS. The gravity anomaly map shows that the regional gravity field generally decreases from west to east. However, there is a local maximum, which correlates well with the shallow halite depths. This is probably an indication of an uplift of the higher density basement rock, where the upper part of K_2tn has undergone erosion and been replaced by younger sediments of N_2Q_{1-3}. This supports a shallower halite layer here as compared with the eastern part of the area. The shape of the halite structure is difficult to determine due to the sparse gravity data.

Rock salt has a relatively high resistivity compared to the overlaying materials, but it would be difficult to identify it with VES since the current probably will not be able to penetrate through the superimposed conductive clay. However, the low resistive clay layer, sometimes lower than 1 ohm-m, could work as an indicator of halite or

at least an indicator of the Thangon formation (K_2tn). These low resistivities can be found in all three areas at depths of 20 to 50 m, and they are always related with very low water contents. Table 3 roughly summarizes the geophysical characteristics obtained in our study for some of the geological formations and stratigraphic units in the region. Our MRS and VES data verify earlier hydrogeological investigation made by Takayanagi (1993) and recognize N_2Q_{1-3} as the main water bearing unit. This unit can be found in all three areas and it is characterized by relatively high water contents, up to 16 %, and with decay times varying between 100 and 400 ms, which suggests a mean pore size equivalent to medium sand to gravel. The resistivity of the aquifer is highly variable, but usually around 10 to 100 ohm-m, suggesting fresh water (Palacky, 1987). The K_2sb has similar MRS characteristics as the K_2tn, i.e. low groundwater potential, but has generally higher resistivity and is usually

Table 3. *A rough summery of typical geophysical parameter like water content (θ_{MRS}), decay time (T_2^*) and resistivity (ρ) for different water bearing units in the Vientiane basin.*

Formation	Rock Material	θ_{MRS} [%]	T_2^* [ms]	ρ [ohm-m]	Comment
Q_4	Sand			450 - 4500	Dry top layer, with a thickness of ca 0.5 m
	Silt				
N_2Q_{1-3}	Silt	4-16	100 - 400	10-250	Main aquifer in the area, usually between 10 and 50 m thick, with highly varying water content.
	Sand				
	Coarse Sand				
	Gravel				
K_2sb	Claystone	<2	100	10-25	Impervious layer with little or no water. Mostly found in area 2 and 3.
	Siltstone				
K_2tn	Breccia	1 - 2.5		0.5 - 8	Impervious layer with little or no water. Find throughout the whole study area. Lower resistivity and water content than K_2sb.
	Clay			0.3 - 0.6	
	Anhydrite				
	Halite			10^6	
K_2cp	Sandstone	<1			Little or no water. Mostly found in outer border of the basin

located closer to the surface, which makes it possible to delineate it from the K_2tn.

The MRS water content (θ_{MRS}) and decay time (T_2^*) are seldom coherent and show often a reverse proportional relationship. That is, when θ_{MRS} is low, T_2^* is usually long. This can be explained by the low initial amplitude that creates an almost horizontal exponential fit of the relaxation, hence creating an artificial long T_2^*. The increase in water content below the non water bearing layer identified as clay of the K_2tn is more difficult to explain. Geological data from boreholes suggests that only mudstone, clay or halite should be found at these depths, which in turn imply little or no water. During large pulse moments, water in shallow aquifers can generate signals equivalent in amplitude to water from deeper aquifer (>40m), creating artifacts of the kind in Fig 5 and Fig. 6 and Fig. 7 (Legchenko, 2005).

The depth of penetration for MRS can be estimated from the skin depth (δ),

$$\delta = 503 \cdot \sqrt{\rho / f} \qquad (7)$$

where the amplitude of the signal has been reduced to 37 %. ρ is the resistivity of the medium and f is the frequency of the transmitted signal. The δ has been estimated for both the water bearing layer as well as for the high conductive layer usually found beneath. The δ determined for the main water bearing layer at different sites (Fig. 13a) show that δ varies in most cases between 35 to 180 m (10 < ρ < 250 ohm-m). The confining layer underlying the aquifer have δ varying between 6 and 150 m (0.3 < ρ < 170 ohm-m). The low resistive layer (Fig. 13b) in the K_2tn sometimes located beneath N_2Q_{1-3} has a δ of 10 to 20 m (0.5 < ρ < 3 ohm-m), hence, it would be difficult to detect an aquifer beneath this layer, which supports the theory of an artifact in the water content model below the main aquifer. Modelling results for a 100 m square loop (Fig. 13c) using the numerical modelling software Samogon (Legchenko, 2001) for a 10 m thick water layer with 10% water content, T_2^*=150 ms, at different depths illustrates the detection limit for different resistive half spaces. The geomagnetic field is set to 43800 nT, with an inclination of 24° corresponding to the conditions in the Vientiane basin. The noise threshold is set to 10 nV. The response of the 100 ohm-m and 50 ohm-m water bearing layers are almost identical, indicating that the difference in these resistivities have little effect on the amplitude of the signal. The difference becomes more significant for lower resistivities. For a 1 Ohm-m halfspace, water can be detected down to about 35 m. In our measurement, the noise level is often higher and the amount of water is in many cases lower than 10%.

Transverse resistance is probably not a good parameter to determine aquifer transmissivity in
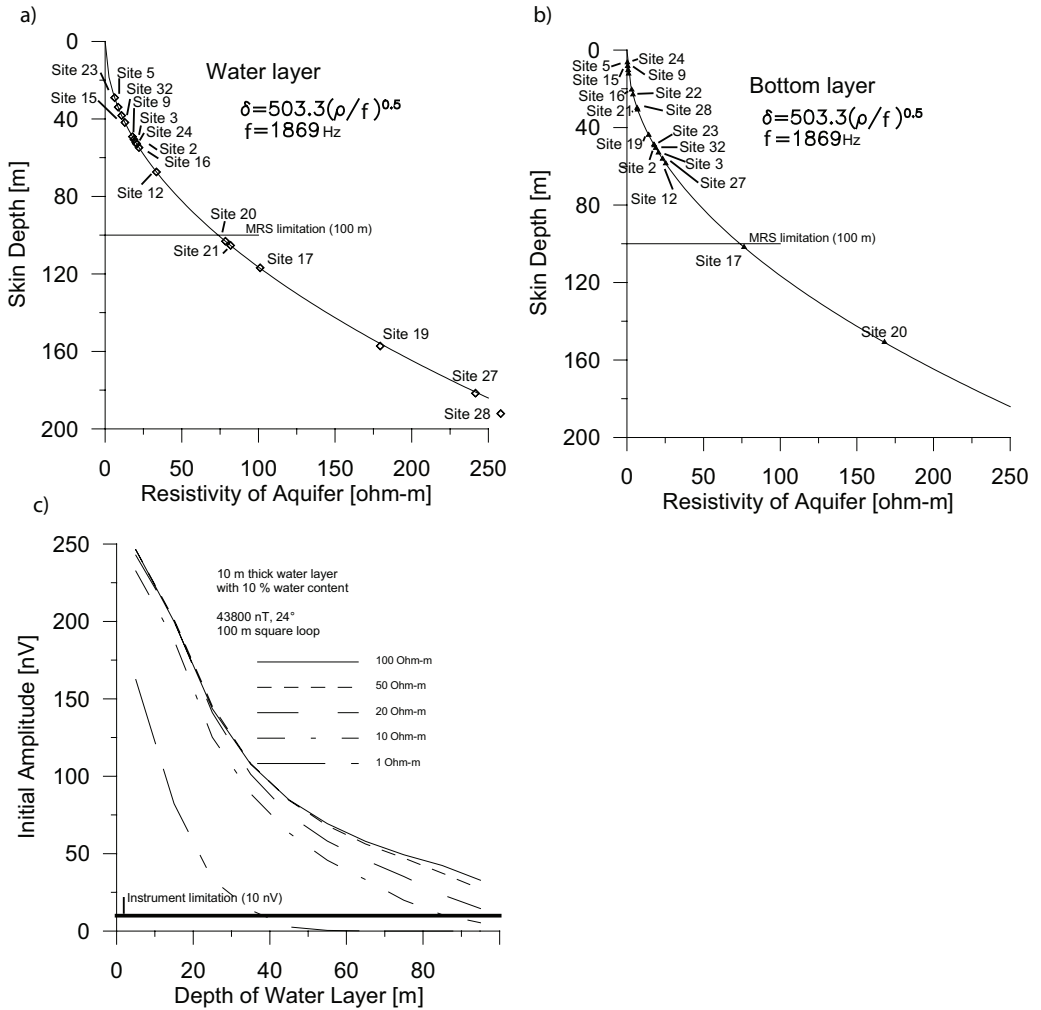
Fig. 13 Skin depths from all VES sites of a) the main aquifer b) the bottom layer, together with c) modeled amplitudes for a 10 m thick water layer with a water content of 10% located at different depths for different resistivities.

the Vientiane Basin, since the aquifer resistivity differs a lot from one site to another.

Since T_2^* repeatedly shows a reverse proportional relationship to θ_{MRS}, transmissivity for low water content layers are often overestimated. However, if letting the T_2^* value for the highest water content layer represent the whole aquifer, it might give a more reliable transmissivity estimate. Rough S_y and S_s estimates for N_2Q_{1-3} correlates quite well with typical values for corresponding Thai unit, determined by Srisuk et al. (1999), although the tabled values for S_R and α for the same type of material varies a lot.

7. Conclusions

The physical conditions in the Vientiane basin, Laos, with small variations in the magnetic field, low magnetic susceptibility of the rocks and sediments and fairly low noise, make MRS a suitable method for groundwater exploration here. MRS demonstrated to be a good tool to identify and characterize aquifers in different geological environments. Where the MRS Signal to noise ratio was too low for a reliable interpretation, MRS and VES together proved to decrease the uncertainty in the interpretation.

Moreover MRS has also shown to be a powerful tool in constraining layer thickness and to identify water layers with medium resistivity in between high and low resistive structures in the VES interpretation (e.g. site 9 and site 16). MRS also helps distinguishing between medium resistive layers of impermeable rock from what could have been interpreted as water if only VES measurements had been carried out.

MRS and VES recognized the stratigraphic unit N_2Q_{1-3}, consisting of alluvial unconsolidated sediments, as the main water bearing unit. The result from the MRS measurements show that within the region there is usually one to two water bearing layers. The aquifer thickness varies between 10 to 40 m and the depth to the main aquifer range from 5 to 15 m. The water content is here relatively high, up to 16 % and decay times varying between 100 and 400 ms, suggesting a mean pore size equivalent to medium sand to gravel. The resistivity of the aquifers is usually between 10 to 100 ohm-m suggesting that the water is fresh. MRS and VES also identify an underlying confining clay layer usually situated between 30 to 50 m depth. Since this clay is most probably related to halite layers and has a resistivity as low as 0.5 ohm-m, it is likely that it is affected by the salt. The clay layer might serve as an indicator of halite, and it probably works as a salinity barrier for the overlying aquifers. Hence, as a future drilling guidance in the Vientiane Basin, one should not drill deeper than 30 to 40 m in area1, 20 to 30 m in area 2 and 20 to 30 m in area 3.

Acknowledgements

References

Allen, D., Andreani, M., Badry, R., Flaum, C., Gossenberg, P., Horkowitz, J., Singer, J., White, J. 1997. How to use borehole NMR. Schlumberger's Oilfield Review summer, 34–57.

Archie, G.E., 1942. The electrical resistivity as an aid in determining some reservoir characteristics. Metallurgical and Petroleum Engineers 146, 54–62.

Cooper, H.H. and Jacob, C.E., 1946, A generalized graphical method for evaluating formation constants and summarizing well field history, American Geophysical Union Transactions, v. 27, pp. 526–534.

Domenico P.A., Mifflin, M. D.1965. Water from low-permeability sediments and land subsidence. Water Resources Research, vol. 1, no. 4, pp.563-576.

Hamill, L., Bell, F.G. 1986. Groundwater Resource Development, Buttersworth, London, p.344.

Japan International Cooperation Agency (JICA), 1994. Drilling logs from the "Vientiane Province Groundwater Development Project". JICA local office in Phon Hong, Vientiane Province, Laos.

Johnson, A. I. 1967. Specific yield- Compilation of specific yields for various materials. U.S. Geological Survey Water-Supply Paper 1662-A.

Kirsh Reinhard (Editor). 2006. Groundwater Geophysics: a Tool for Hydrogeology. Springer –Verlag Berlin Heidelberg 2006, pp. 493.

Legchenko A., 2001 –Samogon, v4.041. Program of numerical modeling of surface magnetic resonance sounding.

Legchenko, A. 2005. Improved modelling of the magnetic resonance signal in the presence of shallow aquifers. NEAR SURFACE GEOPHYSICS 3 (3): 121-130 AUG 2005.

Legchenko, A. 2006. MRS Measurements and Inversion in Presence of EM noise. In: 3rd Magnetic Resonance Sounding Workshop, Spain, Madrid 25-27 October 2006.

Legchenko, A., Baltassat, J.M., Beauce, A., Bernard, J., 2002. Nuclear magnetic resonance as a geophysical tool for hydrogeologists. Journal of Applied Geophysics 50 (1–2), 21–46.

Legchenko A., Valla P. 2002, A review of the basic principles for proton magnetic resonance sounding measurements. Journal of Applied Geophysics 50, 3 – 19

Legchenko A., Valla P. 2003. Removal of power-line harmonics from proton magnetic resonance measurements, Journal of Applied Geophysics 53 (2003) 103– 120.

Legchenko A., Shushakov O. (1998). Inversion of surface NMR data Geophysics, Volume 63, Issue 1, pp. 75-84

Long, N. X., Lam N. X., Canh, N. D. 1986. Report on Geological data for Potassium and Manganese in Thangon Region, Dong Bang, Vientiane, 1986. Department of Geology and Mining, Vientiane, Laos.

Lovatt Smith, P. F., Stokes, R B., Bristow, C., Carter, A. 1996. Mid-Cretaceous inversion in the northern Khorat Plateau of Lao PDR and Thailand. Tectonic evolution of Southeast Asia ; Geological Society Special Publications, vol.106, pp.233-247.

Lubczynski M., Roy J. 2003. Hydrogeological interpretation and potential of the new magnetic resonance sounding (MRS) method. Journal of Hydrology Volume 283, Issues 1-4, 10th December 2003, Pages 19-40

Maillet, R. 1947. The fundamental equations of electrical prospecting. Geophysics, vol.12, no.4, pp.529-556, Oct 1947

Medlicott, K. 2001. Water, sanitation and environmental health in rural Laos PDR. KAP Study for UNICEF, WES Section, August 2001, 20 pp.

Morris, D.A. and Johnson, A.I. 1967. Summary of Hydrologic and Physical Properties of Rock and Soil Materials as Analyzed by the Hydrologic Laboratory of the U.S. Geological Survey 1948-1960. US Geol. Surv. Water Supply paper, 1839-D, p.42.

Na wetcharin, S. 2007. Gravity Anomalies in Vientiane Capital, Lao PDR. 2007. Department of Physics, Faculty of Science, Prince of Songkla University, Hatyai, Thailand, pp. 85.

Niwas, S. and Singhal, D.C., 1981. Estimation of aquifer transmissivity from Dar-Zarrouk-parameters in porous media. J. Hydrol., 50: 393--399.

Palacky, G. J., 1987. Clay mapping using electromagnetic methods. First break, 5, pp. 295-306.

Parasnis, D.S. 1997. Principles of Applied Geophysics. 5th edition. Chapman and Hall, London, UK, p.429.

Ponzini, G., Ostroman, A. and Molinari, M., 1984. Empirical relation between electrical-transverse resistance and hydraulic transmissivity. Geoexploration, 22: l-15.

Salem H.S. 1999. Determination of fluid transmissivity and electric transverse resistance for shallow aquifers and deep reservoirs from surface and well-log electric measurements. Hydrology and Earth System Sciences, vol.3, no.3, pp.421-427, Sep 1999.

Shirov, M., Legchenko, A., Creer, G. 1991. New direct non-invasive ground water detection technology for Australia. Explor.Geophys. 22, 333–338.

Srisuk, K., Sriboonlue, V., and Buaphan, C. 1999. Groundwater flow, saline water and saline soils in the Central Khorat Basin, northeast Thailand. Symposium on Mineral, Energy and Water Resources of Thailand: Towards the year 2000. 238-251.

Sundberg, K., 1932. Effect of impregnating waters on electrical conductivity of soils and rocks. Trans. AIME 97: 367-391.

STEA, State of the Environment Report. 2001: Lao People's Democratic Republic. UNEP, RRC.AP. 2001. URL: http://www.rrcap.unep.org/reports/soe/laosoe.cfm (2007-03-25)

Stuart-Fox, M., Rooney, D.F. 2006. Microsoft Encarta 2006.

Tabakh El. M., Utha-Aroon C., Schreiber B.C. 1999. Sedimentology of the Cretaceous Maha Sarakham evaporites in the Khorat Plateau of northeastern Thailand. Sedimentary Geology, Volume 123, Number 1, January 1999, pp. 31-62(32).

Takayanagi, K. 1993. Basic Design Study Report on the Project for Groundwater Development in Vientiane Province in Lao People's Democratic republic. Japan International Cooperation Agency (JICA), pp.

Theis, C.V., 1935. The relation between the lowering of the piezometric surface and the rate and duration of discharge of a well using groundwater storage, Am. Geophys. Union Trans., vol. 16, pp. 519-524.

Velpen, V. 1988. Resist87: a computer prcessing packaged for dc Resistivity interpretation. M.sc. thesis, ITC-Delft, The Netherlands.

Vouillamoz, J.M., Chatenoux, B., Mathieu, F., Baltassat, J.M., Legchenko, A. 2007. Efficiency of joint use of MRS and VES to characterize coastal aquifer in Myanmar. Journal of Applied Geophysics, Volume 61, Issue 2, February 2007, Pages 142-154

Vouillamoz, J.M., Descloitres, M., Bernard, J., Fourcassier, P., Romagny, L. 2002. Application of integrated magnetic resonance sounding and resistivity methods for borehole implementation; a case study in Cambodia. Journal of Applied Geophysics, vol.50, no.1-2, pp.67-81, May 2002.

Wannakomol, A. 2005. Soil and Groundwater Salinization Problems in the Khorat Plateau, NE Thailand, Integrated Study of Remote Sensing, Geophysical and Field Data. Fachbereich Geowissenschaften, Freie Universität Berlin. http://www.diss.fu-berlin.de/2005/210/indexe.html

Williamson, D R, Peck, A J.Turner, J V.,Arunin,S.1989. Groundwater hydrology and salinity in a valley in Northeast Thailand. Groundwater contamination IAHS-AISH Publication, vol.185, pp.147-154

Worthington, P.F., 1993. The uses and abuses of the Archie equations, 1: The formation factor-porosity relationship. J.Appl. Geophys., 30:215-228.

WRI, 1998. 1998-1999 World Resources: A Guide to the Global Environment, World Resource Institute, Oxford. University Press, New York.

Yaramanci U., Lange G., Hertrich, M. 2002. Aquifer characterisation using Surface NMR jointly with other geophysical techniques at the Nauen/Berlin test location. Journal of Applied Geophysics 50 (2002) 47– 65

Yaramanci, U. 2004. New technologies in ground water exploration; surface nuclear magnetic resonance. Geologica Acta, vol.2, no.2, pp.109-120.

II

Perttu N., Wattanasen K., Elming S-Å., Phommasone K. 2008.

**Determining Water Quality Parameters of Aquifers
in the Vientiane Basin, Laos,
Using Geophysical and Water Chemistry Data**

(Manuscript)

Determining Water Quality Parameters of Aquifers in the Vientiane Basin, Laos, Using Geophysical and Water Chemistry Data

Nils Perttu[1,*], Kamhaeng Wattanasen[2], Sten-Åke Elming[1], Khamphouth Phommasone[3]

[1]*Division of Ore Geology and Applied Geophysics, Luleå University of Technology, SE-971 87 Luleå, Sweden*

[2]*Department of Physics, Faculty of Science, Prince of Songka University, HatYai, 90112 Thailand*

[3]*Department of Physics, National University of Laos, P.O. Box 7322, DongDok Campus Vientiane, Lao PDR*

*Corresponding author: Nils.Perttu@ltu.se, Tel: +46-920-491884, Fax: +46-920-491199

Abstract

The aim of this study is to test the possibility of using MRS and VES together with groundwater chemistry data to distinguish freshwater aquifers from salt affected groundwater and moreover determine water quality parameters directly from geophysical data. Three study areas within the Vientiane basin, including 32 sites and 28 sampled wells have been chosen for the study. The combination of MRS and VES allows distinguishing between the main fresh water bearing unit N_2Q_{1-3} from the salt affected clay layer of K_2tn in all three investigated areas. N_2Q_{1-3} is characterized by relatively high water contents, up to 16 %, and decay times, suggesting a mean pore size equivalent to medium sand to gravel. The resistivity is highly variable, but usually above 10 ohm-m, suggesting predominantly fresh water in the aquifers according to the European drinking water standards (EC= 1500 µS/cm ≈ 6.66 ohm-m). The high conductive clay layer overlying the rock salt of the Thangon formation can be found in all three areas on depth of 20 to 50 m characterized by low water content and resistivity lower than 5 ohm-m.
Several approaches have been used to establish the relationship between the water conductivity collected from wells and the aquifer conductivity determined from VES, including Archie's law. However, the best correlation is achieved using a linear fit between VES conductivity and water conductivity for deep wells (EC[µS/cm]= 0.3821VES[µS/cm], R^2=0.81). Conductivity from shallow wells does not show any relation to VES conductivity (R^2=0.09). This is probably because deep wells usually have higher conductivity than shallow wells and hence contributing more to the aquifer conductivity. Interpolated maps of TDS from deep wells together with maps of the conductivity of the bottom layer, aquifer layer, MRS transmissivity and hydrostatic column indicates that the salt originate from the underlying layer situated beneath the main aquifer. The water quality parameters affecting the water conductivity most are TDS, hardness and chloride, for which all have shown to have a high correlation to the EC of water, and thus VES conductivity. This makes MRS and VES a very promising tool for guidance of future drillings and water quality estimation.

Keywords: magnetic resonance sounding; vertical electrical sounding; resistivity; conductivity, salinity, groundwater quality; Vientiane basin, Laos; Khorat Plateau.

1. Introduction

When evaluating aquifers for drinking water usage, quality of groundwater is as important as its quantity. In Lao People's Democratic Republic (Laos) located in the middle south-east Asia (Fig. 1), only 60% of the urban and 51% of the rural population had direct access to water supply in 1998 (UNEP, 2000). Most Lao people live in rural parts and are heavily dependent on dug wells as their main water source. However deep wells, river water and rainwater are also used (Medlicot, 2001). Dug wells usually dry out during the dry period and in addition, water-borne diseases caused by infiltrations of domestic waste and excreta from farm animals, have

lead to a high morbidity rate (Medlicot, 2001; Takayanagi, 1993). There are small topography differences in the Vientiane basin, which makes it difficult to evaluate the groundwater potential from the visible physical environment. In 1993 the "Project for Groundwater Development in Vientiane Province" was implemented by Japan International Cooperation Agency (JICA), aiming at raising the water supply ratio in the rural areas by drilling deep wells (Takayanagi, 1993). In total 118 deep wells were drilled and when evaluating the project in year 2000, as much as 60% of the wells were not used for drinking due to bad water quality or maintenance problem (JICA, 2000). The bad water quality was mainly due to salt in the groundwater. Rock
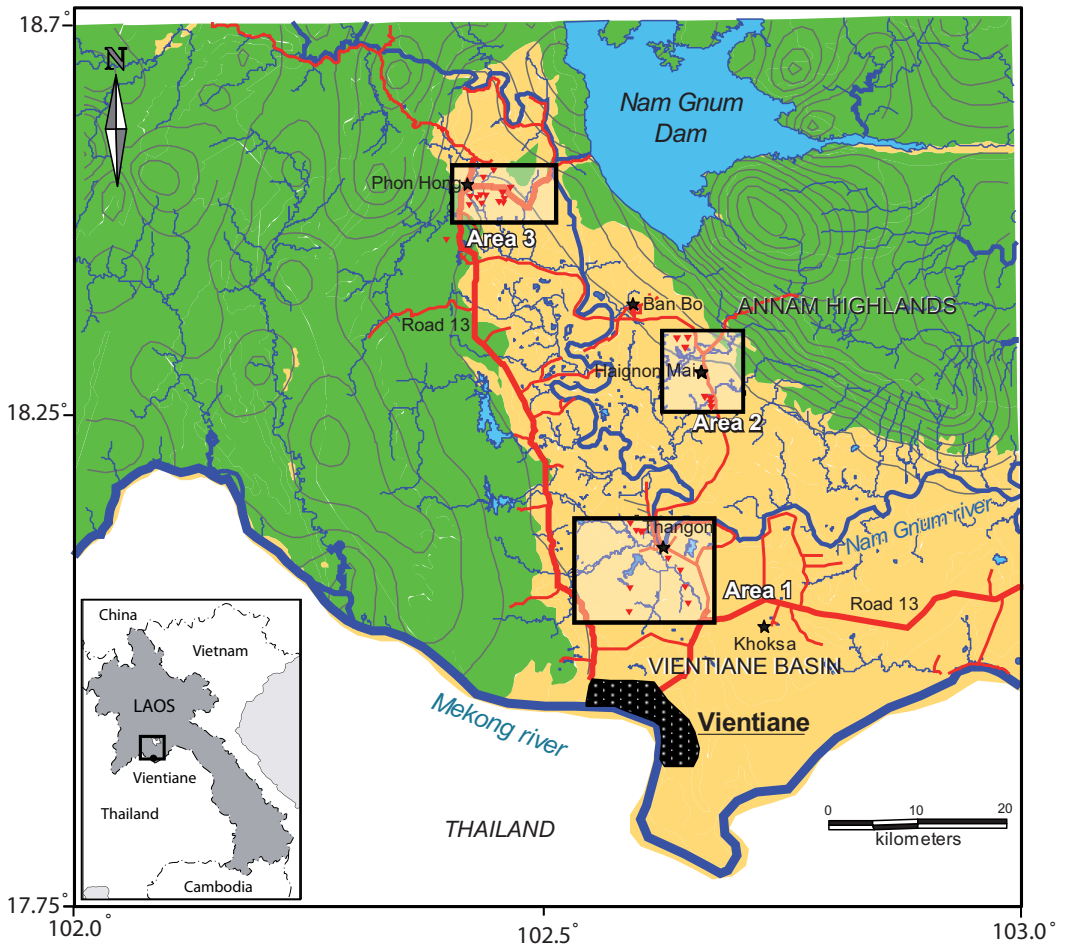

Fig. 1. The Vientiane Province, with the Vientiane Basin located in the drainage basin of Nam Gnum and Mekong river. The three study areas defined with rectangles.

1

salt is naturally occurring within the basin as shallow as 50 m depth in the Thangon formation (Takayanagi, 1993; Wannakomol, 2005; Srisuk et al., 1999 and Williamson et al., 1989).

The aim of this study is to test the possibility of using geophysical techniques to distinguish freshwater aquifers from salt affected groundwater and furthermore explore the possibility to determine the quality of the groundwater directly from geophysical parameters. This we do by combining Magnetic Resonance Sounding (MRS), Vertical Electrical Sounding (VES) and water chemistry data from groundwater in different geological environments in the Vientiane Basin. Resistivity methods have been widely used to characterize aquifers as there is a direct relationship between hydraulic and electric parameters governed by electric conduction through porous media and fluid flow (Sundberg, 1932; Archie, 1942; Worthington, 1993). Moreover, the conductivity also reflects the salinity of the water. However, it is not possible to distinguish high conductive groundwater from e.g. increased clay content. MRS is based on the principal of Nuclear Magnetic Resonance (NMR) and gives a direct image of the water content of the ground and hence the vertical distribution of an aquifer. By combining MRS with VES, salt affected groundwater could be distinguished from high conductive sediments and freshwater aquifers. Similar MRS and VES investigations have been made in Cambodia and in Burma (Vouillamoz et al., 2002 and 2007), but with more emphasis on hydraulic characterization of the aquifers.

2. The Vientiane Basin

The Vientiane Province is located in central Laos (Fig. 1), between latitude 18° and 18.7° and longitude 102° and 103°. The central part of the province is situated in the drainage basin of the Nam Ngum and Mekong rivers and the average elevation of the area is 170 to 190 m. This fertile flat low-land is mainly used for agriculture with big irrigation systems. The surrounding mountain area is covered by forests and the elevations in the area range up to 1600 m. Laos has a tropical monsoon climate with a rainy season from May to October, followed by a cool dry season from November to February and a hot dry period from March to April. The average rainfall is about 1 780 mm, but it varies regionally. The temperature ranges from as high as 40°C in the Mekong lowlands during the hot months to as low as 5°C in the mountain area in the winter (Stuart-Fox and Rooney, 2006).

2.1 Geology

The Vientiane Basin is located in the very northern part of the Sakhon Nakhon Basin within the Khorat Plateau (Fig. 2). The Plateau covers an area of 170000 km^2 between latitudes 101° and 106° and longitudes 14° and 19° in the region of north-eastern Thailand and central Laos. During the Cretaceous, due to relative sea-level rise, the plateau underwent periods of marine influx but was sporadically isolated from the oceans. This created the Maha Sarakham formation, a three layer salt unit separated by red-coloured siliciclastics of fluvial origin. The evaporites include thick successions of halite, anhydrite and potassic minerals like sylvite and carnalite (Tabakh, et al 1999) and can be found as shallow as at 50 m depth.

The equivalent to the Maha Sarakham Formation in the Vientiane Basin is the 550 m thick, middle Cretaceous, Thangon formation (K_2tn). It is most easily found in the south-eastern part of the Vientiane Basin (Long et al, 1986), where the salt structures have been mobilized into pillows and small diapers (Lovatt Smith et al., 1996). The K_2tn is overlain by the Saysomboun formation (K_2sb) (not in map). This formation originates from upper Cretaceous and is composed of red-brown claystone that gradually changes to siltstone with a maximum thickness of 150 m. The K_2sb is mainly found in the northern part of the basin. This formation is overlain by the Vientiane formation (N_2Q_{1-2}) (<70 m) of Neogene to Quaternary origin and the stratigraphic units Q_{2-3} (<25 thick) and Q_4 (<0.5 m thick) of Quaternary origin. N_2Q_{1-2} and Q_{2-3} have similar characteristics and will be treated as one stratigraphic unit in this paper (N_2Q_{1-3}). The N_2Q_{1-3} unit is an alluvial deposit locally found in abandoned river channels, containing mostly gravel, sand and clay. The possibility for
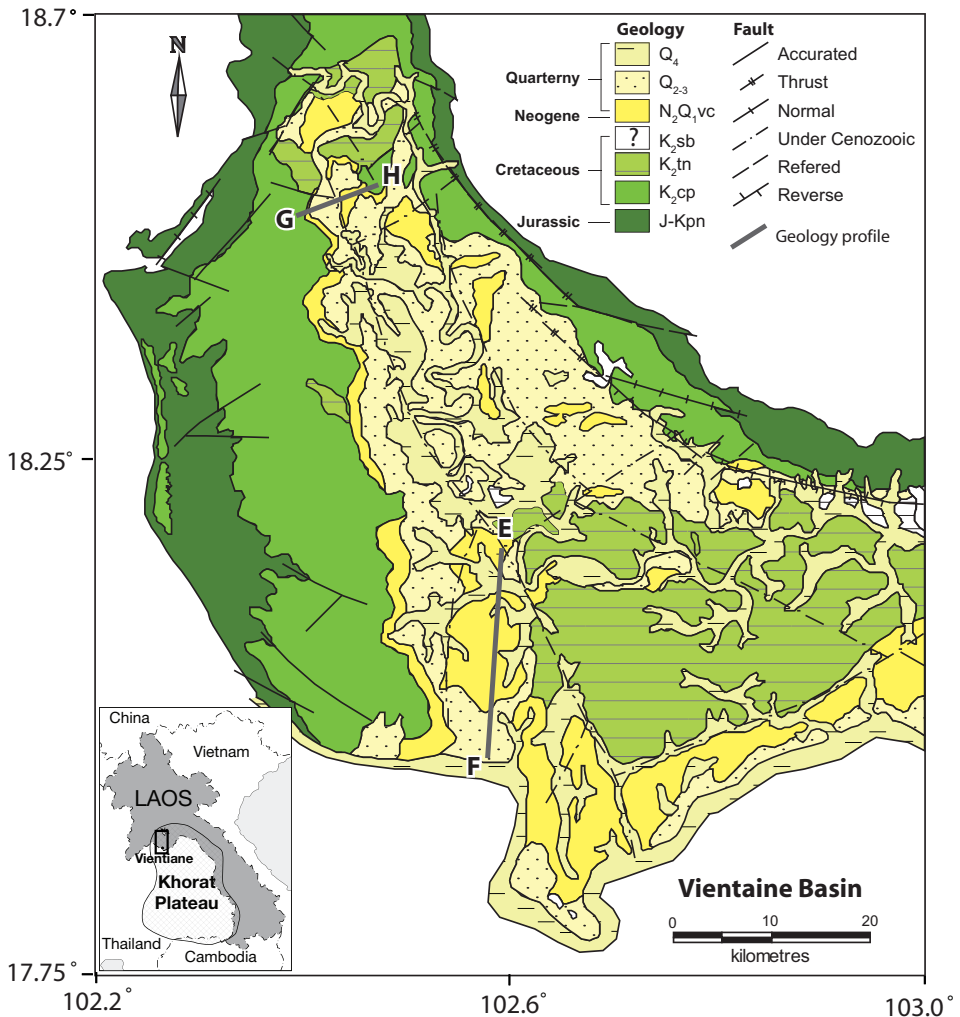
Fig. 2. Geology of Vientiane province (Long et al. 1986). Keymap showing the extent of the Khorat Plateau after Tabakh et al. (1999). Note that the Saysomboun formation (K_2sb) is not presented here.

developing groundwater in this unit is regarded as high (Takayanagi, 1993). Underlying the Thangon Formation is the Khorat Group, which among others consists of the Champa- (K_2cp) and Phu Pha Nang formataions (*J-Kpn*). These up to 400 m and 350 m respectively, thick formations are found primarily in the western and eastern part of the basin. They are largely composed of sandstone of Cretaceous and Jurassic age.

2.1.1 Salinity Caused by Natural and Human Activities

Salinity can arise from natural causes or from human activities. The major source of salinity within the Vientiane Basin, originates primarily from the salt structures of Thangon formation.

Salinity in shallow groundwater, originates from weathered salt accumulated in the upper clastic sediments transported from higher altitudes to nearby lowlands and valleys. Here, the water evaporates, leaving the salt in the upper soil (Löffler and Kubiniok, 1988). Salinity can also

3

arise from deep groundwater flows, when water in a recharge area penetrates down to the rock salt and then is transported to lowland discharge areas. Salt groundwater can also be transported upward through faults and fractures caused by artesian, convective and capillarity flow (Srisuk et al., 1994). Human activity affects the transport of salt in many different ways. Within the Khorat Plateau, soil salinity has been reported due to deforestation, construction of reservoirs, salt manufacturing and irrigation (Arunin, 1987).

2.2 Study Area

Three areas were selected for geophysical studies (Fig. 1), where MRS and VES measurements have been performed in 32 and 18 sites, respectively. Water chemsitry data have been collected from 13 deep and 15 shallow wells in near vicinity of the measuring sites. The sites have been chosen according to differences in geology and water quality, where geological and water chemistry data were retrieved from JICA (Takayanagi, 1993) and from the Department of Geology and Mining in Vientiane (Long et al., 1986). In an initial survey, noise level and accessibility was evaluated, which in most cases resulted in that dry rice paddies were chosen as measuring sites.

3 Geophysical Methods and Interpretation Techniques

The MRS measurements were carried out with the Numis$_{plus}$ equipment manufactured by Iris instruments. The magnetic field was measured using a G 816 magnetometer (Geometrics) with a

resolution of 1 nT. The VES measurements were conducted with a Terrameter SAS4000 (ABEM). Conductivity measurements on water in field and in laboratory were made using the conductivity meter HI 8733 (Hanna Instruments).

3.1 Magnetic Resonance Sounding (MRS)

MRS is a non invasive geophysical technique that energizes the protons in groundwater by transmitting an electromagnetic pulse in the larmor frequency and then measures the resonance signal sent back from the protons. The method and principles are thoroughly described in Legchenko and Valla, (2002), Yaramanci, (2004); Lubczynski and Roy, (2003). The initial amplitude (E_0) of the received signal is directly related to the free water content (θ_{MRS}) and the decay time (T_2^*) is related to the mean pore size of the material. With current limitation of the Numis equipment, the first 30 ms of signals can not be detected. The water content (θ_{MRS}) is determined from the inversion of the E_0 and is presented as a function of θ_{MRS} together with T_2^* versus depth.

Parameters such as porosity (η) and effective porosity (η_e) can be roughly determined directly from E_0 inversion in coarse grained aquifers, under the assumption that bound water, dead-end unconnected porosity is negligible (Lubczynski and Roy, 2003). The measured initial signal E_0 then reflects the porosity ($\theta_{MRS} \approx \eta$). The transverse relaxation time T_2^*, is the characteristic time for the loss of spin rotation coherency and is directly linked to the mean size of the water filled pores. Typical values of T_2^* are presented in Table 1.

Table 1. Values of decay time (T_2^*) for different geological materials (Shirov et al, 1991; Allen et al 1997) .

Decay time	Petrophysical Information	MRS
$T_2^* < 3$ ms	Clay bound water	Undetectable
$T_2^* < 30$ ms	Sandy clays	
$30 < T_2^* < 60$	Clay sands, very fine sands	Detectable
$60 < T_2^* < 120$	Fine sands	
$120 < T_2^* < 180$	Medium sands	
$180 < T_2^* < 300$	Coarse and gravely sands	
$300 < T_2^* < 600$	Gravel deposits	
$600 < T_2^* < 1500$	Surface water bodies	

MRS is able to resolve the aquifer geometry down to half the loop size and detect water down to approximately the depth of the loop size (Lubczynski and Roy, 2003 and Legchenko et al, 2002).

The MRS data was interpreted with the inversion software Samovar, based on the least square solution with regularization (Legchenko and Shushakov, 1998). Legchenko (2006) defines a lower limit of signal to noise ratio of 2 (S/N>2) for reliable interpretation. Due to equivalence, several models can fit the data. The parameter of regularization controls the smoothness of the interpreted water content distribution with depth. Yaramanci et al. (2002) argues that a high regularization will not present sharp boundaries or changes in water content with depth in medium to coarse sand aquifers in an accurate way. A low regularization on the other hand could cause unrealistic variations within small depth ranges. Since the subsurface conductivity influences the depth of penetration of the excitation field (Legchenko and Shushakov, 1998), the MRS interpretation also requires an electrical model of the subsurface.

3.2 Vertical Electrical Sounding (VES)

18 VES measurements were conducted on or in proximity of the MRS sites using a Schlumberger configuration and *AB/2* distances usually up to 200 m. The data were interpreted with the inversion software RESIST87 (Velpen, 1988), and where geological borehole data is present, it has been used to constrain the layer geometry. However, in some sites this kind of information was not available. The interpretation of VES data is complicated by the fact that resistivities for salt water, water saturated clay and sand overlap. Furthermore, due to the high resistivity contrasts between the often high resistive, dry top soil and the low resistive saline aquifer, interjacent freshwater layers with medium resistivities are difficult to detect on the sounding curve (Kirsch, 2006). These problems can be accounted for by using a first MRS model in the interpretation (Vouillamoz et al, 2007).

3.4 Water Quality Related to Conductivity.

Salinity is measured in Total Dissolved Solids (TDS), which is the total sum of cations and anions and the undissociated dissolved species after evaporation and filtration of a sample. TDS however, can also be determined by multiplying the electrical conductivity (EC) in µS/cm at 25°C with the TDS-factor (C_{TDS}) (usually between 0.55-0.90), which depends upon the types of salt present (Reynold and Richards, 1996).

$$TDS[mg/l] = C_{TDS} * EC \qquad (1)$$

TDS is often used for evaluating the water quality for domestic usage. TDS lower than 600 mg/l is considered to be of good quality (Table 2).

Table 2. Palatability of drinking water (WHO, 1996)

Class	TDS (mg/l)
Excellent	<300
Good	300-600
Fair	600-900
Poor	900-1200
Unacceptable	>1200

The main source of cations and anions in groundwater is the slow dissolution of minerals in rocks, and soils and minerals when the groundwater moves through the strata (Reynolds and Richards, 1996). Shoeller (1959) identified three types of sources that contribute to the variation in groundwater chemical characteristics: (1) Variation in mineralogy of the aquifer; (2) Vertical and lateral variations in groundwater flow, i.e. increasing dissolution and hence more ions in solution along the path of the groundwater flow and (3) Difference in climatic factors like rainfall and evaporation, which results in groundwater in arid environments to generally be more saline than groundwater in humid regions.

The European drinking water standards (directive 80/778EEC) have for an acceptable quality suggested a level of no more than 400 µS/cm at 20°C for electrical conductivity (EC) and defines the upper limit of EC to 1500 µS/cm at 20°C (Brassington, 2007). The salt content is

sometimes measured with reference to the level of chloride, which can also be directly related to EC. According to the Swedish National Food Administration, chloride concentrations >100 mg/l can have a corrosive effect on metal pipes and concentrations >300 mg/l can cause taste differences (SEPA, 2007). The major source of natural chloride in groundwater comes from dissolution of halite. Water with a high mineral content, primarily of Calcium (Ca^{2+}) and Magnesium (Mg^{2+}) ions, is considered as hard. Hardness of water is an important criterion for technical and esthetical reasons (Table 3), since hardness can produce a scale in hot water pipes, heaters and boilers. It also requires considerable amounts of soap before lather can be produced and it causes taste differences. Hard water can be expected in regions with large amounts of limestone ($CaCO_3$) or dolomite ($CaMg(CO_3)_2$) (Reynolds and Richards, 1996). Hardness of the water with its polyvalent ions directly contributes to conductivity (Krawczyk and Ford, 2007).

Table 3. *Hardness of water (Reynolds and Richards, 1996)*

Hardness [mg/l] as Ca-HCO₃	Degree of Hardness
1-75	Soft
75-150	Moderately soft
150-300	Hard
300 or more	Very hard

The resistivity ρ, of a porous, water-bearing material, free of clay minerals can be expressed with Archie's law (Archie, 1942), which is an empirically determined formula that expresses the resistivity as a function of the water resisitivity ρ_0, the porosity (η) and the water saturation s.

$$\rho = a \cdot \rho_0 \cdot \eta^{-m} \cdot s^{-n} \qquad (2)$$

The value of n and m depends mostly on the wettability and cementation respectively. If the mineral grains are insulator, then a = 1, which is the main condition for Archie's formula. To a certain degree of decreasing resistivity of the mineral grains, the constant a decreases too (Worthington, 1993). If working in a geological environment without conducting grains (a = 1) and assuming that bound water, dead-end unconnected porosity is negligible, the MRS water content (θ_{MRS}) ≈ porosity (η), ρ is then

deduced from VES resistivity and ρ_0 can be determined from the EC of water from the wells. Together they form the formation factor F= ρ/ρ_0. If the aquifer is assumed to be saturated (s=1), the cementation factor (m) can be determined for a specific geological material.

Vouillamoz (2007) argue that in an environment where aquifers are not free of low resistive clayey material, a "rough estimator" for the water EC can still be made using a linear relationship between ρ determined from VES and water EC measured from water wells. The conductivity of a fluid is strongly dependent on the concentration and mobility of ions, where mobility is highly temperature dependent. Conductivity of water is usually standardized at 25°C. When comparing EC of water with aquifer conductivity it is important to correct for the true temperature of the water. The conductivity of most groundwater varies with about 2% per °C (Clesceri et al. 1998).

4. Results

4.1 Result from the Geophysical Investigation

The inclination of the geomagnetic field in the Vientiane Basin was 24° and the intensity varied between 43620 to 43850 nT equivalent to a larmor frequency of 1859 to 1868 Hz. Depending on the noise, a 100 m square or a 8 shaped loop was used together with 64 to 100 stacks. The power line frequency is here 50 Hz, which allowed for notch filters to be used in presence of industrial noise (Legchenko, 2003). The decay time values matching the highest water content in a water bearing layer have been used to characterize that specific aquifer. The grain size indicated by T_2^* usually agrees well with borehole petrophysical information. However, borehole data can not always be directly related to the sites of measurements.

Examples of measurements from the sites 20, 19 and 22 are presented in Fig. 3. The Signal to noise (S/N) ratios for the different sites typically vary between 2 and 10. The general trend is that the
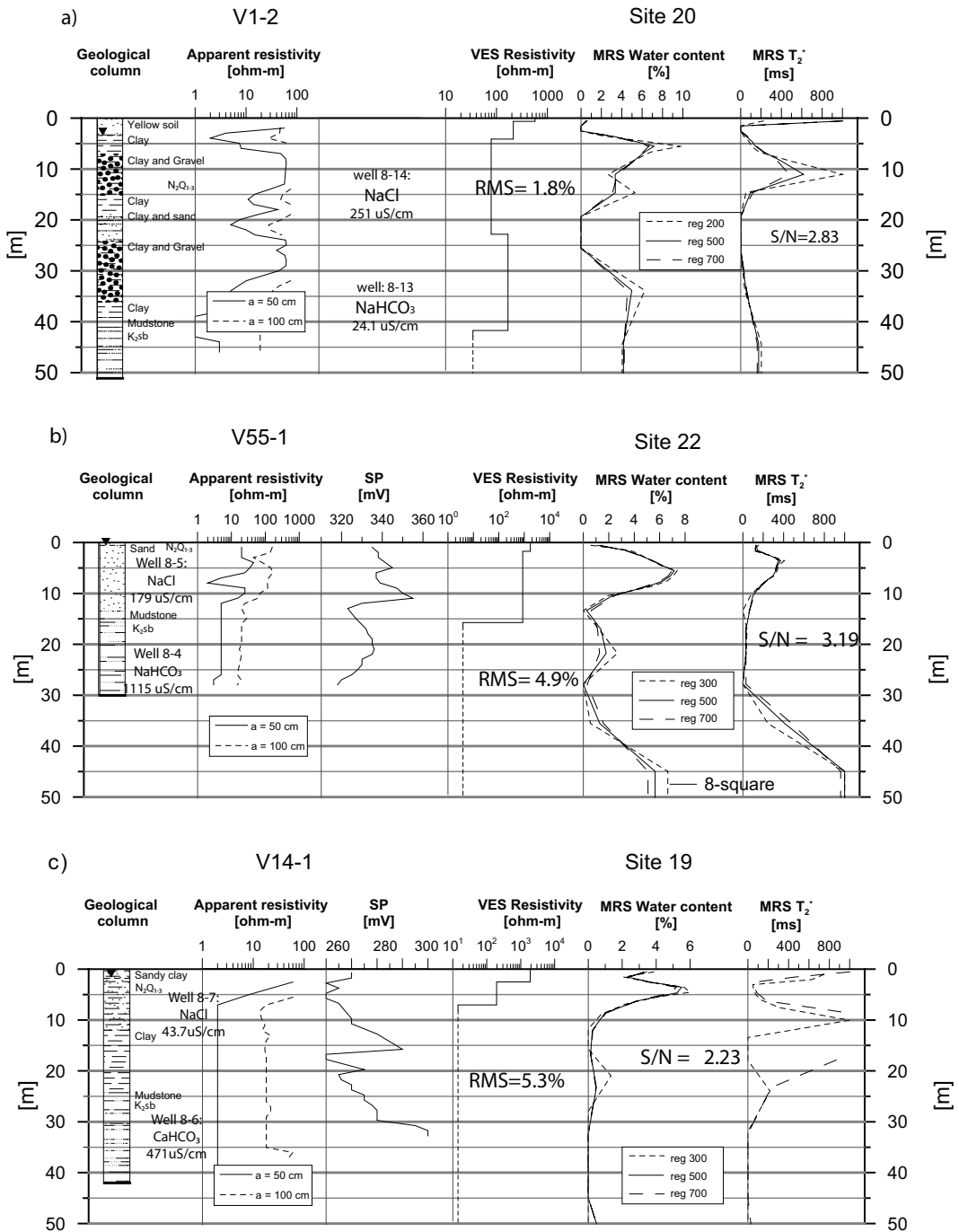
Fig. 3. MRS models illustrating the effect of regularization and VES models together with borehole data in area 3 from a) Site 20, b) Site 19 and c) Site 22.

inverted MRS data seems to fit the raw data quite well for low pulse moments but looses coherency for high pulse moments (Fig. 4). Regularizations between 300 and 700 usually results in a smooth aquifer model geometry, which corresponds quite well with the lithology mapped in adjacent boreholes. T_2^* can vary significantly for different regularization (eg. Site 19). VES measurements are generally of good quality with RMS varying between 2 and 6% (Fig. 4).

materials such as clay and breccia overlying rock salt, all with poor potential for hosting aquifers. MRS usually identifies one shallow and one deep aquifer in the N_2Q_{1-3} (e.g. Site 31, Fig. 5c). The deep, main aquifer generally starts at around 10 to 15 m depth with maximum water content at around 20 to 25 m and the aquifer floor positioned from 30 to 50 m depth. The maximum water content varies between 4 and 12%, but is usually about 6 to 8 %. The T_2^* -values range from 100 ms (Site 24, and 31) to 300 ms (Site 3) corresponding to medium to coarse sand and
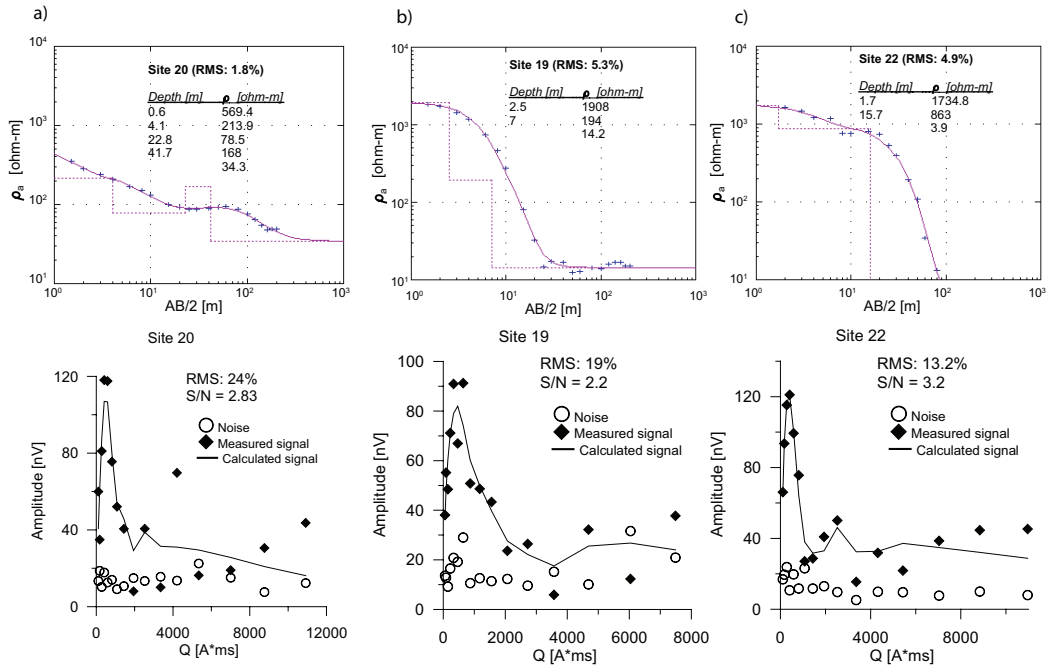

Fig. 4. VES and MRS raw data and model from a) Site 20, b) Site 19 and c) Site 22. Note the poor fit on the MRS model for high pulsemoment with low initial amplitudes.

4.1.1 Identification and Characterization of Geological Structures.

In area 1 (Figs 1 and 5a), the K_2cp is the dominant formation in the western part of the basin, whereas N_2Q_{1-3} is dominant in the central part and the K_2tn in the eastern part. In the geological cross section FE (Long et al., 1986) (Fig. 5b) in area 1, the different characteristics of the N_2Q_{1-3} and the K_2tn are illustrated (Perttu et al., 2008). The N_2Q_{1-3} holds in most parts coarser materials like sand and gravel but also comprises finer sediments like clay and silt. K_2tn on the other hand, contain

gravel sands. The resistivity for these water layers ranges between 20 and 600 ohm-m. The K_2tn is located below the N_2Q_{1-3} with the exception for the south-eastern part where it is found from the surface and down. It is characterized by very low water contents and resistivities lower than 5 ohm-m (Site 24 and 31; Figs. 5c and d).

The area 2 is located in the eastern part of the basin (Figs. 1 and 6a), with the N_2Q_{1-3} as the dominating stratigraphic unit in the southern part and the K_2sb (not in map) in the northern part.
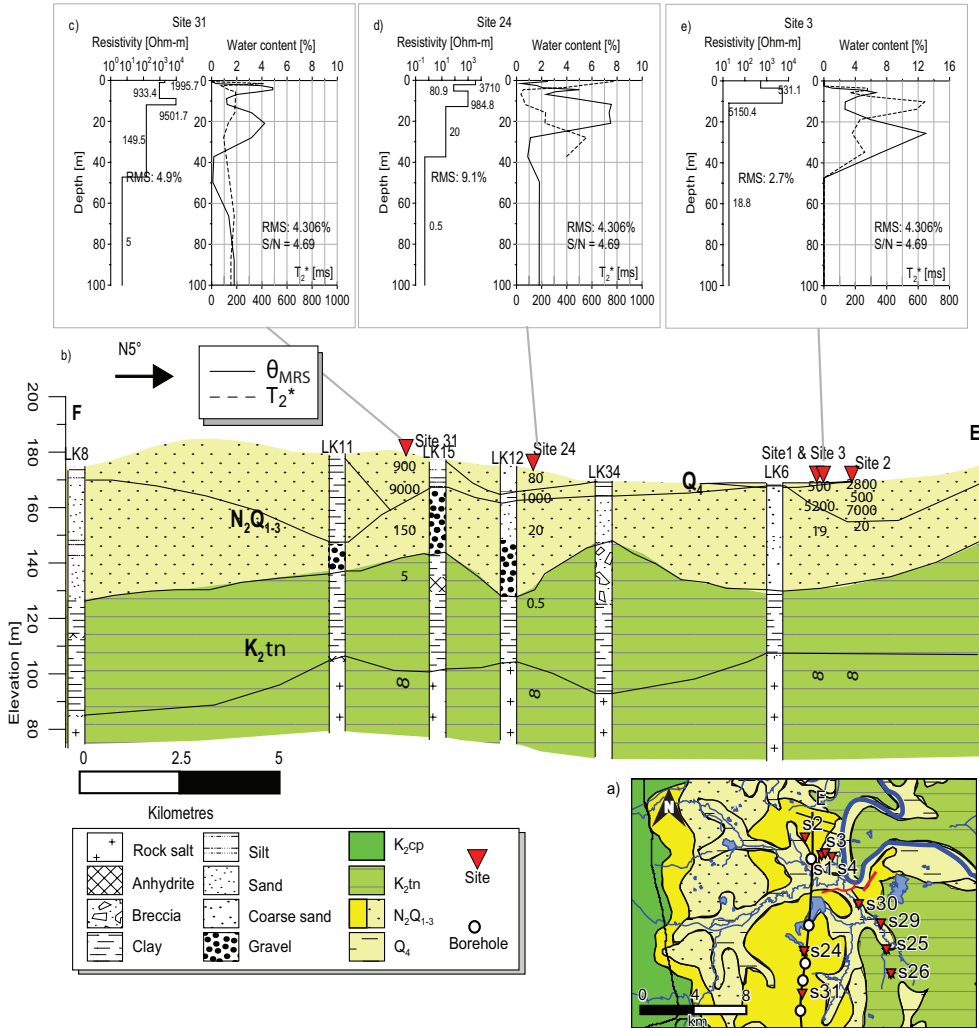
Fig. 5. a) Geological map of Area 1, illustrating the relative position of sites and boreholes along profile 1. b) Modified geological cross sections EF after Long et al. (1986). Inverted MRS data presenting θ_{MRS} and T_2^* together with the VES result from c) site 31, d) site 24 and e) site 3.

However, geological borehole data is sparse in this area, and no measurement has been conducted in close proximity to a borehole. In the southern part, the sites 8 to 11 (Figs. 6a and b) are located at about 500 m apart. From the MRS data, 2 water bearing layers are identified with the main aquifer of about 5 m depth extending down to around 20 to 30 m with the same MRS characteristics as in area 1. The underlying low water content layer has a resistivity of 0.6 ohm-m, which is equivalent to the low resistive clay of the K_2tn in area 1. The northern part includes the sites 5 to 7.

In site 6 only a low water content is found in the upper 10 m of the N_2Q_{1-3}, which then change into the K_2sb (Borehole, B-6; Fig. 6c), where no water is found. At a depth of 45 m, the K_2sb change into clay and anhydrite associated with the K_2tn. The site 5 shared the same MRS characteristics as in the sites in the southern part. However, the resistivity of the two upper water bearing layers is 6.2 ohm-m and. The third deepest water layer, starting at 18 m depth, has a resistivity of 0.3 ohm-m, which could be an indication of salt affected water.
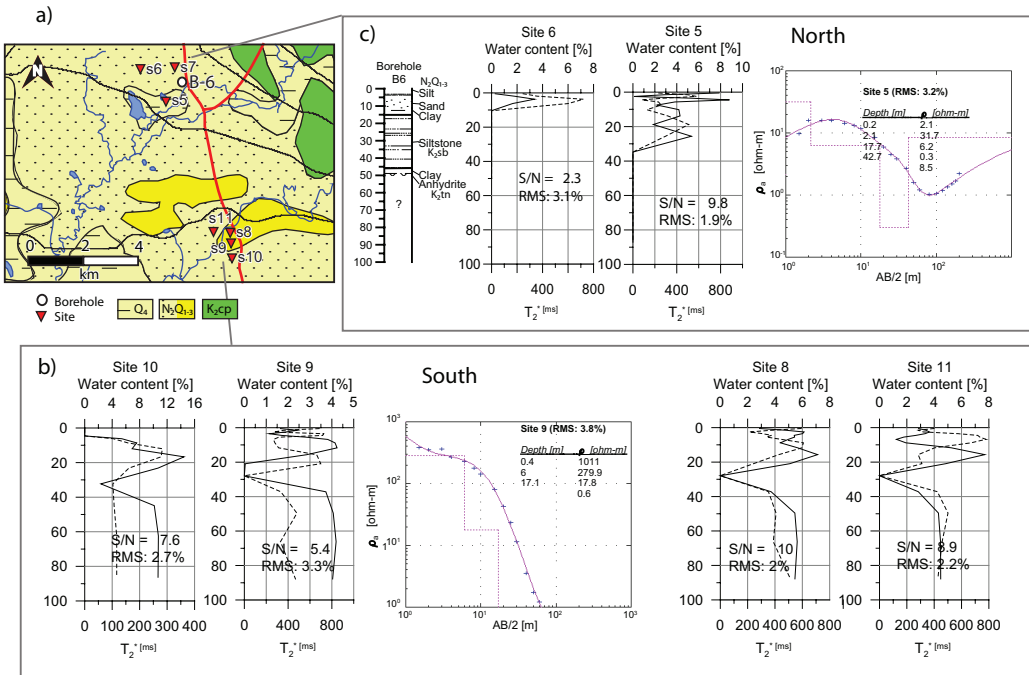
9

Fig. 6. a) Geological map of Area 2 showing the locations of sites and the location of borehole B-6. Sites 5 to 7 are located in the northern part, whereas sites 8 to 11 are situated in the southern part. MRS data presenting θ_{MRS} and T_2^* from b) site 6 and site 5 together with modeled VES and c) site 10, site 9 together with VES model, site 8 and site 11.

The area 3 is located in the narrowing upper part of the Vientiane Basin (Figs. 1 and 7a) with the K_2cp in the western and eastern border of the basin, the K_2tn in the north and N_2Q_{1-3} in the central part. The geological cross section GH (Fig. 7b) compiled from lithology borehole data (JICA, 1994), shown together with VES (Fig. 7c) and MRS (Fig. 7d) data collected in this study, illustrates the geophysical soil and rock characteristics of the area. The stratigraphic unit, N_2Q_{1-3} comprises two water bearing layers (Site 20 and Site 16) in the western part with a thickness of up 40 m, which transcends to one thinner layer, with significantly lower water content in the middle of the cross section. The maximum water content is varying between 4 and 16%, and the T_2^* generally varies between 100 and 400 ms, with longer T_2^* in the western part of the basin. The resistivity for the main water bearing layer varies considerably from site to site but usually ranges between 10 to 250 ohm-m. In the eastern part, the composition of the N_2Q_{1-3} changes to more clayey material and

the water content is lower than 4% and T_2^* lower than 100 ms. The K_2sb underlying N_2Q_{1-3}, consists of mudstone or siltstone (Fig. 7b). It has a fairly low water content (<2%), and T_2^* around 50 to 200 ms. The resistivity varies between 10 to 25 ohm-m (e.g. site 23). Rocks from the K_2tn has not been observed in any boreholes here, but VES measurement from the sites 15, 16 in the middle of the basin, show resistivities (< 5 ohm-m) that may indicate the existence of this formation as characterized in area 1.

4.2 Result from the Groundwater Analysis

Water samples for chemical analysis were collected in January 2007 and 2008, from altogether 15 shallow and 13 deep wells (4 wells in area 1, 7 wells in area 2 and 17 wells in area 3). Chemical analysis for the most common ions together with EC, TDS and alkalinity (Table 4) was made by the Department of Irrigation in Vientiane. pH values from old water quality

10

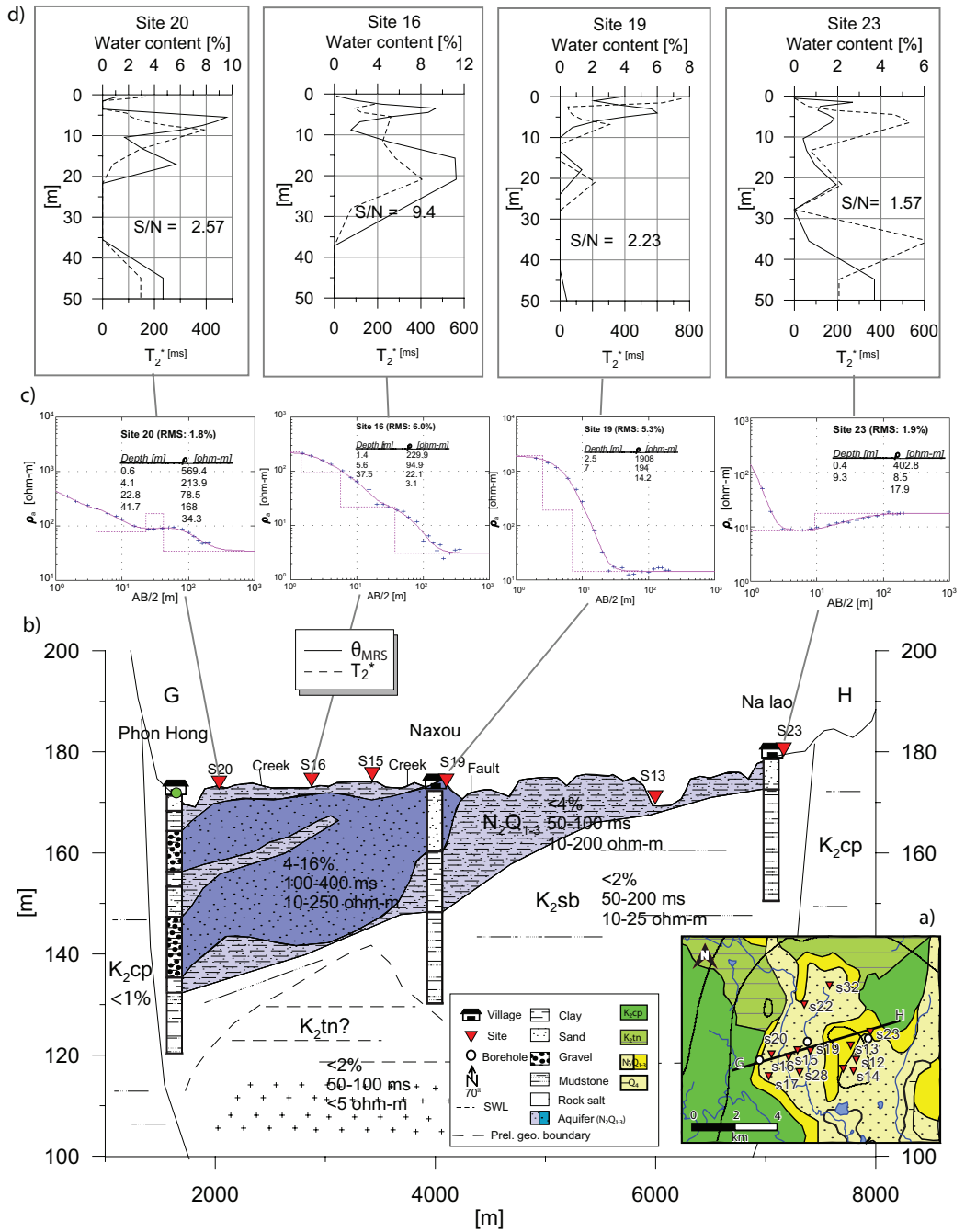**Fig. 7.**a) a) Geological map of area 3 showing the locations of measuring sites together with boreholes relative the profile GH. b) The cross section GH summarizes existing geological information from borehole data, water content, T_2^* and resistivity based on the geophysical measurement with c) VES models and d) θ_{MRS} and T_2^* models from site 20, site 16, site 19 and site 23.

Table 4. Summery of the groundwater chemistry analysis. Grey marked samples exceed limits of water quality standards according to WHO or SEPA. Measured Total Dissolved Solids (TDS), electrical conductivity (EC) TDS-factor (C_{TDS}), passed quality control parameters according to section 4.2.1. S and D denote shallow and deep wells, respectively.

Sample ID	TDS mg/L	EC µS/cm	TDS-factor	Chloride mg/L	Water Type	Calc. Hardness mg/L CaCO$_3$	Quality control 1,2,3,4,5,6	East [°] Long (WGS84)	North [°] Lat (WGS84)	Area 1,2,3	Well Shall./Deep	Geology Layer 1	Layer 2	Layer 3
7-1	11	21	0,53	5,5	Na-Cl	4,14	1,4,5	102,61163	18,15464	1	S	N$_2$Q$_{l-3}$	K$_2$tn	
7-3	24	48	0,50	4	Ca-HCO$_3$	15,84	1,4	102,60747	18,16647	1	S	N$_2$Q$_{l-3}$	K$_2$tn	
7-4	10	20	0,50	4,4	Na-Cl	4,32	1,4,5	102,5993	18,1575	1	S	N$_2$Q$_{l-3}$	K$_2$tn	
7-5	12	25	0,48	2,3	Ca-HCO$_3$	9,13	1,4	102,68113	18,27853	2	S	N$_2$Q$_{l-3}$	K$_2$tn	
7-6	15	29	0,52	2,8	Ca-HCO$_3$	8,63	1,3,4	102,67916	18,28564	2	S	N$_2$Q$_{l-3}$	K$_2$tn	
7-7	17	35	0,49	2,4	Ca-SO$_4$	11,11	1,4	102,67304	18,28525	2	D	N$_2$Q$_{l-3}$	K$_2$	
7-8	29	59	0,49	7,8	Ca-Cl	18,41	1,4,5	102,67325	18,28467	2	S	N$_2$Q$_{l-3}$	K$_2$tn	
7-9	46	92	0,50	18,1	Ca-Cl	35,75	1,4	102,65963	18,34006	2	D	N$_2$Q$_{l-3}$	K$_2$tn	
7-10	139	277	0,50	47,2	Ca-Cl	98,90	1,3,4,5	102,65621	18,33047	2	D	N$_2$Q$_{l-3}$	K$_2$tn	
7-11	15	30	0,50	7,9	Ca-Cl	8,88	1,4	102,66138	18,33774	2	D	N$_2$Q$_{l-3}$	K$_2$tn	
7-12	64	129	0,50	19,9	Ca-Cl	51,29	1,3,4	102,45911	18,48735	3	S	N$_2$Q$_{l-3}$	K$_2$sb	
7-13	50	101	0,50	1	Ca-HCO$_3$	48,57	1,3,4	102,43498	18,48783	3	S	N$_2$Q$_{l-3}$	K$_2$sb	
7-14	123	245	0,50	15,1	Ca-HCO$_3$	107,65	1,3,4	102,42404	18,49725	3	S	N$_2$Q$_{l-3}$	K$_2$sb	
8-1	6	12,2	0,49	1,6	K-Cl	2,99	1,4	102,58786	18,0913	1	D	N$_2$Q$_{l-3}$	K$_2$sb	
8-2	67	134	0,50	0,85	Na-HCO$_3$	19,28		102,39073	18,56783	3	D	N$_2$Q$_{l-3}$	K$_2$sb	
8-3	86	173	0,50	14,7	Ca-HCO$_3$	60,65	1,3,4	102,39073	18,56783	3	S	N$_2$Q$_{l-3}$	K$_2$sb	
8-4	558	1115	0,50	165	Na-HCO$_3$	117,23	1	102,43307	18,50745	3	D	N$_2$Q$_{l-3}$	K$_2$sb	K$_2$tn?
8-5	90	179	0,50	53,9	Na-Cl	46,04	1,4,5	102,43353	18,50472	3	S	N$_2$Q$_{l-3}$	K$_2$sb	
8-6	236	471	0,50	9,62	Ca-HCO$_3$	152,77	3,4	102,43515	18,49747	3	D	N$_2$Q$_{l-3}$	K$_2$sb	
8-7	22	43,7	0,51	10,1	Na-Cl	10,33	1,4	102,43515	18,49747	3	S	N$_2$Q$_{l-3}$	K$_2$sb	K$_2$tn?
8-8	91	183	0,50	23,4	Ca-HCO$_3$	45,91	1,3,5	102,45259	18,48718	3	D	N$_2$Q$_{l-3}$	K$_2$sb	
8-9	34	68,2	0,50	13,4	Na-Cl	12,35	1,3,5	102,45259	18,48718	3	S	N$_2$Q$_{l-3}$	K$_2$sb	
8-10	79	158	0,50	11,1	Ca-HCO$_3$	64,21	1,3,4	102,46684	18,4959	3	D	N$_2$Q$_{l-3}$	K$_2$sb	
8-11	86	172	0,50	36,5	Ca-Cl	52,48	1,3,4,5	102,46652	18,49545	3	S	N$_2$Q$_{l-3}$	K$_2$sb	
8-12	296	592	0,50	11,1	Ca-HCO$_3$	306,30	1,3	102,46878	18,49405	3	D	N$_2$Q$_{l-3}$	K$_2$sb	
8-13	12	24,1	0,50	2,56	Na-HCO$_3$	3,73	1,4	102,41207	18,48718	3	D	N$_2$Q$_{l-3}$	K$_2$sb	
8-14	126	251	0,50	35,6	Na-Cl	52,91	1,3,4	102,41932	18,49265	3	S	N$_2$Q$_{l-3}$	K$_2$sb	
8-15	247	494		0,084				102,44778	18,52132	3	D	N$_2$Q$_{l-3}$	K$_2$sb	

12

analysis (JICA, 1994) has been used from the same wells or neighboring wells (in area 2 and 3) to calculate HCO_3 and CO_3 from alkalinity. Chloride and EC data from area 3 collected by Takayanagi (1993) have also been used in the interpretation.

4.2.1 Quality Control of Chemical Analysis

The following quality assurance tests (Standard Methods 1030 E.) are applicable to samples where relatively complete analysis are made, including pH, conductivity, TDS and major anions and cations. Here, 6 tests are presented, where the first 3 are considered to be of greater importance and reliability: Anion-Cation Balance (1), Measured TDS = Calculated TDS (2), Measured EC = Calculated EC (3), Measured EC and Ion Sums (4), Calculated TDS and EC Ratio (5) and Measured TDS and EC Ratio (6) (Clesceri et al. 1998).

All samples except 8-2 and 8-6 passed the criteria for electroneutrality (1) and neither anions nor cations are more dominant when looking at all the samples. None of the samples passed the criteria for measured TDS = calculated TDS (2), where the calculated TDS is always higher than the measured. The measured TDS to conductivity ratio (6) is always less than 0.55, which implies that the measured TDS is suspect. The conductivity has in some wells been measured in field with a good correspondence to the laboratory analysis, which even more implies that the measured TDS is too low. Measured EC matches or almost matches calculated conductivity (3) and Ion Sums (4) in many of the samples, but is generally lower than the calculated conductivity, which suggests that other constituents can be poorly analyzed as well. Many of the samples meet the criterions of calculated TDS to EC ratio (5) but are sometimes higher (>0.7), which could imply poorly dissociated calcium and sulfate. In summary, the most reliable parameter to reflect the salinity in the sampled groundwater is the measured EC.

4.2.2 Water Quality

With reference to the analyzed TDS values, the groundwater from most wells can be classified of excellent quality (<300 mg/l) or at least of good quality (<600 mg/l) according to WHO international standard (Table 5). The calculated TDS (TDS_c) on the other hand indicates water of unacceptable (>1200 mg/l) quality in two wells in area 3 (8-4 and 8-6) but indicates good quality in all other wells (Table 5). The EC of water is usually lower than 300 µS/cm with the highest value of 1115 µS/cm in well 8-4 in area 3. However, it does not exceed the limit of 1500 µS/cm for unacceptable quality according to the European water quality standard (directive 80/778EEC). The chemical characteristics of the sampled water are listed in Table 4 where the water has been characterized according to their main constituents. Most Na-Cl type of water is collected from shallow wells whereas water from deep wells are dominated by $Na-HCO_3$ or $Ca-HCO_3$, This may imply that salinity in shallow wells are caused from evaporation rather than migration of salt from deeper structures. The analyzed TDS-factor does not vary much in the three areas, with an average value of $C_{TDS} \approx 0.5$, and prove to be insensitive to different types of water. The calculated TDS_c factor determined from regression analysis gives a C_{TDS} of 0.86 ($R^2=0.93$), which instead is too high compared to quality control test (6) ($0.55<C_{TDS}<0.7$). The TDS_c factor seems to be lower for Na-Cl and K-Cl type of water than for water of the type $Na-HCO_3$ or $Ca-HCO_3$. Chloride concentration usually varies between 1 and 50 mg/l. One sample exceeds the risk of pipe corrosion (165 mg/l; well 8-4) according to SEPA. However, no sample exceeds the limits of taste effects WHO or SEPA (>300 mg/l, SEPA or >250 mg/l, WHO). Water samples from area 3 were also analyzed by Takayanagi (1993), where EC >1000 µS/cm and chloride concentration >100 mg/l were determined for water from some deep wells. Salt (NaCl) from the salt factory of Ban Bo has been diluted using de-ionized water and then measured in the laboratory at Luleå University of Technology for EC for a wide range of concentrations (Fig. 8). This analyze show an almost perfect linear fit (EC = 2.5841*Cl⁻, $R^2=0.998$). Chloride concentrations from water samples in different wells in the three areas are here plotted against EC (Fig. 8). The EC of the chloride concentrations is quite scattered and exceeds the EC of the diluted chloride graph, which could be explained by other ions
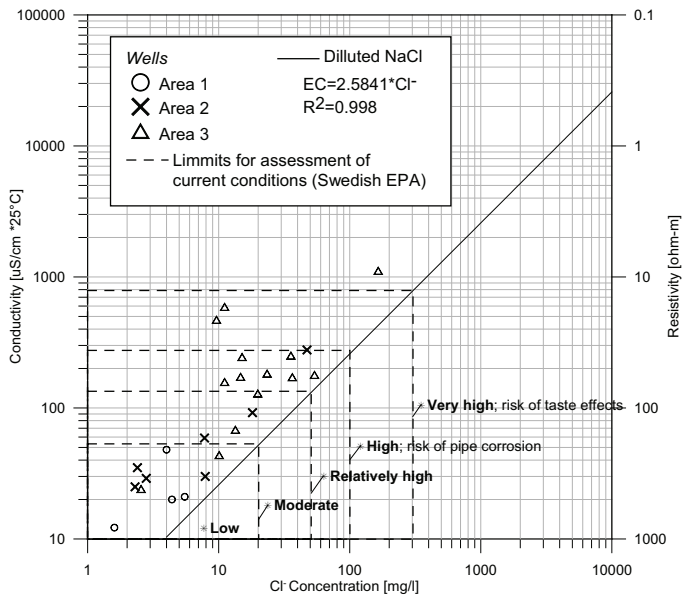
Fig. 8. Salt (NaCl) from the Ban Bo salt factory has been diluted for different concentration and measured for EC at 25°C (−), with an almost perfect linear fit. Chloride data from sampled wells in area 1 (O), area 2 (X) and area 3 (Δ) plotted against EC are quite scattered but the overall gradient is the same as the diluted salt curve.

Table 5. *Correlation coefficients between different water chemistry parametrar. EC show a high correlation to TDS, chloride, sodium and alkalinity.*

	EC	TDS	Cl	SO₄	Ca	Mg	Na	K	Alkalinity
EC	1								
TDS	1.00	1							
Cl	0.76	0.76	1						
SO₄	0.36	0.36	0.42	1					
Ca	0.70	0.70	0.25	0.24	1				
Mg	0.73	0.73	0.33	0.23	0.96	1			
Na	0.88	0.88	0.93	0.29	0.30	0.34	1		
K	0.22	0.22	0.25	0.32	0.05	0.17	0.18	1	
Alkalinity	0.85	0.85	0.40	0.11	0.89	0.88	0.56	0.12	1

contributing to the EC. However, the gradient of the diluted chloride curve and the sampled EC and chloride concentration from wells, seems to be about the same.

The correlation matrix, including all 28 sampled wells for 9 variables is presented in Table 5, where each cell provides the correlation coefficient for two sets of analytes.

EC and TDS have correlation coefficient of 1, which suggests that the measured TDS reflects the change is conductivity perfectly. EC and TDS also show a strong and positive correlation

to Na, Cl and alkalinity but also to Ca and Mg, which suggest that EC can be directly related to hardness. Furthermore, chloride shows a significant correlation to sodium, which indicates that chloride concentration, can be directly related to halite. Magnesium and calcium show a strong positive correlation to one another and to alkalinity.

Total hardness (H_T) can be calculated from the Ca^{2+} and Mg^{2+} content in the water from the equation

$$H_T\left[\text{mg/l as CaCO}_3\right] =$$
$$2.497\left[Ca^{2+},\text{mg/l}\right] + 4.118\left[Mg^{2+},\text{mg/l}\right] \quad (5)$$

as described in Standard Methods 2340 B (Clesceri et al. 1998). High values are found in well 8-6 and 8-12 (Hard >150 mg/l). Here, H_T is plotted against EC (Fig. 9) with a best fit using H_T=0.43*EC-11.07 (R^2=0.90).

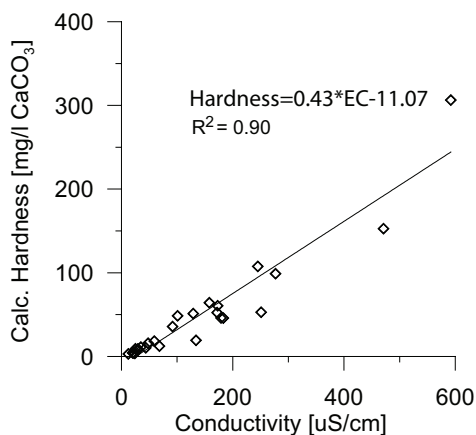**Fig. 9.** Measured EC plotted against calculated hardness. Best fit is obtained from H_T=0.43*EC-11.07 (R_2=0.90).

from Equation 2). Since various unconsolidated sediments of different grain sizes comprises the N_2Q_{1-3}, water bearing layers have been grouped according to mutual grain sizes indicated by T_2* value (Table 1), where m has been determined for each group using simple regression (Table 6).

A better correlation between F and θ_{MRS} is then achieved for clay sands and fine sands but there was no correlation found for coarse and gravely sands. The number of samples in medium sands is too few for interpretation.

The measured water EC (25°C) corrected for temperature has been compared to the modeled VES conductivity. The best fit is obtained using EC[μS/cm]= 0.3821VES[μS/cm], R^2=0.81 for water from deep wells (Fig. 10a), although the data is quite scattered. A good fit is also achieved with the double squared method: EC[μS/cm]= $\sqrt{(17972,8 + 0,16538*VES[\mu S/cm]^2)}$, R^2=0.78. For shallow wells the coefficient of determination is very low (R^2<0.1). This is because the data is very scattered for low VES conductivity (< 200 μS/cm or >50 ohm-m) (Fig. 10b). This equation does not take the aquifer

Table 6. Unconsolidated sediments of N_2Q_{1-3} have been grouped according to mutual grain sizes indicated by T_2*, where the cementation factor (m) have been determined from regression analysis.

Soil characteristics	m	R^2	no of samples
Clay sands	1.75	0.72	4
Fine sands	1.18	0.42	10
Medium sands			2
Coarse and gravely sands	0.56	0.03	8

4.3 Estimation of Water Conductivity from Geophysical data

Within the basin, VES data suggests vertical variations in the aquifer resistivity, which is confirmed by the EC measurements of water from nearby deep and shallow wells. However, no significant correlation could be found from plotting the MRS water content (θ_{MRS}) against the VES resistivity (ρ) for the N_2Q_{1-3}. This implies that the change in θ_{MRS} within N_2Q_{1-3} is not reflected in the ρ. The cementation factor (m) is determined by a regression analysis of the formation factor (F=ρ/ρ_0) and θ_{MRS} on a bilogarithmic cross plot, where m is the slope of the curve (deduced

material into consideration. In a recharge area, composed of fine grained material with soluble minerals, one could expect the water to have more dissolved solids, than in a recharge area containing coarser, less soluble material (Back and Hanshaw, 1966). Waxman and Smits (1968) provided a model for current flow in porous media, where one part of the current is conveyed through the pore water, whereas the other part is associated with the electrical double layer (i.e. clay), and the total resistivity is the sum of the two. Analogous to this, it should be possible to roughly estimate the contribution from the finer sediments/clay using the petrophysical information from T_2*. The EC-estimator for
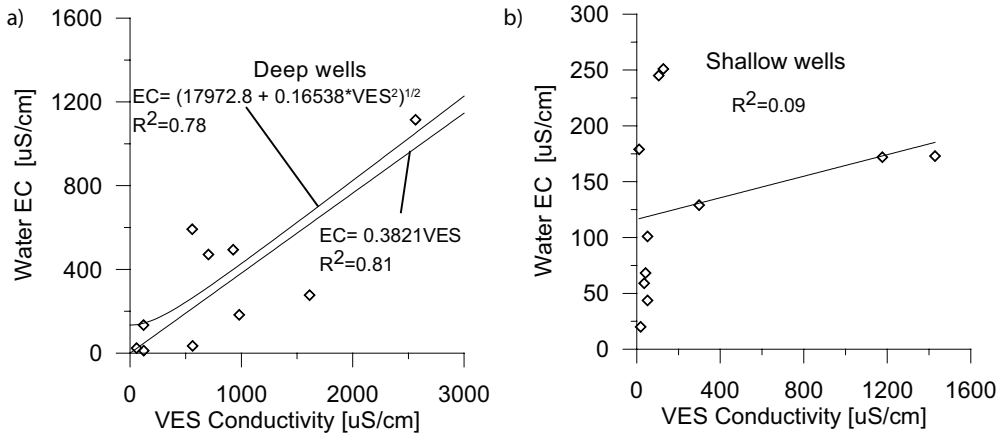
Fig. 10. a) Conductivity of aquifers (VES) against water EC from a) deep and b) shallow wells. The best fit for deep wells is obtained using EC[μS/cm]= 0.3821VES[μS/cm] , R^2=0.81. For shallow wells the R^2 <0.1, and the data is very scattered for low aquifer conductivity.

deep wells would then transform to *EC[μS/cm]= 0,345*VES[μS/cm]- 0,221* T_2*[ms]*, for deep wells with an unchanged R^2 of 0.81 using the least square method. Since, the P-value = 0.76 > 0.05 (operating at the 0.05 significance level) for T_2*, there is no indication of serial autocorrelation and T_2* should be removed from the model. This implies that the deep aquifer conductivity is controlled by the conductivity of water and not the material of the aquifer.

4.4 Comparison of TDS to Aquifer Conductivity and Hydrogeological Parameters

The Salinity (TDS) is caused by differences in mineralogy, topography, flow paths of the groundwater and climate factors. Therefore, the spatial distribution of TDS [mg/l] from area 3 is here plotted together with the VES conductivity of the bottom confining layer (Fig 11a) and the conductivities of the main aquifer layer (Fig. 11b). TDS is also plotted together with hydrogeological parameters like MRS transmissivity (T_{MRS}) (Fig. 11c) and hydrostatic column (H_w) (Fig. 11d) together with the topographic gradients, where the length of the arrow indicate the relative change in elevation. H_w estimated from MRS, gives a direct volumetric estimate of the free water content in an aquifer:

$$H_W = \theta_{MRS} \cdot \Delta z \qquad (6)$$

where Δz is the aquifer thickness of the N_2Q_{1-3} unit. T_{MRS} is a measure of the hydraulic properties of the aquifer (Legchenko et al. 2002; Vouillamoz et al, 2002) and is estimated from

$$T_{MRS} = C_T \int_{\Delta z} \theta^4 \cdot T_2^{*2} dz \qquad (7)$$

where the site specific constant C_T= 1.81*10^{-13} (Perttu et al. 2008) was derived from MRS data from site 17 and 20 and pumping test transmissivity from well 8-13.

The measured TDS is too low according to the quality control, although it correlates perfectly with the conductivity of the groundwater and hence reflects the relative difference in salinity of the aquifer. TDS determined on water from 7 deep wells has a maximum in the upper middle part of the basin, with the highest value of 558 mg/l in well 8-4. The TDS decreases towards the south, but also to the east in area 3. This agrees fairly well with the conductivity of the bottom layer located beneath the main aquifer on depths of 20 to 40 m in the western part and at about 10 m in the eastern part. It has also a maximum in the middle of the basin, although shifted more to the south part (Fig. 11a). The main aquifer conductivity has a similar relation with the TDS, although the conductivity seems to be high in the eastern part of the basin as well (Fig. 11b).
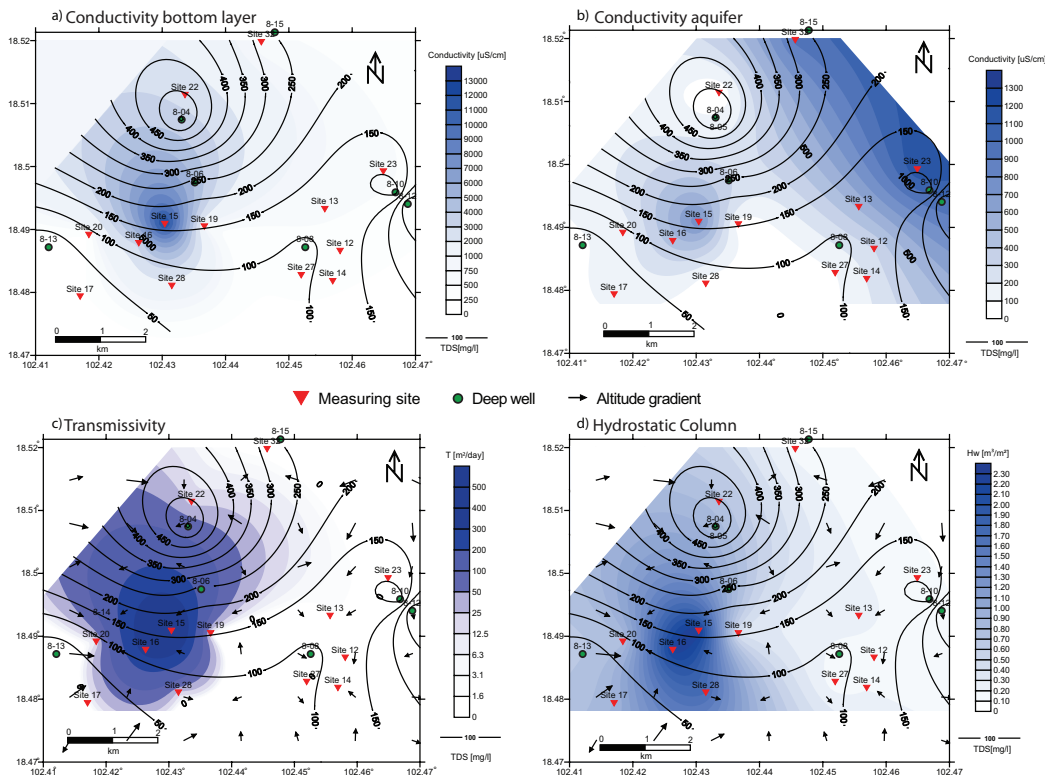
Fig. 11. TDS contours together with maps of VES conductivity a) of the bottom layer and the b) aquifer layer, c) transmissivity (T_{MRS}) and d) hydrostatic column (H_w) together with topographic gradients expressed by arrows, where the length denotes gradient amplitude. The maximum conductivity of the bottom layer and the aquifer layer correlates well to the maximum H_w and T_{MRS} but is shifted to the south compared to the maximum TDS.

This might be an indication that the salinity of deep wells is more affected by the bottom layer than the main aquifer. The topographic gradient correlates well with increasing T_{MRS} and H_w in the western part, and the maximum T_{MRS} (Fig. 11c) and H_w (Fig. 11d) correlates very well with the conductivity of the bottom layer and the aquifer and is thus also located somewhat different compared to the TDS maximum. This could be an indication that the amount of water and the rate of circulation could have an impact on the salinity of the underlying layer and the aquifer layer. It could also be an indication that salt in the upper part of area 3 is diluted and transported southward, where it contributes to the higher conductivity in the main aquifer layer and the underlying layer. Still the number of data is too small and scattered spatially to make a more quantitative interpretation possible.

5. Discussion

The geophysical data are of overall good quality, although some VES data are more scattered towards the end of the sounding, usually associated with low resistivity. The water content (θ_{MRS}) and T_2^* are seldom coherent and often show a reverse proportional relationship. That is, when θ_{MRS} is low, T_2^* is usually high. This can be explained by the low initial amplitude that creates an almost horizontal exponential fit of the relaxation, hence creating a long artificial T_2^*. The increase in water content below the non water bearing layer identified as clay from $K_2 tn$ is more difficult to explain. Geological data from boreholes suggests that only clay or halite should be found on these depths, which in turn imply little or no water. In large pulse moments, water in shallow aquifers can generate signals equivalent in amplitude to water from deeper aquifer, creating artifacts of

the kind in figure 3, 5 and 6 (Legchenko, 2005). The EC of water samples have been determined both in laboratory and in field, with a good coherency, which makes EC a reliable parameter. This is also the parameter which can be directly related to VES conductivity. Although the measured TDS factor (C_{TDS}) is too low and hence the TDS as well, it still reflects the variations in EC in water perfectly and is hence a reliable parameter to illustrate the variation in salinity. The vertical variations in the aquifer conductivity are reflected in the water EC collected from shallow and deep wells. In most cases, the EC is higher for water from deeper wells than from shallow wells, which can be explained either by a natural dissolution of minerals as the water moves through the strata or from salt dilution from the deeper positioned Thangon formation. NaCl-type of water could work as an indicator of halite polluted water in deeper wells. However, most NaCl-type of water is found in shallow wells, which might be explained by salt water moving from higher areas to lower areas where the water evaporates leaving the salt in the upper surface. In many deep wells, even those with high conductivity, the water is of $CaHCO_3$ type. The halite structures in the Thangon formation is usually overlain by a thin layer of anhydrite ($CaSO_4$) which could contribute to the increased calcium and hardness in some deep wells. The interpolated map of TDS and the VES conductivity bottom layer underlying the aquifer indicates that the high TDS originates from there and the similarity between the bottom conductivity map and hydrogeological maps of H_w and T_{MRS} could imply that the amount of water and rate of circulation could have an affect on the salinity of water in deep wells. It is also possible that the salt is transported from the northern part of area 3 southward, where the salt affected water is trapped in the bottom of the thicker parts of N_2Q_{1-3}, contributing to the salinity of the aquifer and the underlying layer.

The higher R² for VES conductivity and water EC in deeper wells than for shallow wells may depend on the often higher water conductivity in deeper wells, which contribute more to the VES conductivity. Shallow wells (shallow aquifer) are also more vulnerable to local anthropogenic activities whereas deeper wells (deeper aquifer)

are more homogenous. The water EC estimation relating VES conductivity and decay time (T_2*) show that T_2* is insignificant in the model and thus should be removed. This implies that that deeper aquifer is more controlled by conductivity of water than the aquifer material, but also that T_2* is not a good parameter to estimate the conductivity contribution from finer sediments. The water EC estimation in shallow wells suggest that for very low VES conductivities (<200 µS/cm), there is no correlation at all. However, for higher VES conductivity there seem to be some correlation. Archie's law works poorly in the N_2Q_{1-3}, since the unit is quite heterogonous and contains high conductive sediments. Furthermore, the porosity estimated from θ_{MRS} is probably underestimated in finer sediments, where more water is bound to the pore walls, which can not be detected by MRS. Still, a better result can be achieved when sediments within the N_2Q_{1-3} have been grouped in different grain sizes, indicated by T_2*. Yet, another method is needed to estimate the conductivity contribution from the aquifer material. Different approaches are described by Waxman and Smits, 1968; De Lima and Sharma, 1990; Johnson and Sen, 1988.

6. Conclusions

In the Vientiane basin, the combination of MRS and VES allows to distinguish between the main fresh water bearing unit N_2Q_{1-3} from the salt affected clay layer of K_2tn in all three investigated areas. N_2Q_{1-3} is characterized by relatively high water contents, up to 16 %, and decay times, suggesting a mean pore size equivalent to medium sand to gravel. The resistivity is highly variable, but usually above 10 ohm-m, suggesting predominantly fresh water in the aquifers according to the European drinking water standards (EC= 1500 µS/cm ≈ 6.66 ohm-m). The high conductive clay layer overlying the rock salt of the Thangon formation can be found in all three areas on depth of 20 to 50 m characterized by low water content and resistivity lower than 5 ohm-m.

Several approaches have been used to establish the relationship between the water EC and the aquifer conductivity, including Archie's law

and a model where the total conductivity is the sum of the water EC and the conductivity contribution from finer sediments indicated by T_2^*. Both models, returned poor results. There is still a strong relationship between water EC from deep wells and VES conductivity, where the best fit is obtained using: EC[μS/cm]= 0.3821VES[μS/cm], R^2=0.81. No relation is found between conductivity from shallow wells and VES conductivity (R^2=0.09). This is probably because the often higher water conductivity in deeper wells contributes more to the VES conductivity. Interpolated maps of TDS from deeps wells together with maps of the conductivity of the bottom layer, aquifer layer, MRS transmissivity and MRS hydrostatic column may indicate that the salt originate from the underlying layer situated beneath the main aquifer, but it could also have been transported from the northern part area 3 southward where it is trapped in the bottom of the thicker part of the aquifer. No wells in the investigated areas have water chemistry parameters exceeding the limit for unacceptable drinking water according to WHO or the European water quality standard. The main water quality parameters affecting the water conductivity in the Vientiane Basin are TDS, hardness and chloride, which all have shown to have a high correlation to the water EC and thus VES conductivity. This makes MRS and VES a very promising tool for guidance of future drillings and water quality estimation.

Acknowledgements

References

Allen, D., Andreani, M., Badry, R., Flaum, C., Gossenberg, P., Horkowitz, J., Singer, J., White, J. 1997. How to use borehole NMR. Schlumberger's Oilfield Review summer, 34–57.

Archie, G.E., 1942. The electrical resistivity as an aid in determining some reservoir characteristics. Metallurgical and Petroleum Engineers 146, 54–62.

Arunin, S., 1987. Management of Saline Soil and Alkaline Soils in Thailand, Paper presented at the Regional Expert Consultant on the Management of Saline/Alkaline Soils, FAO Regional Office for Asian and the Pacific, August 25-29, 1987, Bangkok, Thailand, 15 p.

Back, W., Hanshaw B., 1965. Chemical geohydrology. Advances in hydroscience, V. 2. Academic press, New York, pp. 49-109

Brassington, R. 2007. Field Hydrogeology. 3rd edition. West Sussex, England, pp. 264.

Clesceri, L. S.(Editor), Greenberg, A. E. (Editor), Eaton, A. D. (Editor), 1998. Standard Methods for the Examination of Water and Wastewater, 20th Edition. Americal Public Health Association (Washington), American Water Works Association (Denver), and Water Environment Federation (Alexandria, VA), pp. 1220.

De Lima, O. A. and Sharma, M. M., 1990. A Grain Conductivity Approach to Shaly Sandstone, Geophysics 55(10), 1347-1358.

Directive 80/778/EEC. 1980. Council Directive of 15 July 1980 relating to the quality of water intended for human consumption. European drinking water standard.

Japan International Cooperation Agency (JICA), 2000. The study on rural water supply and sanitation improvement in the northwest region in the Lao People´s Democratic Republic, Ministry of health, National center for environmental health and water supply, Progress report 2, 14 pp

Japan International Cooperation Agency (JICA), 1994. Drilling logs from the "Vientiane Province Groundwater Development Project".

JICA local office in Phon Hong, Vientiane Province, Laos.

Johnson , D. L. and Sen, P. N., 1988. Dependence of the Conductivity of a Porous Medium on Electrolyte Conductivity, Phys. Rev. B 37.

Kirsh Reinhard (Editor). 2006. Groundwater Geophysics: a Tool for Hydrogeology. Springer –Verlag Berlin Heidelberg 2006.

Krawczyk W.E., and Derek C. Ford, DC, 2007. Correlating specific conductivity with total hardnessin gypsum karst waters. Earth Surface Processes and Landforms, Earth Surf. Process. Landforms 32, 612–620 (2007).

Legchenko, A. 2006. MRS Measurements and Inversion in Presence of EM noise. In: 3rd Magnetic Resonance Sounding Workshop, Spain, Madrid 25-27 October 2006.

Legchenko, A. 2005. Improved modelling of the magnetic resonance signal in the presence of shallow aquifers. NEAR SURFACE GEOPHYSICS 3 (3): 121-130 AUG 2005.

Legchenko, A., Baltassat, J.M., Beauce, A., Bernard, J., 2002. Nuclear magnetic resonance as a geophysical tool for hydrogeologists. Journal of Applied Geophysics 50 (1–2), 21–46.

Legchenko A., Valla P. 2002, A review of the basic principles for proton magnetic resonance sounding measurements. Journal of Applied Geophysics 50, 3 – 19

Legchenko A., Valla P. 2003. Removal of power-line harmonics from proton magnetic resonance measurements, Journal of Applied Geophysics 53 (2003) 103– 120.

Legchenko A., Shushakov O. 1998. Inversion of surface NMR data
Geophysics, Volume 63, Issue 1, pp. 75-84

Long, N. X., Lam N. X., Canh, N. D. 1986. Report on Geological data for Potassium and Manganese in Thangon Region, Dong Bang, Vientiane, 1986. Department of Geology and Mining, Vientiane, Laos.

Lovatt Smith, P. F., Stokes, R B., Bristow, C., Carter, A. 1996. Mid-Cretaceous inversion in the northern Khorat Plateau of Lao PDR and Thailand. Tectonic evolution of Southeast Asia ; Geological Society Special Publications, vol.106, pp.233-247.

Lubczynski M., Roy J. 2003. Hydrogeological interpretation and potential of the new magnetic resonance sounding (MRS) method. Journal of Hydrology Volume 283, Issues 1-4, 10 December 2003, Pages 19-40

Löffler, E. & Kubiniok, J., 1988. Soil Salinization in North-East Thailand, Erdkunde, Band 42, Heft 2, s. 89-100.

Medlicott, K. 2001. Water, sanitation and environmental health in rural Laos PDR.
KAP Study for UNICEF, WES Section, August 2001, 20 pp.

Perttu N., Wattanasen K., Elming S-Å., Phommasone K. 2008. Characterization of Aquifers in the Vientiane Basin, Laos, Using Magnetic Resonance Sounding and Vertical Electrical Sounding.

Reynolds, T., Richards, P. 1996. Unit operations and processes in Environmental Engineering, 2nd edition.PWS Publishing Company. Boston, USA, pp 798.

Shirov, M., Legchenko, A., Creer, G. 1991. New direct non-invasive ground water detection technology for Australia. Explor.Geophys. 22, 333–338.

Shoeller. H. 1959. Arid Zone Hydrology: Recent Developments, UNESCO, Paris, p.125.

Srisuk, K., Sriboonlue, V., and Buaphan, C. 1999. Groundwater flow, saline water and saline soils in the Central Khorat Basin, northeast Thailand. Symposium on Mineral, Energy and Water Resources of Thailand: Towards the year 2000. 238-251.

Srisuk, K. & Toth, K., 1994. Groundwater Salinity and Three-Dimensional Groundwater Flow Model at Ban Nong Khai Nun, Khon Kaen, 186 p.

Stuart-Fox, M., Rooney, D.F. 2006. Microsoft Encarta 2006.

Sundberg, K., 1932. Effect of impregnating waters on electrical conductivity of soils and rocks. Trans. AIME 97: 367-391.

Swedish Environmental Protection Agency (SEPA) 2007. URL: http://www.internat.naturvardsverket.se/ (read: 2007-04-11)

Tabakh El. M., Utha-Aroon C., Schreiber B.C. 1999. Sedimentology of the Cretaceous Maha Sarakham evaporites in the Khorat Plateau of northeastern Thailand. Sedimentary Geology, Volume 123, Number 1, January 1999 , pp. 31-62(32).

Takayanagi, K. 1993. Basic Design Study Report on the Project for Groundwater Development in Vientiane Province in Lao People's Democratic republic.

UNEP, RRC.AP. 2001. State of the Environment (STEA) Report 2001: Lao People's Democratic Republic. URL: http://www.rrcap.unep.org/reports/soe/laosoe.cfm (2007-03-25)

Velpen, V. 1988. Resist87: a computer prcessing packaged for dc Resistivity interpretation. M.sc. thesis, ITC-Delft, The Netherlands.

Vouillamoz, J.M., Chatenoux, B., Mathieu, F., Baltassat, J.M., Legchenko, A. 2007. Efficiency of joint use of MRS and VES to characterize coastal aquifer in Myanmar. Journal of Applied Geophysics, Volume 61, Issue 2, February 2007, Pages 142-154

Vouillamoz, J.M., Descloitres, M., Bernard, J., Fourcassier, P., Romagny, L. 2002. Application of integrated magnetic resonance sounding and resistivity methods for borehole implementation; a case study in Cambodia. Journal of Applied Geophysics, vol.50, no.1-2, pp.67-81, May 2002.

Wannakomol, A. 2005. Soil and Groundwater Salinization Problems in the Khorat Plateau, NE Thailand, Integrated Study of Remote Sensing, Geophysical and Field Data. Fachbereich

Geowissenschaften, Freie Universität Berlin.
http://www.diss.fu-berlin.de/2005/210/indexe.
html

Waxman, M. H. and Smits, L. J. H. Electrical conductivities in oil-bearing shale sands. Soc. Petrol. Eng. J. June 1968, pp. 107-122; Trans. AIME, vol 243.

WHO. 1996. Guidelines for drinking-water quality, 2nd ed. Vol. 2. Health criteria and other supporting information. World Health Organization, Geneva, 1996.

Williamson, D. R., Peck, A J.Turner, J. V., Arunin, S. 1989. Groundwater hydrology and salinity in a valley in Northeast Thailand. Groundwater contamination
IAHS-AISH Publication, vol.185, pp.147-154

Worthington, P.F., 1993. The uses and abuses of the Archie equations, 1: The formation factor-porosity relationship. J.Appl. Geophys., 30:215-228.

WRI, 1998. 1998-1999 World Resources: A Guide to the Global Environment, World Resource Institute, Oxford. University Press, New York.

Yaramanci U., Lange G., Hertrich, M. 2002. Aquifer characterisation using Surface NMR jointly with other geophysical techniques at the Nauen/Berlin test location. Journal of Applied Geophysics 50 (2002) 47– 65